# DOGS AS A MODEL OF HUMAN RETINAL DISEASE: EXTENSIONS OF THE FULL-FIELD ELECTRORETINOGRAM TO CHARACTERIZE NORMAL AND ALTERED RETINAL FUNCTION AND APPLICATIONS TO TRANSLATABLE GENE AUGMENTATION THERAPY

By

Nathaniel Pasmanter

A DISSERTATION

Submitted to
Michigan State University
in partial fulfillment of the requirements
for the degree of

Comparative Medicine and Integrative Biology—Doctor of Philosophy

2021

## ABSTRACT

DOGS AS A MODEL OF HUMAN RETINAL DISEASE: EXTENSIONS OF THE FULL-FIELD ELECTRORETINOGRAM TO CHARACTERIZE NORMAL AND ALTERED RETINAL FUNCTION AND APPLICATIONS TO TRANSLATABLE GENE AUGMENTATION THERAPY

By

Nathaniel Pasmanter

Dogs are an important model of human retinal disease and are frequently used to develop and test translational therapies. Accurate characterization and quantification of the full-field electroretinogram (ERG) is essential in assessing potential treatments, yet many methods used to study the human ERG are rarely used in canine studies. This study aims to assess the utility of several mathematical models of the a- and b-waves and expanded protocols - such as chromatic, increasing background luminance, extended flickers, and long-duration flashes - in characterizing and analyzing the canine ERG. This study establishes baseline parameters for normal canine retinal function and quantifies the altered function in several dog models of human retinal disease. The results of this study demonstrate that mathematical models of the ERG waveforms provide excellent fits in normal dogs, and that expanded protocols better characterize rod and cone contributions to the canine ERG. These methods additionally enable direct comparison of quantified parameters between normal dogs and dog models of human disease as well as longitudinal assessment of disease progression and response to treatment with gene augmentation therapy. The results indicate that incorporating these methods adds valuable information of retinal function. Further research is needed to assess the reliability of these methods across breeds and different recording conditions.

This thesis is dedicated to my younger sister Danya.
Your memory will always live on.

## ACKNOWLEDGMENTS

I would like to thank Zachary Pasmanter for his constant, unrelenting support of all my endeavors, both great and small. He is always my ray of sunshine even on a cloudy day.

I would also like to extend a special thanks to Laurence Occelli and Janice Querubin for their help and support throughout this journey.

And finally, I want to thank my friends and family, and my adviser Dr. Simon Petersen-Jones.

**TABLE OF CONTENTS**

## LIST OF TABLES

## LIST OF FIGURES

## KEY TO ABBREVIATIONS

AC alternating current

CSNB congenital stationary night blindness

DC direct current

DFT discrete Fourier transform

ECVO European College of Veterinary Ophthalmologists

ERG electroretinogram

ERP early receptor potential

ISCEV International Society for Clinical Electrophysiology of Vision

L-AP4 2-amino-4-phosphonobutyrate

mfERG multifocal ERG

NCQX sodium-calcium exchanger

NMDA N-methyl-D-Aspartate

OP oscillatory potential

PDA *cis* 2,3-piperidine-dicarboxylic acid

PERG pattern ERG

PhNR photopic negative response

POAG primary open-angle glaucoma

PRA progressive retinal atrophy

PRCD progressive rod-cone dystrophy

RBC rod bipolar cell

RP retinitis pigmentosa

RPE retinal pigment epithelium

SARDS sudden acquired retinal degeneration syndrome

STR scotopic threshold response

TTX tetrodotoxin

# CHAPTER 1.

# INTRODUCTION

## Background

Electroretinography (ERG) assesses retinal function by recording the electrical response of the retina to light stimulus. The characteristic waveforms in the recorded response are used to assess the health and function of retinal cells [1]. Since it was first performed in 1865, the use of ERG has expanded to clinical, translational, and research investigations in multiple disciplines. In humans and other species, ERG is a critical tool in the diagnosis, characterization, and monitoring of a variety of inherited and acquired retinal diseases, as well as assessment of the recovery of retinal function following treatments such as gene augmentation therapy [2–4].

Dogs are an important large animal model of human retinal disease [5,6]. Spontaneous inherited retinal dystrophies such as the progressive retinal atrophies (PRAs) in dogs show much similarity to analogous conditions such as the retinitis pigmentosas (RPs) in humans [6,7]. They are commonly used to study these conditions and develop translational therapies [5,8–11]. The presence of a retinal region of high photoreceptor density with a cone-rich center, the area centralis, in canine eyes make them particularly valuable because of the similarity to human retina which has a macula with central fovea [12]. Accurate characterization of canine retinal function and dysfunction is critical, both in identification of potential dog models of human retinal disease as well as assessment of translational therapies.

Many diseases present with classic or pathognomonic ERG findings. In the clinical setting, patients are typically assessed for abnormalities using the ISCEV/ECVO standards (for humans and canines, respectively) for the scotopic (dark-adapted) and photopic (light-adapted) ERG [1,13]. The use of different flash strengths and background luminance preferentially assesses the function of different populations of retinal cells. The photopic ERG, with complete suppression of rod responses using a background light, reflects cone function. In scotopic

conditions with dim flashes, rod responses predominate. With brighter flashes, the response reflects both contributions of rods and cones and the interactions between the two [14–17]. The ERG in response to a moderate strength flash of light consists of an initial negative a-wave, whose leading slope can be modeled to assess photoreceptor function [15,18]. The second waveform, the positive b-wave, increases with amplitude with stimulus strength. The amplitude increase can be modeled as a means of assessing retinal sensitivity [19].

**Focus and Value**

Expanding the standard ERG assessment with additional protocols and post-recording analysis provides valuable information on retinal function. These methods can be broadly categorized as 'modalities', which vary in recording apparatus, stimulus and luminance, and 'models', which analyze mathematical models and transformations of the recorded waveforms. A variety of modalities and models are used in human ERG recordings. These include flashes with high frequency flickers, which are a sensitive measure of cone function, and mathematical models of rod and cone photoreceptor responses [15,18,20,21]. These methods have been used to accurately establish the presence and characterize the progression of a variety of degenerative retinal dystrophies in humans and mice [22–24]. However, many of these modalities and models are infrequently used in ERG studies of canine retinal electrophysiology.

Different ERG modalities, such as long flash, flicker, chromatic, and changing background illumination, as well as mathematical models and transformations of the ERG waveforms, can be used to effectively characterize normal parameters of retinal function in wildtype dogs. Furthermore, these models can be extended to dogs with inherited retinal diseases to demonstrate the presence of retinal disease, monitor disease progression, and determine the effectiveness of gene therapy treatment in rescuing photoreceptor function. Specifically, this

thesis shows that these models can be used to determine the phenotypes of a population of research animals, as well as evaluate the functional rescue in affected animals treated with novel therapies (e.g. gene therapy in *Cngb1*$^{-/-}$ dogs as a model of RP in humans).

**Aims**

1. Establish baseline features of normal canine retinal function using flicker, chromatic, long flash, and different background illumination ERGs. Disease models with either lack of rod function or cone function are used to show photoreceptor specificity of the parameters measured as well as the effect of loss of interaction between rods and cones. Specifically, this research demonstrates the effectiveness of the rod a-wave model in characterizing normal rod photoreceptor function.
2. Examine the effectiveness of the cone a-wave model and frequency-based analysis methods in dogs. This research further demonstrates the effectiveness of these ERG modalities and mathematical models in establishing the presence of inherited retinal dystrophies in dogs, as well as monitoring disease progression and the results of gene therapy treatment.

**Objectives**

1. Quantify and establish baseline parameters for normal retinal function in dogs using additional ERG modalities and mathematical models.
2. Analyze dogs with inherited retinal disease and determine physiological and biochemical correlates of baseline retinal function and disease progression.
3. Longitudinal assessment of dogs treated with gene augmentation therapy, and determination of functional rescue through comparison to phenotypically normal dogs and untreated controls.

4. Develop additional mathematical models and protocols for characterization of normal canine retinal function and assessment of inherited retinal disease.

# CHAPTER 2.

# A REVIEW OF ELECTRORETINOGRAPHY WAVEFORMS AND MODELS AND THEIR APPLICATION IN THE DOG

## 2.1. Introduction and background

Since it was first performed by Holmgren in 1865, the electroretinogram (ERG) has become a mainstay in evaluating retinal function in both clinical and research ophthalmology. The standard technique, full-field flash ERG using alternating current (AC) recording, most commonly involves using a corneal contact electrode and a skin reference electrode as well as a ground electrode. The potential difference between the corneal electrode and the reference electrode records the summed electrical activity across the corneal surface [1]. A direct current (DC) method, although less frequently used, provides investigation of a response over several minutes and can add additional information on the function of the retinal pigment epithelium (RPE) [25]. The ERG is generated by retinal cellular responses resulting from light stimulation. Electrical currents that can be recorded at the cornea are generated when a current flows in radially orientated cells from electrical source to sinks. Recording and assessment of these radial currents as the electroretinogram provides insight into the function of different populations of retinal cells, enabling characterization and measurement of retinal dysfunction [2], progression of retinal changes in disease [3], and efficacy of therapy for retinal conditions [4]. More recently, mathematical models for ERG analysis have been developed and used in both human and non-human primate (as a model for human) research to better characterize responses and link them to biochemical events [18]. However, mathematical modeling of the ERG response has not been frequently used in dog studies.

The stimulus and adaptation state of the eye enables recording of rod and cone responses in scotopic (dark-adapted, to enable recording from rod initiated responses and with flashes of higher luminance both rod and cone mixed responses) and photopic (light-adapted to isolate cone driven responses) conditions. The ERG recorded as a result of a moderately strong flash of light

consists of an initial negative component, the a-wave, whose leading slope can be modeled to assess rod photoreceptors in the dark-adapted eye and cone photoreceptor function in the light-adapted eye [18]. The second waveform, the positive b-wave, is primarily the result of currents generated by bipolar cells. The threshold for a rod-mediated b-wave is at a lower stimulus level than that of the a-wave. Both the a-wave and b-wave increase in amplitude with stimulus strength, which can be modeled as a means of assessing retinal sensitivity [26]. The a- and b-waves are the primary ERG components used for assessing retinal function. However, other waveforms are recognized and are discussed in more detail below.

Expanding on the early work of Holmgren, there have been numerous advances in our understanding of visual electrophysiology. Gotch discovered the characteristic positive and negative deflections of an ERG performed on excised frog eyes [27], and Einthoven and Jolly labelled these characteristic deflections [28]. Expanding on the work of other researchers, much of the pioneering work on ERGs was performed by Granit in the 1930s. He successfully isolated the different components of the ERG waveform, showing the presence of three components (which he named processes: PI/PII/PIII) based on their sequential elimination from the cat ERG under increasing depth of ether anesthesia [29]. He further tied these components to the overall waveforms which make up the ERG providing the basis for our current understanding of the underlying physiological components.

Although conventional ERG recordings are non-invasive and utilize a corneal contact electrode, invasive intraretinal ERG recording using micropipette electrodes inserted into the retina with an electrode inserted in the vitreous humor used as reference have been used to localize the origin of the electrical response. Components of the intraretinal ERG are named based mainly on conventional ERG recordings, but both the shape and amplitude of recorded

responses depends on the depth of electrode insertion [30–33]. Transmission of the light induced response occurs from distal to proximal retina – photoreceptors are in the distal retina, while bipolar cells are proximal to the photoreceptors, and third order neurons such as ganglion cells proximal to bipolar cells. Thus, deeper insertion of the intraretinal microelectrode measures potentials generated more distally in the retina. Intraretinal recordings have been used to better characterize near threshold ERG responses, localizing their origin to locations proximal to photoreceptors [34]. The intraretinal ERG has also been used to characterize differences in shape and amplitude of the response across different species [35].

Drug dissection studies of the retina, using intravitreally administered drugs to block activity of specific neurons, have improved understanding of the cells and pathways that contribute to different ERG waveforms [36,37]. Several of these drug classes will be discussed here. Application of aspartate blocks responses in second order neurons from glutamate released from the synaptic terminal of photoreceptors and thus isolates photoreceptor and retinal pigment epithelium derived responses [38]. Glutamate analogs such L-AP4 mimics the action of endogenous glutamate on metabotropic glutamate receptors, resulting in sustained cone ON-bipolar cell membrane hyperpolarization and suppression of light-evoked responses [39]. Selective antagonists of ionotropic glutamate receptors such as *cis* 2,3-piperidine-dicarboxylic acid (PDA) block both cone OFF-bipolar and horizontal cell responses. PDA additionally eliminates third-order neuronal responses in the inner retina [40]. Both N-methyl-D-Aspartate (NMDA), which acts as a partial agonist at NMDA receptors, and tetrodotoxin (TTX), a selective sodium channel blocker, suppress third order neuronal amacrine and ganglion cell activity but leave bipolar cell activity intact [39,41,42].

While the purpose of this review is not to provide direct instructions on how to complete an ERG it is important to mention some factors that can influence the recorded ERG, several of which will be discussed. Technical considerations of ERG recording include signal amplification and bandpass filter parameters, which can affect the quality of the recorded signal. Filtering is used to help remove electrical interference, known as "noise", thus enhancing the signal to noise ratio resulting in a cleaner ERG recording. However, setting a low level for the low pass filter eliminates higher frequency signal components, while setting a high level for the high pass filter will alter the shape of the waveforms recorded [43]. Narrowing the bandpass filter can be used to extract ERG components such as the oscillatory potentials. Additionally, increasing the number of recordings obtained and averaged improves the signal-to-noise ratio of the composite signal. Different electrode types can vary significantly in recorded signal amplitudes, while increasing the distance of the reference electrode from the lateral canthus typically increases signal amplitude [44–47]. Anesthetic type and depth is an additional consideration; light anesthesia may allow for additional background noise generated by muscle activity, whereas deep anesthesia can reduce recorded signals, and different types of anesthetic agents have different effects on recordings [48]. Thus for recordings to be comparable identical anesthesia protocols should be used and the depth of anesthesia monitored closely. For research purposes ERGs are often recorded under anesthesia while a quick retinal check in the clinic may be performed in the conscious animal.

There are many other factors that contribute to variation in ERG recordings. These include length of dark and light adaptation for scotopic and photopic ERG recordings, respectively, this affects bleaching of rod photoreceptors and amplitude of responses [49]. Additional factors include individual variation, pupil dilation, breed differences, eye axial length,

and subject age [50–53]. Care should be taken to standardize recording conditions and parameters to enhance reproducibility and enable comparisons to be made between different subjects.

### 2.2. Physiological processes underlying the ERG

Photoreceptors employ a somewhat unique system in signaling visual responses. In the dark, a proportion of cyclic nucleotide-gated channels in both rod and cone photoreceptor outer segments are open as a result of the presence of cyclic GMP. These channels allow an influx of positive ions into the cell maintaining a relatively depolarized cell membrane. This coupled with active transport of cations out of the cell through the NCQX $Ca^{2+}/Na^{+}$, $K^{+}$ exchange channel causes an electrical current to flow along the length of the photoreceptor, known in rods as the dark current[54–57]. In the depolarized (dark-adapted) state, voltage-gated calcium channels in the synaptic terminal remain open, allowing an influx of calcium ions which triggers a steady release of glutamate at the photoreceptor synapse with second order neurons; retinal bipolar cells and horizontal cells. Glutamate causes hyperpolarization of ON-Bipolar cells (via a metabotropic glutamate receptor) and depolarization of OFF-Bipolar cells (via an ionotropic glutamate receptor) [58,59]. Light stimulus results in isomerization of the photoreceptor G-coupled receptor – the visual pigment (11-*cis*-retinal combined with an opsin; e.g. forming rhodopsin in rods). Rhodopsin and the cone opsins are densely packed in the membranes of the rod and cone photoreceptor outer segments [60,61]. Isomerization of the 11-*cis*-retinal causes a conformational change in the opsin and activation of the associated G-protein, transducin, which subsequently activates the phosphodiesterase holoenzyme (PDE6). Activated PDE6 catalyzes the hydrolysis of cyclic GMP to 5'-GMP, leading to closure of cyclic nucleotide-gated ion channels [55]. This channel closure leads to photoreceptor cell membrane hyperpolarization and the reduction of the dark current. This contributes to the PIII response which underlies the resulting corneal negative

a-wave of the ERG [54,62,63]. The voltage-gated calcium channels at the photoreceptor synaptic terminal also respond to the altered membrane voltage, decreasing the influx of calcium which in turn leads to decreased glutamate release, with a resultant depolarization of ON-Bipolar cells (primarily responsible for the PII response and making a major contribution to the positive b-wave). In the cone pathway this also results in hyperpolarization of OFF-Bipolar cells (which has an effect on the shape of the flash ERG and in the response to longer flash stimuli contributes to the d-wave) [58,59,64]. Upon cessation of light stimulus, several factors mediated by low intracellular calcium concentrations restore the photoreceptor to its native 'dark-adapted' state [54,64,65].

### 2.3. ERG waveforms

The basic studies investigating the origins of the ERG waveforms as reported here have been performed in several different species showing similarities between species but also differences in the degree that each component shapes the final waveform (e.g. differences between species in OFF-bipolar cell contributions). There are a limited number of specific studies dissecting waveform components in dogs but the basic waveform components are similar to those described by in-depth studies in other species.

1. A-wave

The a-wave is visualized as an initial negative deflection of the ERG and has major contributions from the activity of rod and/or cone photoreceptors [56]. The a-wave of the scotopic ERG is primarily the result of the reduction in the rod dark current (Figure 2.1A). The photopic cone mediated a-wave has a more complex origin with significant contributions from inner retinal cells, particularly at lower stimulus strengths [40,66] (Figure 2.1B). The a-wave is one of the most studied of the ERG components and increases in amplitude and decreases in implicit time

with increasing stimuli strength until it reaches saturation. Care must be taken to distinguish it from another negative waveform, the scotopic threshold response (STR) which is a response recorded from weak stimuli in a well dark-adapted eye and appears at response threshold at stimuli below b-wave threshold. With increasing stimulus strength, the b-wave appears and increases in amplitude such that it obscures the STR (which is considered in more detail below). In contrast to the STR, the scotopic a-wave is typically not visualized until stimuli strength several orders of magnitude above the initial appearance of the b-wave.

Drug dissection studies have confirmed photoreceptors to be the primary source of the rod-driven a-wave and significant contributors to the cone-driven a-wave. ERG recorded from aspartate-treated eyes isolates the PIII response by eliminating postreceptoral responses (which are major contributors to b and d-waves, oscillatory potentials [OPs], and the STR). These studies show the major contribution of the photoreceptor PIII responses to the ERG a-wave [38,67,68]. Further studies of the scotopic ERG demonstrate that both NMDA and PDA reduce the amplitude of the a-wave response and eliminate a 'trough' that appears between the a and b-waves. This suggests that postreceptoral contributions to the dark-adapted a-wave derive not only from OFF-bipolar cells, but also from amacrine and ganglion cells [41,42]. Additional investigations have revealed a 'slow' negative P-III component only visible when the retina was separated from the RPE to remove its positive contribution with a similar time course. This slow contribution to the a-wave has been attributed to both postreceptoral contributions from OFF-bipolar cells, as well as Müller cells responding to changes in extracellular potassium concentration caused by activation of photoreceptors [69–71].

Understanding the physiologic processes that underlie the ERG is key to recognizing normal features of the ERG, as well as identifying and localizing abnormal responses.

Classically, the a-wave of the scotopic ERG represents the summed response of retinal photoreceptors. Under scotopic conditions, responses to brief light flashes of low-stimulus strength represent the sole contribution of rod photoreceptors to the ERG a-wave response, as cone photopigment is several of orders less sensitive to photon stimulation than rhodopsin. With increasing stimulus strength, cone photoreceptors also activate, and the a-wave then represents the summed response of rods and cones. Rod responses are suppressed in photopic conditions so the resultant a-waves are driven by the cone responses [14–17].

As stated above, near threshold the photopic a-wave has major contributions from postreceptoral components. These postreceptoral components are blocked by the action of PDA which indicates they originate from the OFF pathway [40]. It is of note that the size of OFF pathway responses differs between species and thus there is probably a difference in the contribution to the photopic a-wave [66,72]. The photoreceptor component of the photopic a-wave increases with stronger stimuli [40,73].

Classical a-wave analysis measures both the amplitude (measured from pre-flash ERG baseline to the a-wave trough) as well as implicit time (time to trough from the start of flash stimulus). These parameters are subject to the saturation kinetics of phototransduction amplification. Increases in flash stimulus strength increase both the quantity and speed of photoreceptor responses, with a commensurate increase in a-wave amplitude and decrease in implicit time with increasing stimulus strength [62]. Modelling of the slope of both rod and cone a-wave has been established to more accurately measure photoreceptor responses and are discussed below.

2. B-wave

The b-wave is visualized as a corneal positive deflection of the ERG and is primarily shaped by the PII response. It appears in response to weaker stimuli than the scotopic a-wave (Figure 2.1C). To stronger stimuli it follows the initial negative deflection of the a-wave. There has been some debate about the origin of the b-wave, but it is now widely accepted that the major contribution is from the ON-bipolar cells. Typically, the largest amplitude response in the ERG, the b-wave amplitude is measured from the trough of the preceding a-wave to the following positive peak, accounting for the intrusion of OPs in the measurement (See Figure 2.1A).

Studies of isolated PII recordings, compared to patch-clamp single-cell current recordings of rod bipolar cells (RBCs), which are an ON form of bipolar cell, support RBCs as the main generator of the rod-driven b-wave [74,75]. Additionally, several drug dissection studies have provided invaluable insights into the pathways responsible for the generation of the cone-driven b-wave. Studies utilizing L-AP4 demonstrate that L-AP4 largely eliminates the early positive component of the cone b-wave, thus confirming ON-bipolar cells as the primary originator of the photopic b-wave response. In contrast, a later negative component that reduces the amplitude of the positive b-wave, in addition to influencing its shape, is eliminated by PDA application, suggesting that OFF-bipolar cells are responsible for this modulating process. The combination of opposing underlying waveforms thus shape the b-wave, a process that has been described by Sieving et al. as a 'push-pull' mechanism [73,76].

While electrical activity emanating from RBCs predominantly fashions the scotopic b-wave, and the combination of forces from cone ON and OFF-bipolar cells shape the photopic b-wave, there are other factors that contribute to both the amplitude and shape of the b-wave (See

Figures 2.1D and 2.2). This includes Müller cell responses to changes in extracellular potassium concentration caused by activity in adjacent neurons. Indeed, electrical current flow along Müller cells was originally posited as the source of the b-wave – however, studies of the retina exposed to barium, which functions to decrease Müller cell potassium permeability, failed to abolish the b-wave, and in some circumstances even augmented the b-wave response [77–79]. However, intravitreal barium injection also diminished the response of a 'slow' component of the scotopic b-wave in the cat, which may indicate a possible role of electrical fields developed across the length of Müller cells in shaping the late b-wave response [41]. Additional studies have investigated possible contributions from amacrine and ganglion cells to effect changes on the ERG b-wave. Intravitreal TTX injection, in addition to bicuculline and strychnine to block GABA and glycine receptors, respectively, demonstrated that additional postreceptoral contributions impact both the amplitude and kinetics of the b-wave response. TTX-treated eyes demonstrated a substantial delay in b-wave response, while blockage of both Glycine and GABA receptors caused an increase in b-wave amplitude [80,81]. Thus, while ON-bipolar cells are responsible for generating the major portion of the b-wave, additional postreceptoral components influence the shape of the response.

3. Oscillatory Potentials

OPs are characteristic high frequency waveforms superimposed on the rising edge of the scotopic and photopic b-wave. Activity of several cell types appear to contribute to the OPs. They originate in the proximal retina, mainly from amacrine cells but with additional contribution from ganglion cells [82,83]. There is some debate over potential spatial localization of early vs late OPs, with some evidence that in the photopic ERG early OPs may originate in the ON pathway while late OPs originate in the OFF pathway [82]. OPs are one of the most sensitive

ERG components with respect to blood flow and may be diminished before other waveforms in mild retinal ischemia [84].

Measuring the stimulus:response characteristics of the OPs requires extracting the signal, typically utilizing a bandpass filter that removes low-frequency components of the ERG [85] (Figure 2.3). Although OPs are of a much higher frequency than the a and b-waves, they can be further subdivided into 'low-frequency' OPs, centered near 80Hz and originating from amacrine cells, and 'high-frequency' OPs, which are centered near 160Hz and originate from ganglion cells. Examining these separate features of OPs can be done utilizing a transform that accounts for frequency localization with time, such as the Discrete Wavelet Transform [86].

4. Scotopic Threshold Response (STR)

Although a single photon can stimulate the photoisomerization of a rhodopsin molecule in rod photoreceptors, a minimum level of light is required to generate a detectable ERG response. In the scotopic ERG, at stimulus strength near the psychophysical limit of vision, a waveform known as the STR, can be recorded. Believed to represent changes in extracellular potassium concentration affecting Müller cells, with additional contributions from amacrine and retinal ganglion cells, the STR has been recorded in multiple species [87–89]. Additionally, drug dissection studies of proximal retinal contributions to the STR have suggested potential inter-species differences in origin, with reports suggesting the STR in monkeys originates from retinal ganglion cells, and that of humans, cats, and mice, from amacrine cells [87,90]. Although the dominant component is typically a negative waveform (nSTR), there may also be a preceding positive waveform (pSTR), with pharmacological evidence of similar origins for both components [91]. As stimulus strength increases, the STR becomes overwhelmed by the developing b-wave [87,88] **(**Figure 2.4).

5. C-wave

When using DC recording, the c-wave is seen as a slow positive deflection after the b-wave and derives from changes in the transepithelial potential of the RPE [92]. Recording from a retina separated from the RPE eliminates the c-wave entirely. Furthermore, the c-wave demonstrates a linear relationship between amplitude and stimulus strength [93]. Although infrequently measured due to the technical considerations of DC recordings, the c-wave may have clinical and research utility in characterizing diseases featuring RPE disruption, including choriocapillaris atrophy and some types of retinitis pigmentosa (RP) [94,95].

6. D-wave

Typically only detectable with prolonged (>100ms) intense light stimulus, the d-wave originates from OFF-bipolar cell activity in the cone pathway [96,97] (Figure 2.5). The OFF response from a longer flash stimulus is positive in humans, primates and chickens and predominantly negative in other species such as rats and dogs [98,99]. In contrast to ON-bipolar cells, which are stimulated through metabatropic glutamate receptors, OFF-bipolar cells are primarily stimulated through glutamate stimulation of ionotropic AMPA and kainite receptors [100]. The differential response of bipolar cells to glutamate release is highlighted by the continued presence of an OFF-bipolar cell response even in the absence of ON-bipolar cell activity (as in certain types of complete congenital stationary night blindness) [99,101].

7. Early Receptor Potential (ERP)

The ERP is a brief, biphasic electrical response that appears immediately following bright flashes, and is believed to result from light-induced conformational changes in the visual pigment of the photoreceptors. The ERP is the earliest quantifiable response that can be detected following a flash stimulus. A function of both stimulus strength and quantity of isomerizable

photopigment, the ERP typically occurs within 1.5ms of flash, making it difficult to measure using a standard ERG protocol [102]. Although infrequently measured, it is suggested to provide insight into photopigment density in retinas otherwise not showing signs of disease [103].

8. I-wave

The ERG i-wave is a positive deflection that may be seen following the b-wave in photopic ERGs, the i-wave is also believed to reflect some late contribution of ganglion cells (See Figure 2.1C). Its mechanisms are poorly understood, although there is some evidence that it may decrease in amplitude with glaucoma, perhaps making it useful in assessing patients with this disease [104–106].

9. Photopic Negative Response (PhNR)

Under photopic conditions, a negative waveform directly following the b-wave peak can be visualized (See Figure 2.1C). The PhNR, though not well-described physiologically, is thought to reflect retinal ganglion cell activity. The basis for this derives from several studies on optic neuropathies – pathologies that impair ganglion cell function, such as primary open angle glaucoma and several causes of retinal ischemia, which lead to a decreased amplitude to the PhNR. TTX injection also reduces PhNR amplitude, further supporting 3$^{rd}$ order neurons as the source of this waveform [107–109].

10. X-wave

In the dark-adapted ERG, direct photoreceptor responses can be temporally separated under certain stimulus conditions. The dark-adapted cone response, the x-wave, is best visualized with dim flashes of red light after sufficient dark adaptation [110]. In cone-rich species, the x-wave is a positive response that precedes the rod-driven b-wave response [111,112]. With brighter red flashes, and with flashes of substantially different wavelengths, the x-wave is often masked by

the scotopic b-wave and may only appear as a positive deflection along the leading edge of the b-wave [110,113].

### 2.4. Selected Additional ERG Modalities

1. Pattern ERG

PERG derives responses from both ON and OFF pathways and measures retinal response to a contrast-reversing pattern, typically using a checkerboard pattern [114]. In humans it provides information on macular function, as well as that of retinal ganglion cells, and can be used to investigate diseases affecting the retina and optic nerve, such as glaucoma [115]. In dogs with glaucoma, studies have found a reduction in PERG function corresponding to increases in IOP [116]. Several waveforms unique to the PERG have been identified and named. P1 and N2, the major positive and negative deflections seen following pattern reversal, respectively. In humans, these waveforms are denoted P50 and N95 as they are seen at 50 and 95 milliseconds following pattern reversal. The timing of the responses varies across species [114,117,118]

2. Multifocal ERG (mfERG)

mfERG provides better spatial resolution of retinal function than regular full-field flash ERG. While the full-field ERG examines the function of the retina as a whole, mfERG creates a topographic map of the retina, allowing analysis of local retinal activity. After mathematical extraction of the electrical response, different areas of the retina can be examined for localizing potential dysfunction. This is typically performed in photopic conditions, and thus primarily measures cone responses [119]. mfERG can be used to better localize and evaluate conditions such inherited diseases which tend to preferentially affect certain retinal areas such as Stargardt macular dystrophy, better classifying the effects of retinitis pigmentosa, and evaluating for

retinal damage after surgical treatment [120]. It has also been used to demonstrate regional rescue of retinal function as a result of retinal gene augmentation therapy [11].

3. Long flash ERG

As described earlier, the long-duration flash ERG, also known as the ON-OFF ERG, is mainly used to separate the pathways responsible for the cone-driven contributions to the photopic ERG response. With a typical ERG protocol, where a very brief duration flash (<4 ms) is used, the ON and OFF responses are merged. By extending flash duration (eg. >100 ms), the flash offset response is separated from the onset response (See Figure 2.5). The long flash ERG has been used in characterizing postreceptoral abnormalities in diseases with abnormal b-waves, such as congenital stationary night blindness (CSNB) [121–124].

In separating the responses to flash onset and offset, the long flash ERG provides several observable components. The corneal-negative a-wave follows flash onset, followed by the corneal-positive b-wave (not identical to the regular short flash b-wave, as it lacks the flash offset response seen in the short flash ERG protocol). The post b-wave response has clear differences between species – in the rat, there is a notable positive plateau, while the guinea pig demonstrates a sharp negative deflection [98]. Finally, the isolated OFF response, which may be positive or negative depending on species, occurs shortly after flash offset. Administration of PDA and L-AP4 demonstrate differential effects on the aforementioned features, varying by species, suggesting that contributions and interactions of cone photoreceptors, ON and OFF postreceptoral pathways contribute to the size and shape of the components of the long flash ERG in different ways in a species-dependent manner [73,76,98,125,126].

4. Flicker ERG

Typical full-field flash ERG protocols focus mainly on responses to single light flashes. Indeed, the current ISCEV standard ERG protocol includes only a single recommendation with altered frequency of ERG flashes (30Hz photopic flashes) [1]. Including flashes beyond the standard single flash and 30Hz flicker protocols may provide additional insight into retinal function. Flicker protocols using different shape of stimulus waveform such as saw-tooth have been used to extract additional information from the ERG [127]. Recent analysis of control and mouse models with specific genes knocked out has enhanced our understanding of the potential contribution of an expanded scotopic flicker protocol to characterizing postreceptoral retinal function [22]. With flash stimuli in the mixed rod-cone range, three frequency bands were identified as quantifying the activity of different classes of retinal bipolar cells in the scotopic ERG– under 5Hz, the ERG response represents the contributions of rod bipolar cells. Between 5 and 15Hz, cone ON-bipolar cell contributions predominate. Above 15Hz, the main contribution derives from cone OFF-bipolar cells (Figure 2.6).

Drug dissection studies of the photopic flicker ERG using PDA and L-AP4 further support the substantial postreceptoral contribution of the cone ON and OFF pathways to the retinal response to high-frequency stimuli. Additionally, these studies indicate that there are substantial postreceptoral contributions to high-frequency photopic flicker stimuli [128,129]. There is also evidence of inter-species differences in response to fast-flicker ERG, potentially due to variations in spectral sensitivity [130–132]. With sufficiently high frequency stimuli, patients subjected to flash flicker ERG are unable to temporally separate different flashes. The critical fusion frequency (CFF) is defined as the lowest flash frequency at which flash flickers cannot be temporally resolved on ERG. CFF varies between species, depending both on size and metabolic

rate [133]. Early ERG studies indicated a CFF of 20Hz in dogs; however, behavioral studies indicate a CFF for cones near 80Hz, higher than the 60Hz reported in humans. CFF may be lowered in certain disease processes, such as cone degeneration [134,135].

5. Chromatic ERG

Standard full flash ERG protocols often recommend the use of white light stimuli, which consists of the full spectrum of visible wavelengths. However, dogs possess two cone types (M/L and S) in addition to rods, which contain different opsins that are sensitive to specific wavelength ranges. S-cones in dogs are preferentially stimulated by short wavelength, or blue, light (peak spectral sensitivity at 430-435nm), while M/L-cones are preferentially stimulated by longer wavelength, or red, light (peak spectral sensitivity at 555nm). Conversely, rods, which do not convey color information, are nevertheless most sensitive to middle wavelength, or green, light (peak sensitivity at 508nm) [136].

In the photopic ERG, specific wavelength flashes and backgrounds can be used to isolate the responses of one class of cones. Such protocols have been used to characterize and diagnose achromatopsia and dyschromatopsia in humans. In the dark-adapted ERG, selective use of red and blue flashes can be used to preferentially stimulate dark-adapted cones and rods, respectively [113]. Protocols matching b-wave amplitudes of red and blue flashes have been used in several investigations, such as the characterization of negative ERGs (referring to waveforms with smaller b-wave than a-wave amplitude) [137]. Recently, a ‘silent substitution’ method, which uses sine wave stimuli with 180° phase difference presented at different frequencies and luminance, has been used to separate rod, M/L-cone, and S-cone responses in dogs [138].

## 2.5. Modeling of ERG waveforms

While ERG waveforms can be measured for implicit time and amplitude, these provide limited insight into retinal function as it relates to the underlying processes, for example of phototransduction. Models provide a quantitative measure of retinal function that is based on biochemical events. The first model utilized is the most common method used to analyze the b-wave change in amplitude over a range of stimuli strengths; based on a Michaelis-Menten function and named after the first scientists to utilize it; the Naka-Rushton equation. Naka and Rushton described this modeling in 1966, the equation is fit to the first limb of the dark-adapted b-wave, plotting amplitude against increasing stimulus luminance [139]. The parameters of the resulting sigmoidal curve can be compared both within and between subjects to assess retinal responsiveness, homogeneity, and sensitivity of bipolar cells in the inner nuclear layer [26].

Lamb and Pugh provided an impetus for the use of models of photoreceptor function, connecting the biochemical processes of phototransduction with the electrical changes measured by ERG. Noting that photocurrent response follows saturation kinetics, they developed several equations for rod photoreceptors which measure the rate of current change as a function of time and light intensity in terms of a single photoreceptor [63]. The overall response visualized on the ERG depends on the number of functional photoreceptors in the population, and can be modeled after subtracting matched light-adapted from dark-adapted responses to provide the rod-only response [62]. Several models for the photopic a-wave have been proposed and applied in humans, including a Michaelis-Menten type saturation function, as well as application of an additional function to the scotopic model [15]. Postreceptoral contributions to the cone-driven a-wave, in addition to interspecies differences in cone membrane capacitance, subtypes, and spectral sensitivity make development of a generalizable model of the photopic a-wave difficult.

Quantification of a and b-wave responses using optimally fitted mathematical models provides insight into the health of these retinal cells [23]. Modeling of the leading edge of the rod a-wave solely characterizes the function of rod photoreceptors (featuring a maximum amplitude parameter $R_{max}$, sensitivity parameter log S, and time delay parameter $t_d$) [18]. Additionally, Naka-Rushton fitting of the rod b-wave (defined by an amplitude parameter $V_m$, a semisaturation constant *k*, and a slope parameter *n*) assesses retinal sensitivity (mainly originating from second-order neurons) [19]. Evaluation of model parameters enables comparison of ERG responses, both individually and across a population, over time. (Figure 2.7).

In humans, modeling of the a-wave and b-wave of the ERG have been applied to the characterization of different inherited and isolated phenotypes of retinal disease [140], the evaluation of differential effects of diseases such as glaucoma on the retina [141], as well as the progression of retinal dystrophies [142]. They have also been used in pharmacologic and toxicologic studies, both in assessing drug effects on retinal function [143] and as potential biomarkers of drug distribution to the CNS [144]. More recently, and demonstrating future promise, these models have been used in assessing the effects of gene therapy treatment on animal models of inherited retinal disease in humans [5,145].

ERG waveforms can also be analyzed using frequency-based analysis. Photopic flicker ERG can be quantified by Fourier analysis in the frequency domain and used to detect retina functional changes from diseases such as diabetic retinopathy [146]. Another method, the discrete wavelet transform, operates in the time-frequency domain and examines the intensity of different frequencies that contribute to the overall ERG waveform as a function of time. Given that different retinal components contribute to the response at different frequencies, such an analysis could help to differentiate different cell contributions to the overall ERG response at different

points in time, and potentially identify specific sources of retinal dysfunction [147]. Additionally, wavelet transform can aid in the analysis of morphological changes in the ERG waveform [148]. The use of frequency-domain analysis may enable the extraction of useful information in very low amplitude ERG responses barely detectable above noise, as it separates out different frequency contributions to the overall waveform and removes potential noise contamination in the time domain. In one study using this technique it was possible to monitor progression of RP in a human patient for years after conventional time-domain analysis was impossible [149].

### 2.6. Applications of ERG to the study of different canine retinal dystrophies

ERG has utility in both clinical and research ophthalmology. It is commonly used in the diagnosis of sudden acquired retinal degeneration syndrome (SARDS) and early progressive retinal atrophy (PRA), two of the leading causes of incurable blindness in dogs [150]. The European College of Veterinary Ophthalmologists (ECVO) provided guidelines for clinical ERG protocols for dogs [13], while the International Society for Clinical Electrophysiology of Vision (ISCEV) establishes analogous guidelines for use in human patients. Although the limited range of recommended flash strengths restricts the utility of these protocols in ophthalmology research, ISCEV recently issued a protocol for the stimulus-response series of the dark-adapted ERG, with a focus on Naka-Rushton fitting of the rod-driven b-wave [151]). ERG is an important component in the investigation and characterization of newly identified retinal dystrophies and when performed early in the disease process can indicate the type of retinal dysfunction that underlies the condition [8]. It is also used to monitor disease progression in large animal retinal dystrophy models [152], and correlate changes to human forms of inherited retinal dystrophies[5,9]. ERG can also be used in toxicological studies as a sensitive method to detect adverse retinal effects [153].

Dogs with retinal dysfunction have been studied both to advance veterinary medicine and as models of human retinal disease, and more recently have been very important in developing translational therapies [5,6]. Dogs and cats have an advantage over laboratory rodent models in that they have a retinal region of high photoreceptor density with a cone-rich center; the area centralis [12]. This is analogous to the human macula which is critical for high-acuity vision. The remainder of this paper provides examples of characteristic ERG findings in a variety of canine retinal dystrophies.

Dogs with a range of different types of spontaneous retinal dystrophies have been identified. These include achromatopias, the progressive retinal atrophies (equivalent to the retinitis pigmentosas and cone-rod dystrophies in man), models of Leber congenital amaurosis, congenital stationary night-blindnesses and canine multifocal retinopathy (analogous to bestrophinopathies in man). The ERG is a useful tool in the study of these conditions and can give an indication of retinal functional changes prior to degeneration. This can be useful in the characterization of newly recognized conditions. Below are included a few examples of ERG changes that occur with some of the canine retinal dystrophies.

Achromatopsia. Loss of cone function with preservation of rod function is seen in dogs with achromatopsia. The scotopic ERG is relatively normal whereas the photopic ERG is absent reflecting the lack of cone function [154].

Congenital Stationary Night Blindness. There are different forms of CSNB recognized in humans, with characteristic ERG changes which depend on the function of the mutated gene. The ERG changes of patients can show whether the abnormality is a lack of normal synaptic transmission from rod, or rod and cone photoreceptors to rod bipolar cells, or both rod bipolar and cone ON- and OFF-bipolar cells respectively. Such absence of synaptic transmission is

suggestive of mutations of photoreceptor expressed genes [155]. In other instances the mutation may directly affect ON-bipolar cell function (both rod bipolar and cone ON-bipolar cells) while sparing OFF-bipolar cell function. This is typical of mutations in genes involved in ON bipolar cell signaling.

A recessive CSNB in beagles has been identified [99]. The ERG of the affected dogs lacks a b-wave and has a relatively normal a-wave. OFF-bipolar cell responses are still detectable in the ERG suggesting that the mutation perturbs normal ON-bipolar cell function. A mutation in LRIT3 was recently identified in these dogs [156].

Progressive retinal atrophy (PRA). PRAs represent a collection of retinal dystrophies with a similar clinical presentation of a progressive, generalized, bilateral retinal degeneration. Mutations have been identified in several different genes resulting in this presentation. Dogs with classic PRA have an initial loss of rod function with a slower loss of cone function. Many of the causal gene mutations are in genes expressed in rod photoreceptors. The progressive loss of rods leads to a secondary loss of cones even if the mutant gene is not expressed in cones. Conversely, mutations of genes expressed in both rods and cones can result in a cone-rod dystrophy where cones are initially affected to a similar degree to rods, or may be even more severely affected than rods [6,7,157].

ERG studies in the early stages of the disease process can distinguish between the rod-led dystrophies and the cone-rod dystrophies, while the funduscopic changes of a generalized retinal degeneration typically do not distinguish the sub types. Some gene mutations result in a loss of function that precedes structural loss, while in other mutations do not initially reduce photoreceptor function appreciably but do result in a progressive loss of photoreceptors. In the

latter instances the ERG responses may initially be normal, with longitudinal ERG recordings demonstrating declining amplitudes as there is a progressive loss of photoreceptors [152,158,159]. An example of a form of PRA with an initial normal ERG with declining amplitudes paralleling progressive loss of photoreceptors is the progressive rod-cone degeneration (*PRCD*) form of PRA, which is the commonest form of PRA. Use of ERG for early detection of *PRCD* is possible if normal breed and age matched controls are available in the investigating laboratory. However identification of the *PRCD* mutation and genetic testing means that ERG is not needed as a pre-breeding screen for breeds with *PRCD*.

PRA that is caused by mutations that impact rod phototransduction result in a loss of rod mediated ERG responses prior to significant (and thus ophthalmoscopically detectable) retinal thinning. Loss of function mutations in PDE6 subunits are one cause of this presentation. The first form of PRA for which the causal gene mutation was identified was the rod-cone dysplasia 1 form of PRA in the Irish Setter which is caused by a mutation in *PDE6B* [160]. Subsequently a mutation in the other active subunit of PDE6 was identified; *PDE6A* in the Cardigan Welsh Corgis [161]. As described earlier in this article, PDE6 hydrolyzes cGMP in rod photoreceptors in response to light stimulation activating rhodopsin and then transducin. Without functional PDE6 there is a failure in rod phototransduction, and an elevation of cGMP levels leading to rapid death of the non-functional rod photoreceptors. The lack of phototransduction is reflected in the scotopic ERG stimulus:responses series where ERG responses are absent until the stimulus is sufficiently strong to result in a cone response. ERG readily detects the lack of rod responses from the earliest age the ERG can be recorded **(**Figure 2.8). At the early-stages the photopic responses may be essentially normal although in *PDE6A*-mutant Cardigan Welsh Corgis an early

reduction in cone a-wave was apparent reflecting the stunted development of cone outer segments [159,161].

### 2.7. Summary

In conclusion, the full-field flash ERG has been and continues to remain an invaluable tool in both clinical and research ophthalmology, aiding in the diagnosis of retinal disease and the characterization of normal and abnormal retinal function. The potential of the ERG is often not fully utilized in veterinary medicine, where typically a limited range of stimuli are used and analysis is confined to subjective assessment of the overall waveform shape, and measurement of the amplitudes and timing of the a- and b-wave. With use of a greater range of stimulus conditions (from threshold of response to a strong stimulus), chromatic stimuli and different flicker stimuli, as discussed in this paper, coupled with a more in-depth analysis of the responses, additional information on retinal function can readily be obtained, allowing for a greater understanding of normal retinal function as well as the altered function that occurs in retinal disease.

# APPENDIX

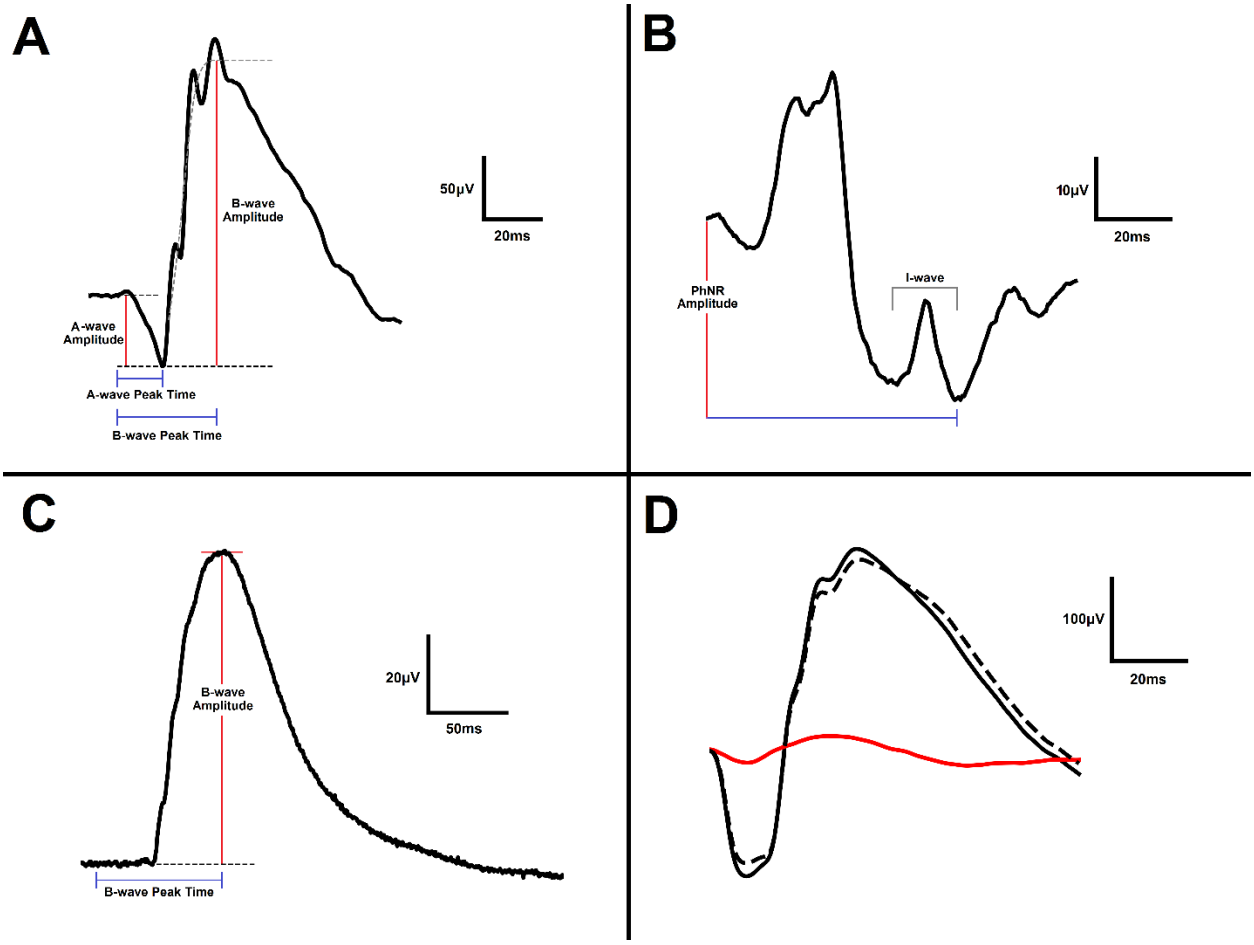


**Figure 2.1. Dark- and light-adapted single flash waveforms**

A. Dark-adapted ERG of a normal dog as a result of a -0.4 log cd.s/m$^2$ white light flash stimulus. With this luminance stimuli, there is a mixed rod-cone response contributing to the ERG. The peak time and amplitude measurements for the a and b-waves are shown. Note that the b-wave amplitude is measured from the trough of the a-wave to the maximum positive response with OPs removed (dashed gray line on figure).

B. Light-adapted ERG of a normal dog in response to a 0.86 log cd.s/m$^2$ flash stimulus. With use of a 30 cd/m$^2$ background light to suppress rod responses, the ERG shows a cone-only response. The i-wave and PhNR are noted following the b-wave.

**Figure 2.1. (cont'd)**

C. Scotopic ERG of a normal dog with -2.41 log cd.s/$m^2$ flash stimulus. With weak stimuli, the scotopic ERG shows a rod-only response, and no a-wave is present. The peak time and amplitude measurements for the b-wave is shown.

D. Mixed dark- (black line) and light-adapted (red line) ERG of a normal dog with 1.36 log cd.s/$m^2$ flash stimulus. The waveform obtained by subtracting the light-adapted from the dark-adapted response (dashed line) theoretically represents a rod-mediated response.

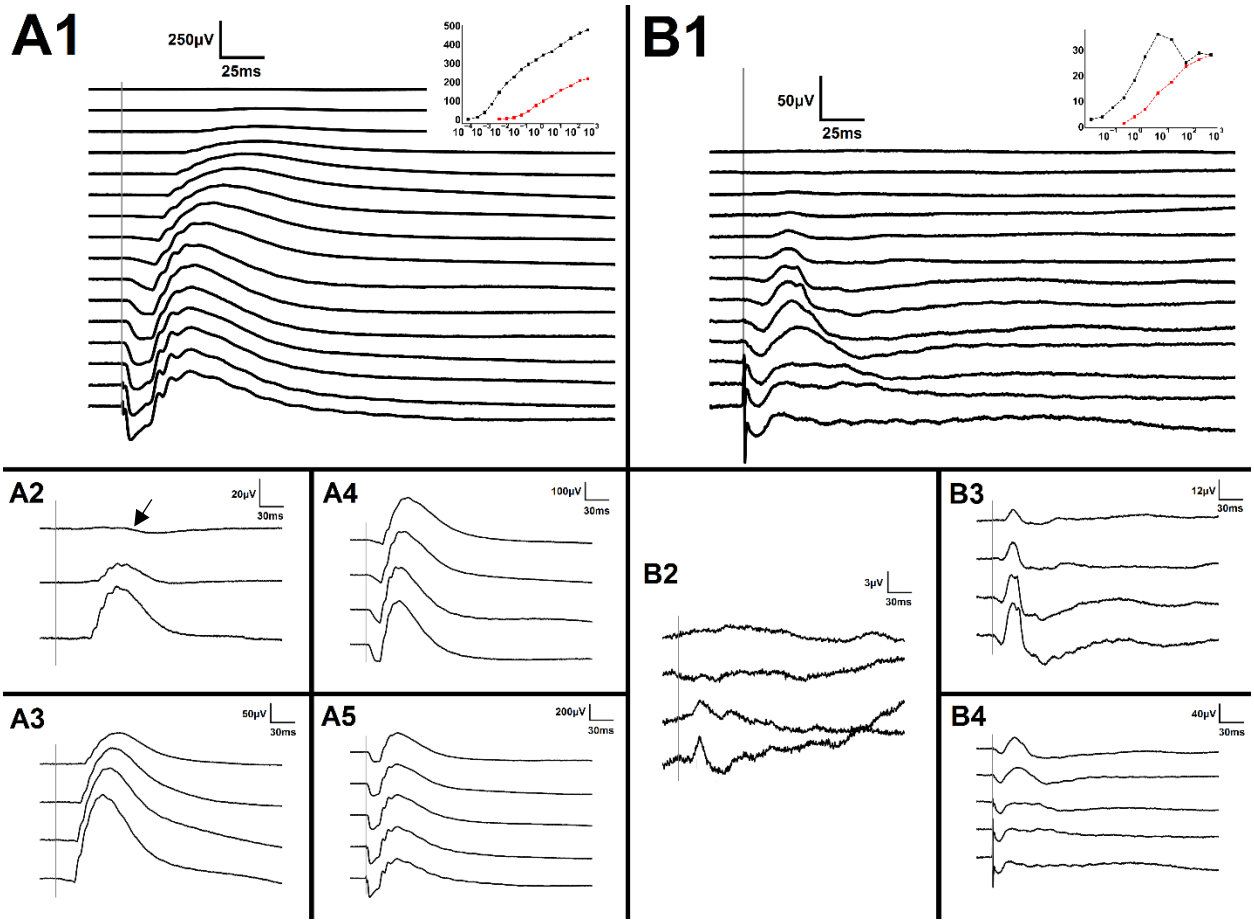


**Figure 2.2. Dark- and light-adapted montages of single flash ERG series, shown at equivalent stimulus strength**

A1. Montage of dark-adapted responses from a normal dog. Note the lower stimulus threshold required to effect a measurable response, as compared to the light-adapted ERG (B1), as well as the greater amplitude of responses at comparable stimulus strength. A b-wave response is detectable in the second tracing, at -3.19 log cd.s/$m^2$ stimulus strength. The inset shows the luminance:response curves for the a-wave amplitude in red and b-wave amplitude in black. The y-axis shows amplitude in microvolts and the x-axis luminance of the stimulus in log cd.s/$m^2$). The same series is shown in more detail in A2-A5.

**Figure 2.2. (cont'd)**

A2. Dark-adapted ERG responses elicited from -3.7, -3.19, and -2.8 log cd.s/$m^2$ flash stimuli. The upper tracing shows a scotopic threshold response (denoted by the arrow; see Figure 2.4 for more details of an STR).

A3. Dark-adapted ERG responses elicited from -2.41, -2, -1.6, and -1.19 log cd.s/$m^2$ flash stimuli.

A4. Dark-adapted ERG responses elicited from -0.8, -0.4, 0.0, and 0.39 log cd.s/$m^2$ flash stimuli.

A5. Dark-adapted ERG responses elicited from 0.86, 1.36, 1.9, 2.39, and 2.82 log cd.s/$m^2$ flash stimuli.

B1. Montage of light-adapted responses from a normal dog. Light-adapted response amplitudes are lower in amplitude compared to equal stimulus strength dark-adapted flashes. There is no detectable response until the third tracing, at -1.6 log cd.s/$m^2$ stimulus strength, a stimulus 1.6 log units greater than that required to elicit a response in the dark-adapted ERG. The inset shows the luminance:response curves for the a-wave amplitude in red and b-wave amplitude in black. Note the presence of a photopic hill effect whereby the b-wave amplitude peaks and then declines with increasing stimulus strength. The y-axis shows amplitude in microvolts and the x-axis luminance of the stimulus in log cd.s/$m^2$). The same series is shown in more detail in B2-B5.

B2. Light-adapted ERG responses elicited from -2.41, -2, -1.6, and -1.19 log cd.s/$m^2$ flash stimuli.

B3. Light-adapted ERG responses elicited from -0.8, -0.4, 0.0, and 0.39 log cd.s/$m^2$ flash stimuli.

B4. Light-adapted ERG responses elicited from 0.86, 1.36, 1.9, 2.39, and 2.82 log cd.s/$m^2$ flash stimuli.

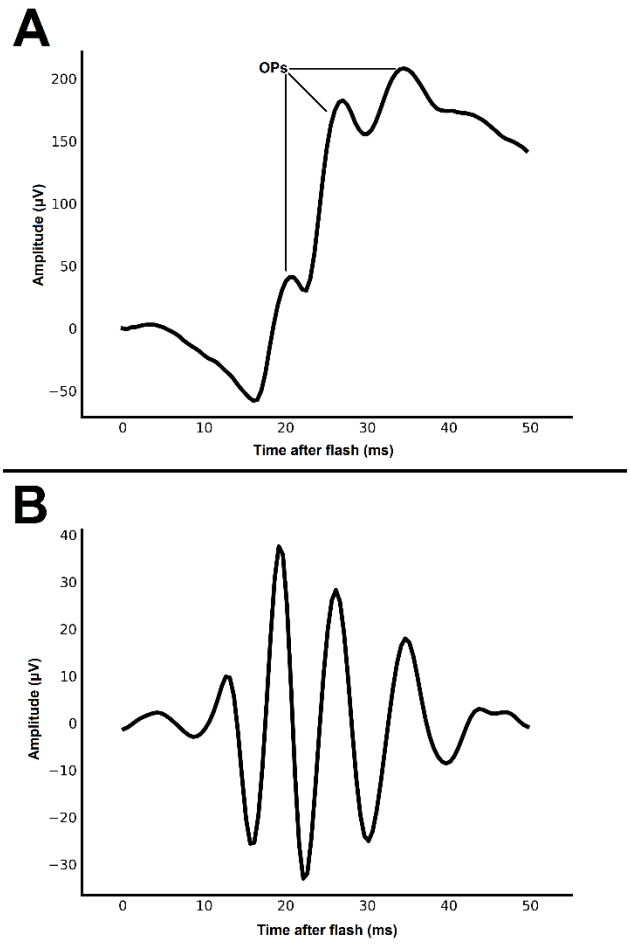


**Figure 2.3. Oscillatory potentials of a standard dark-adapted full-field flash ERG**

A. ERG in response to a -0.4 log cd.s/$m^2$ flash stimulus (see Figure 2.1B). OPs are denoted along the rising edge of the b-wave.

B. Isolated OPs were extracted using a $5^{th}$ order Butterworth filter to bandpass the signal from 75Hz to 300Hz.

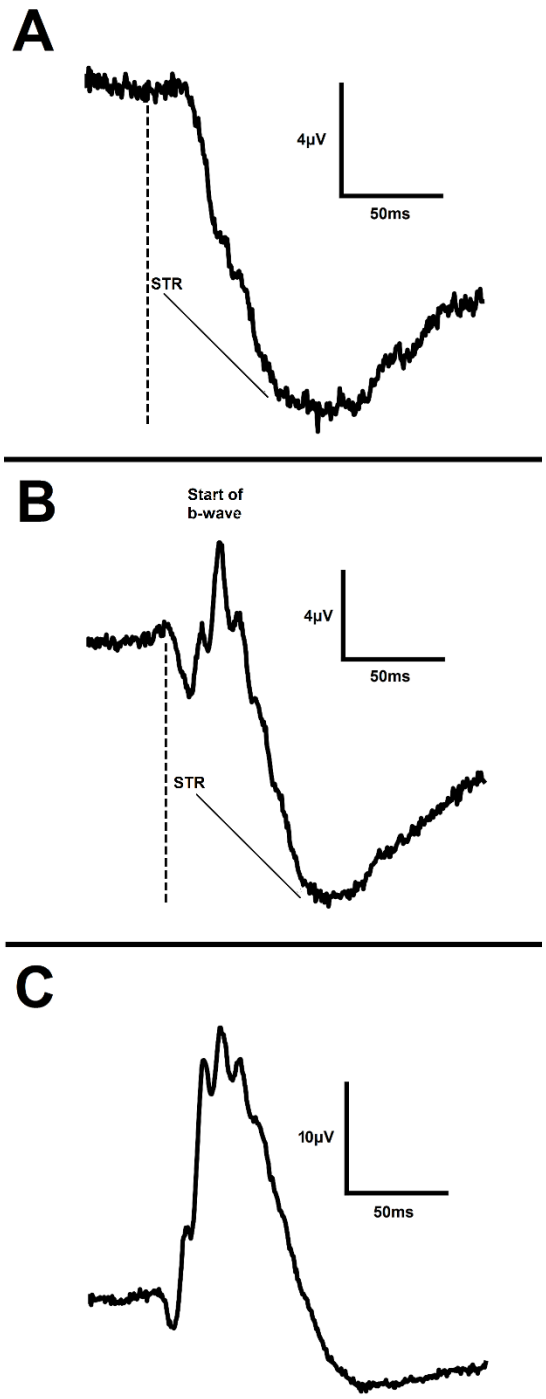


**Figure 2.4. STR visualized in standard dark-adapted full-field flash ERG**

A. ERG performed with a -3.7 log cd.s/$m^2$ flash stimulus, shown from flash onset. Compared to the a-wave, the STR occurs at substantially later times post-flash.

**Figure 2.4. (cont'd)**

B. ERG performed with a -3.2 log cd.s/$m^2$ flash stimulus in the same dog, shown from flash onset. The growing b-wave is shown superimposed on the descending slope of the STR.

C. ERG performed with a -2.8 log cd.s/$m^2$ flash stimulus in the same dog, shown from flash onset. The STR is mostly masked by the b-wave at the relatively dim stimulus shown here, although the initial downslope of the STR can be still seen and should not be mistaken for an a-wave which has a much higher threshold.

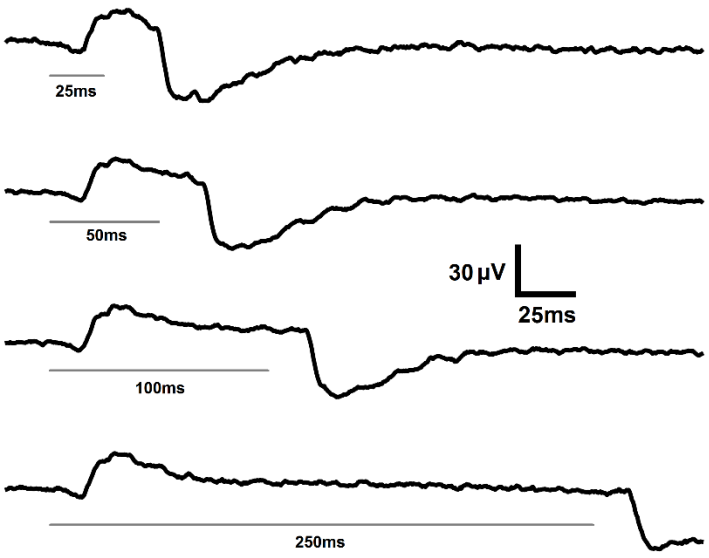


**Figure 2.5. Standard long-duration flash ERG from a normal dog**

ERG was performed with 3.1 log cd/m$^2$ flash stimulus on a rod-saturating 42 cd/m$^2$ background. Flash duration, from top to bottom, was 25ms, 50ms, 100ms, and 250ms, respectively. The grey lines indicate the duration of the light stimulus. The separation of the ON and OFF response become obvious. The off response in the dog may consist of a very small positive d-wave with a larger following negative component (as in series 4, 250ms flash duration).

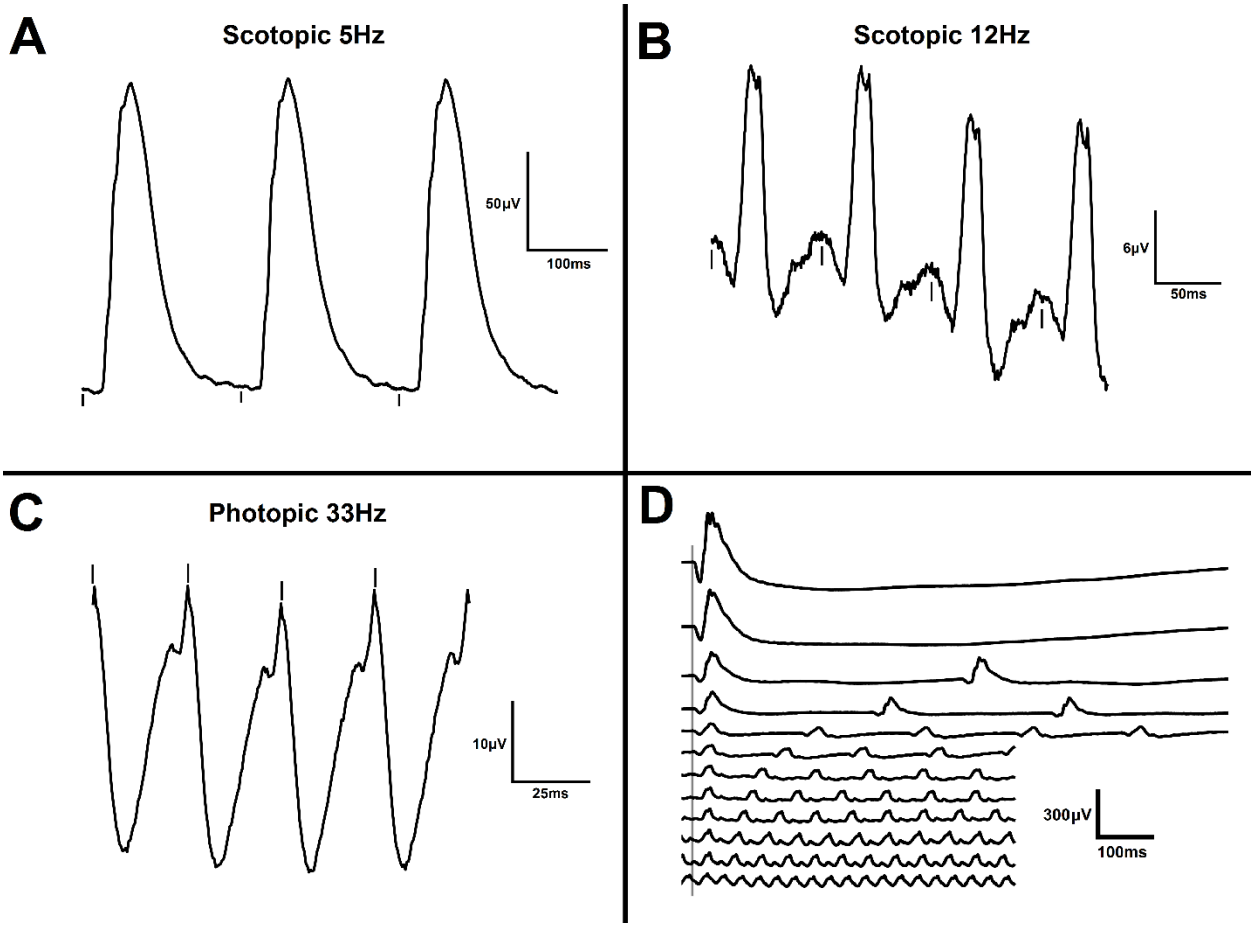


**Figure 2.6. Reponses from flicker ERG protocols performed in a normal dog**

A. Dark-adapted ERG of 5Hz flicker with 0.025 cd.s/$m^2$ stimulus strength. Low-frequency flickers have been shown to represent the contributions of Rod Bipolar cells.

B. Dark-adapted ERG of 12Hz flicker with 0.592 cd.s/$m^2$ stimulus strength. Mid-frequency flickers have been shown to mainly represent the contributions of Cone ON-Bipolar cells.

C. Light-adapted ERG of 33Hz flicker with 3.0 cd.s/$m^2$ stimulus strength (after 10 minutes of light adaptation to a rod suppressing 30 cd/$m^2$ background light). High-frequency flickers have been shown to mainly represent the contributions of Cone OFF-Bipolar cells.

D. Dark-adapted ERG flicker series with 3.2 cd.s/$m^2$ stimulus strength. Flickers ranged from 0.5Hz to 30Hz.

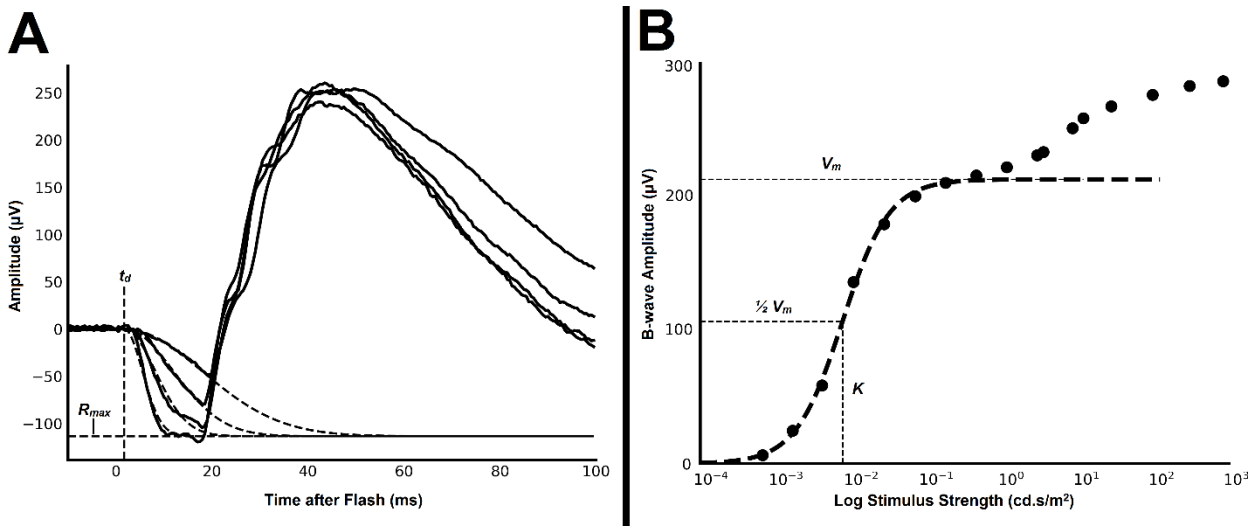


**Figure 2.7. Models of the a and b-waves**

A. Model of the leading edge of the rod a-wave, using the Hood & Birch adaptation of the Lamb & Pugh model (Hood & Birch 1990). Using a least-squares minimization algorithm, the equation

$$R = R_{max}\cdot(1-exp[-I\cdot S\cdot(t-t_d)^2])$$

was fit to flash stimuli ranging from -0.4 and 0.86 log cd.s/m$^2$. The amplitude $R$ is a function of the retinal luminance $I$ and time $t$ after the flash and $t_d$ is a brief delay. $S$ is a sensitivity factor and $R_{max}$ is the maximum amplitude of the response. For this dog, model parameters were $R_{max}$ = -113.4μV; $S$ = 1.976 log 1/(scotopic td · sec$^3$); $t_d$ = 1.69ms.

B. Naka-Rushton fitting of the dark-adapted b-wave amplitude $R$ plotted against stimulus strength $L$ by fitting the data to the equation

$$R/V_m = L^n/(L^n+K^n)$$

$V_m$ represents the maximum response amplitude of the first limb of the b-wave luminance:response plot, $K$ is a semi-saturation constant considered a measure of retinal sensitivity, and $n$ is a dimensionless constant dependent on of the slope of the plot at the position of $K$, which may reflect retinal homogeneity. For this dog, model parameters were $V_m$ = 213.0 μV; $K$ = -2.14 log cd.s/m$^2$; $n$ = 1.419.

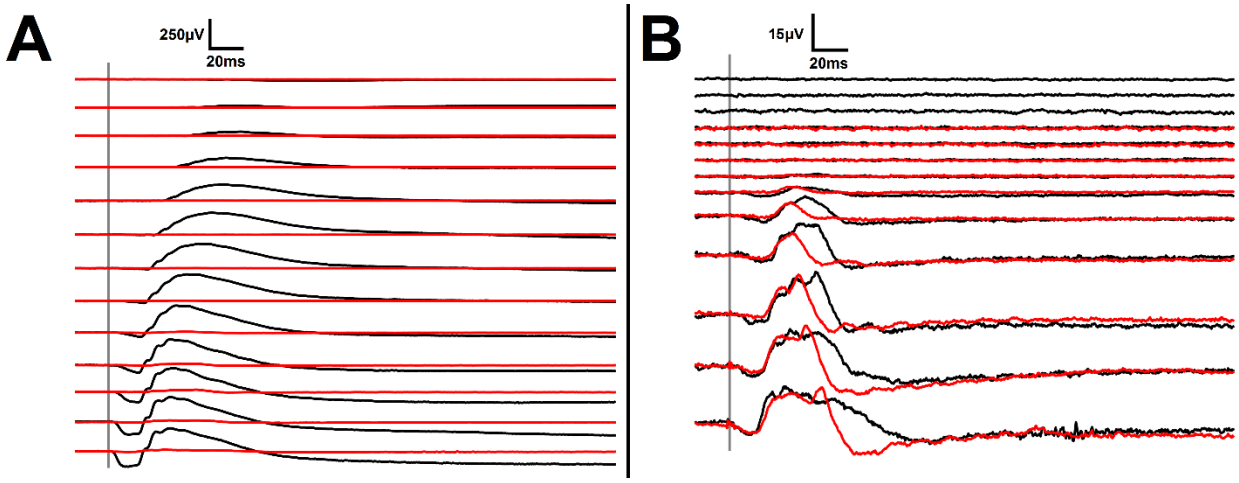


**Figure 2.8. Montages of a dark-adapted ERG series comparing responses from a normal dog and a *PDE6A*$^{-/-}$ dog which has a failure in rod phototransduction and lacks all rod ERG response**

A. Montage of a dark-adapted luminance series from a normal (black) and *PDE6A*$^{-/-}$ (red) dog at two months of age. Responses were elicited from a series of white flashes from -3.7 to 1.36 log cd.s/m$^2$. Note the markedly decreased responses in the affected dog, compared to the normal dog, at every recorded stimulus.

B. The dark- (black) and light-adapted (red) responses from the same *PDE6A*$^{-/-}$ dog show the low amplitude responses recorded. Responses are cone-driven, as dogs with this form of PRA completely lack rod function. The difference between the overlain waveforms represents the difference between dark- and light-adapted cones.

# CHAPTER 3.

# MATHEMATICAL MODELS AND TRANSFORMATIONS OF THE CANINE ERG: UTILITY IN ASSESSING ALTERED RETINAL FUNCTION IN DISEASE MODELS AND MONITORING OF RESPONSE TO TRANSLATABLE GENE AUGMENTATION THERAPY

### 3.1. Introduction

A model is defined as ‘a conceptual or mathematical representation of a system that serves to understand and quantify it’. In the biological sciences, mathematical models serve to take observational data and hypotheses and organize them into a quantifiable framework. Such parameterization of biological systems enables further study into the effects of changing both components of the model as well as environmental factors [162]. One of the earliest, and best known, biological models is the Michaelis-Menten equation used to describe enzyme kinetics [163]. The Gaussian function is another model that has applications across many disciplines, including the biological sciences.

In visual electrophysiology, mathematical models bridge the gap between the summed retinal electrical current flow to light stimulus as recorded at the corneal surface and the underlying molecular mechanisms that generate these currents [62,63]. By quantifying the sensitivity and amplitude responses of populations of retinal cells based on the biochemical processes that occur in single cells, these models accomplish several goals. They accurately establish response ranges in normal individuals and enable detection and direct comparisons of deviations from normal [53,164]. Moreover, the models aid in the determination of the underlying cause of dysfunction [23,62]. Additionally, they provide a succinct method of characterizing progression of retinal disease as well as potential improvements with gene augmentation therapy and other treatments [5,9].

Traditional single full-field flash electroretinographic (ERG) recordings use a limited number of stimuli in scotopic and photopic conditions to assess the health and function of the retina. These standard flashes provide a basis for global assessment of normal retinal function as well as detection and characterization of a variety of diseases, which makes them an invaluable

tool in both clinical and research ophthalmology [165]. However, further quantifiable information can be obtained through mathematical models and transformations of the recorded waveforms. Additional mathematical modeling of ERG waveforms, such as the Birch & Hood fit of the rod-driven a-wave [164], as well as frequency-domain transformations such as the discrete Fourier transform (DFT) [149], have seen limited use in analysis of canine ERGs. Mathematical models and transformations of the ERG a-wave and b-wave enable further characterization of the function of populations of retinal neurons in both wildtype dogs and those with inherited retinal degenerations [5,155].

In the models for rod and cone phototransduction (Eqs. 2-4 below), the *R* parameter quantifies the maximal photoreceptor response (the total circulating current of rod photoreceptors in the retina when recording in the dark adapted state, after subtraction of cone responses, and of cones when rod responses are suppressed with a background light) and reflects the population of healthy photoreceptors, while the *S* parameter quantifies the sensitivity of the a-wave response and reflects the speed of the biochemical reactions of phototransduction [15,18]. A reduction in the *R* parameter indicates reduced circulating current of the total population of photoreceptors, which may be caused by photoreceptor death, shortening of outer segments, or substantial alterations in membrane permeability. In contrast, a reduction in the *S* parameter suggests dysfunction in the biochemical reactions of phototransduction. In heterogeneous conditions such as retinitis pigmentosa, quantification of these parameters in both rods and cones can aid in characterizing the nature of retinal dysfunction as well as identify potential underlying pathology [21,62].

Photoreceptor signaling is a complex and unique process. In the dark, rods and cones maintain a relatively depolarized cell membrane due to influx of positive ions through cyclic

nucleotide-gated channels in outer segments in conjunction with active transport of cations out of the cells. In rods, the dark current refers to this electrical flow along the length of the photoreceptor [55,56]. Experimentally, when exposed to a light stimulus of progressively increasing strength (thus closing increasing proportions of cyclic nucleotide gated channels and hyperpolarizing the cell), the increase in normalized rod photocurrent is described by the Lamb & Pugh equation:

$$F(t)=1-exp(-1/2*\Phi*(t-t_{eff}/t_{\Phi})^2)=exp(-1/2*\Phi*A*(t-t_{eff})^2) \qquad \text{(Equation 1)}$$

$T_{eff}$ is the sum of the brief delays in amplification, $\Phi$ represents the number of photoisomerizations of rhodopsin per rod (a function of flash strength), and A is the amplification constant of phototransduction – this encompasses the events beginning with photons activating rhodopsin and ultimately resulting in cyclic nucleotide channel closure and a cessation of positive inward current, known as the dark current. These parameters represent the sensitivity of individual rods and impact the latency of response. Saturation kinetics explain the rate of current change as a function of time and flash stimulus strength, but in terms of a single photoreceptor [21,62,63].

To adapt the equation to represent the response of the massed retinal photoreceptors Birch & Hood developed the following equation for the leading edge of the rod a-wave:

$$R(I,t)=(1-\exp[-I\cdot S\cdot(t-t_d)^2])\cdot R_{max} \quad for\ t>t_d \qquad \text{(Equation 2)}$$

The amplitude $R$ is a function of the retinal luminance $I$ and time $t$ after the flash and $t_d$ is a brief delay. $S$ is a sensitivity factor and $R_{max}$ is the maximum amplitude of the response. This model takes the experimentally validated equation for normalized photocurrent and multiplies it by the amplitude parameter $R_{max}$ [23,164].

Two different equations, described by Birch & Hood [15], have been used to successfully characterize the human cone a-wave:

$$R(I, t) = (\{1-\exp[-I\cdot \mathbf{S}\cdot(t-t_d)^2]\}\cdot R_{mp_3})^{*}exp(-t/\tau) \text{ for } t>t_d \qquad \text{(Equation 3)}$$

The equation fits the same parameters as that of the rod-driven a-wave and convolves the function ($^{*}$ denotes convolution function) with a negative exponential function, where $\tau$ is the time constant of the RC (lowpass) filter. Given the technical difficulties in model construction and fit of the convolution function, and the observation that the model typically approximates semi-saturation kinetics, this function has been simplified to:

$$R(I,t)=(I\cdot S_c\cdot(t-t_d)^3)/(I\cdot S_c\cdot(t-t_d)^3+1)\cdot R_{mp_3} \text{ for } t>t_d \qquad \text{(Equation 4)}$$

The amplitude $R$ is a function of the retinal luminance $I$ and time $t$ after the flash and $t_d$ is a brief delay. $S$ ($S_c$ in the simplified model) is a sensitivity factor and $R_{mp_3}$ is the maximum amplitude of the response.

The equations used to model the rod- and cone-driven a-wave are derived from the biochemical events of a single photoreceptor that are subsequently applied to a population of cells. An older model, Naka-Rushton fitting, is used to model the ON-bipolar cell-driven dark-adapted b-wave [75]. This requires measurement of dark-adapted b-wave amplitudes, which are subsequently plotted against stimulus strength. This model provides insight into the second order cells that contribute to the visual response.

$$R/V_m = L^n/(L^n+K^n) \qquad \text{(Equation 5)}$$

$V_m$ represents the maximum response amplitude of the first limb of the b-wave luminance:response plot, K is a semi-saturation constant considered a measure of retinal sensitivity, and n is dependent on of the slope of the plot at the position of K, which may reflect retinal homogeneity [139,166,167].

In addition to mathematical models of specific ERG waveforms, further analysis of both ISCEV/ECVO standard flashes as well as expanded protocols can be performed through frequency-domain transformations of standard recordings [1,13]. Typical ERG analysis occurs in the time domain (TD) only, measuring the electrical response of the retina to a series of light flashes of varying stimulus strength. While measurements made from this information can provide crucial information about the health of various components of retinal function, including fits of mathematical models to components of the ERG waveform, they fail to provide potentially useful information about the differing frequency components of the retinal response. The Fourier transform is the most obvious method of analyzing frequency domain (FD) information contained in a signal. This analysis can be extended to wavelet transforms such as the discrete wavelet transform (DWT), which is a compromise between TD and FD analysis. Although few studies have investigated the application of these methods, several recent reports found that different populations of retinal cells make different frequency contributions to the human ERG and suggest that these contributions vary significantly between normal subjects and those with retinal dystrophy [148,149].

Dogs homozygous for a *PDE6A* null mutation were used to assess cone only response with almost no active rod interaction. Cone ERG a-waves are slightly reduced in young affected dogs while cone b-wave is not significantly altered in young dogs. They do progressively lose cone ERGs over the first 12 months of age, and so ERGs must be recorded at a young age to assess cone-only function [159]. Given the early and severe course of the disease, treatment in affected dogs must occur at a young age. Successful treatment has been implemented via gene augmentation therapy using adeno-associated virus (AAV). This treatment restores rod function and preserves both rod and cone photoreceptors [9].

A mutation in the *CNGB1* gene causes an autosomal recessive form of inherited retinal dystrophy in dogs, with early decrease in rod function and relatively preserved cone vision. Vision loss in this disease is much slower than in *PDE6A* mutant dogs. Although there is a reduction in rod a and b-wave amplitudes, dark-adapted ERGs recorded at a young age demonstrate desensitized residual rod responses, with considerably elevated scotopic b-wave threshold compared to wildtype dogs [unpublished data]. The residual rod response is slower than normal response and slowly diminishes with age [152]. *CNGB1* AAV-mediated gene augmentation therapy restores dark-adapted vision and results in long-term preservation of rod function [5].

The purpose of this paper is to assess the applicability of mathematical models of ERG waveforms in normal dogs and those with retinal disease, that are important models of human retinal disease such as retinitis pigmentosa. Additionally, we assess the strength of potential linear and predictive relationships between the models through correlation and regression analysis. As previously stated, time-domain analysis of a limited number of flashes provides substantial information about retinal function within the time constraints often present in the clinical setting. However, relatively limited expansion of the number of ERG flashes greatly increases the potential to fit models and perform frequency-domain analysis. Here, we discuss several established mathematical models of ERG waveforms and their application to normal dogs and those with retinal dysfunction, as well as an overview of frequency-based analysis with a potential application of the DFT to assessing signal and noise in ERG recordings.

## 3.2. Materials and Methods

### Ethics Statement

All procedures were performed in accordance with the ARVO statement for the Use of Animals in Ophthalmic and Vision Research and approved by the Michigan State University Institutional Animal Care and Use Committee.

### Animals

Purpose bred *PDE6A*$^{-/-}$, *CNGB1*$^{-/-}$, and unaffected dogs maintained in a colony at Michigan State University were investigated in this study. They were housed under 12hr:12hr light:dark cycles. 11 phenotypically normal adult (> 2 months of age) beagle and beagle crosses were included in the study. *CNGB1*$^{-/-}$ dogs included both 11 untreated animals and 4 young dogs (between 15-22 weeks of age) who received a single subretinal injection of the recombinant AAV2/5 vector with the canine *CNGB1* cDNA controlled by a human G protein–coupled receptor kinase 1 (*GRK1*) promoter (AAV5-*hGRK1-cCngb1*) [5]. Untreated dogs were tested at a young age (1-3 months), which is prior to loss of cone function and at which time there is a desensitized residual rod response. *PDE6A*$^{-/-}$ dogs included both 10 untreated animals and 6 young dogs (between 4-8 weeks of age) who received a single subretinal injection of an adeno-associated viral vector serotype 2/8 delivering human *PDE6A* cDNA under control of a human rhodopsin promoter (AAV8-*hRHO-hPDE6A*) [9]. Untreated dogs were tested at a young age (1-3 months), which is while they have well preserved cone function and little to no rod response. Treated dogs were tested between 1 and 9 months following gene therapy.

*Methods*

Dogs were induced (by isoflurane mask for puppies and by IV propofol for older animals), intubated, and subsequently maintained under anesthesia

with isoflurane (IsoFlo, Abbott Laboratories, North Chicago, IL, USA) [between 2-3.5% in a 1-2L/min oxygen flow via a rebreathing circle system for dog over 10 kg and via a Bain system for dog under 10 kg].

**Electroretinography (ERG)**

Electroretinograms were recorded as previously described [168]. Specific apparatuses are noted below. Briefly, dogs were dark-adapted for one hour and pupils dilated with tropicamide (Tropicamide Ophthalmic Solution UPS 1%, Falcon Pharmaceuticals Ltd., Fort Worth, TX, USA). A gold-ringed electrode contact lens (ERG-Jet electrode, Fabrinal Eye Care, La Chaux-De-Fonds, CH) was used and for reference and grounding platinum needle skin electrodes (Grass Technologies, Warwick, RI, USA) were placed 5mm lateral to the lateral canthus and over the occiput, respectively. ERGs were recorded using an Espion $E^2$ Electrophysiology system with ColorDome Ganzfeld (Diagnosys LLC, Lowell, MA).

**White Flash ERG**

For low strength stimuli, each flash was presented at one second intervals, and repeated to generate an averaged response detectable against background electrical noise. As stimulus strength was increased the time between flashes was lengthened to prevent light-adaptation of rod photopigment. After completion of the dark-adapted flashes, the animal was light-adapted (exposed to continuous, bright white light at 30 cd/$m^2$) for 10 minutes to suppress rod responses, and the trials repeated in the light-adapted eye.

**Curve fitting**

Calculation of model parameters was performed using the *lmfit* curve-fitting program in the Python 3.6 environment. This calculation uses the Levenberg-Marquardt algorithm to calculate optimal parameter values via least squares minimization [169].

Briefly, the residual of a model fit is defined as the difference between the value of the dependent variable of the actual data and the value predicted by the model:

$$r_i = y_i - f(x_i,\beta)$$

Where $r_i$ denotes the value of the residual $r$ at data point $i$, $y_i$ is the value of dependent variable, and $f(\boldsymbol{X}_i,\boldsymbol{\beta})$ is the model function $f$ with independent variables $\boldsymbol{X}$ and model parameters $\boldsymbol{\beta}$. Least squares minimization calculates optimal model parameters $\boldsymbol{\beta}$ through minimizing the sum of the square of the residuals $S$ [170]:

$$S = \sum_{i=1}^{n} r_i^2$$

The Levenberg-Marquardt algorithm is an iterative process that begins with estimates of the function parameters $\boldsymbol{\beta}$ [171,172]. As the accuracy of the model depends in part on choice of initial parameters, reasonable approximations were used for each model fit based on preliminary fits in control dogs. For example, for the rod-driven a-wave model, initial parameters were set at $t_d$ = 3, log S = 2, and $R_{max}$ = a-wave amplitude for stimulus strength $I$. These parameters are replaced by $\boldsymbol{\beta}+\boldsymbol{\delta}$ and a linear approximation of the function:

$$f(\boldsymbol{X}_i,\boldsymbol{\beta}+\boldsymbol{\delta}) \approx f(\boldsymbol{X}_i,\boldsymbol{\beta}) + \mathbf{J}_i\,\boldsymbol{\delta}$$

Where $\mathbf{J}_i$ is the gradient of $f$ with respect to $\boldsymbol{\beta}$. Successive calculation of the parameter $\boldsymbol{\delta}$ that minimizes the sum of square of the residuals $S$ is performed computationally until final model parameters are obtained.

Model goodness-of-fit is determined by the least-squares parameter, with values less than 0.25 considered a good fit [164]:

$$lsq = \frac{\sum_{i=1}^{n}(y_i - f(X_I, \boldsymbol{\beta}))^2}{\sum_{i=1}^{n}(y_i - mean(y))^2}$$

Goodness-of-fit can also be assessed with the $R^2$ parameter, defined as:

$$R^2 = 1 - \frac{variance(residual)}{variance(data)}$$

$R^2$ varies from 0 to 1, with values near 1 indicating a better fit.

**Mathematical Models**

**Flash Stimuli**

In several older ERGs, the ISCEV standard flashes of 0.48 and 1.0 were substituted with 0.4 and 0.86 log cd.s/m$^2$, respectively. All newer ERG protocols included both sets of stimuli. We determined that using either set of stimuli yields virtually identical model fits. Although we used the 0.4 and 0.86 log cd.s/m$^2$ stimuli for consistency in comparing model parameters, either set may be used and considered interchangeable.

**Rod-driven a-wave**

For determination of model parameters for the rod-driven a-wave (Eq. 2), we restricted our initial analysis to flashes ranging in strength from -1.6 to 1.4 log cd.s/m$^2$. For our calculations, model parameters were calculated after subtracting photopically matched ERG waveforms.

**Cone-driven a-wave**

For determination of model parameters for the cone-driven a-wave (Eqs. 3 & 4), we restricted our initial analysis to photopic ERG flashes ranging in strength from 0 to 1.4 log cd.s/m$^2$. We attempted to fit both models to recorded waveforms in order to determine which provided the best fit.

**Naka-Rushton b-wave fitting**

Amplitudes were measured from the trough of the preceding a-wave to the peak of the following b-wave, accounting for OP intrusion along the leading edge of the b-wave. Model parameters were calculated by fitting the Naka-Rushton function to the first limb of the

luminance:response plot from flash stimuli ranging from -3.2 to 0 log cd.s/m$^2$ (Eq. 5), whose maximum value was assessed through visual assessment of this plot. Although the stimulus eliciting the maximal ($V_m$) response varied somewhat between different subjects, in normal dogs it typically fell between -1 and 0 log cd.s/m$^2$ flash stimulus.

**Significance calculations**

All variables were assessed for homoscedasticity using the Breusch-Pagan test, and for normality using the Shapiro-Wilks test, prior to calculation of the t-statistic using the independent t-test and the F-statistic using the F-test of the linear mixed effects model (LME). An LME model was employed utilizing the Statsmodels package in Python to examine statistical significance of serial ERGs performed in dogs treated with gene augmentation therapy, as well correlations between model parameters in all dogs, fitting the following equation:

$$Y_{ij} = \beta_0 + \beta_1 X_{ij} + \gamma_i + \varepsilon_{ij}$$

$Y_{ij}$ is the $j^{th}$ measured response for subject $i$, $X_{ij}$ is the covariate for this response, $\gamma_i$ is the random effects parameter for subject $i$, and $\varepsilon_{ij}$ is the error parameter for this response. $\beta_0$ and $\beta_1$ are fixed effect parameters for all subjects, corresponding to intercept and slope, respectively, and are fit according to the restricted maximum likelihood (REML) optimized with the Broyden-Fletcher-Goldfarb-Shanno (BFGS) algorithm [173].

**Frequency-domain analysis**

Let $x_0, \ldots, x_{N-1}$ be complex numbers. The DFT is defined by the formula [174]:

$$X_k = \sum_{n=0}^{N-1} x_n \, e^{-i2\pi kn/N} \qquad k = 0, \ldots, N-1$$

Where $e^{i2\pi/N}$ is a primitive $N$th root of 1.

With real input, the algorithm satisfies the symmetry:

$$X_{N-k} = X_k^*$$

Given a real signal *y* of length *N* and bandwidth frequency *f*, the DFT

$$\frac{2}{N} abs(DFT(y))^2$$

yields power spectral density data from *0Hz* to *f/2* with *N/2* bins of length *f/N*, with amplitude normalized to the number of frequency bins. For our recordings, a typical single flash ERG is recorded at bandwidth 2,000Hz from *t=-20ms* to *t=299.5ms* for a signal length of 640. Therefore, the DFT of a standard signal yields power spectral density (PSD) from *0-1000Hz*, with 320 bins of length 3.125Hz each.

The power of specific frequency bands can be calculated by integrating the PSD function over the desired minimum and maximum frequency. As the function is discrete, the integral can be approximated by calculating the area under the curve using the trapezoidal rule [175]:

$$\int_a^b f(x)dx \approx \frac{\Delta x}{2} \sum_{k=1}^{N} (f(x_{k-1}) + f(x_k))$$

Given a signal cutoff of 200Hz (chosen to include the higher frequency OPs centered ~160Hz but exclude higher frequency noise), this rule can be used to calculate the 'signal' power by integrating between 0-200Hz, and the 'noise' power from 200-1000Hz. The signal-to-noise ratio calculated using PSD is given by:

$$SNR = \frac{P_{Signal}}{P_{Noise}}$$

Additional information can be calculated using the PSD, such as subsets of the 'signal' power (e.g. OP power, integrating between 75-200Hz) [13,176].

### 3.3. Results

**The Birch & Hood adaptation of the Lamb & Pugh rod-driven a-wave model (Figures 3.1-3.3).**

As assessed by both the *lsq* and $R^2$ parameters, the model provided an excellent fit in the 12 eyes of 6 phenotypically normal adult dogs assessed in this study. Several examples of the model are shown with fit parameters (Figure 3.1). Additionally, we applied the model to multiple combinations of stimulus strengths to optimize recording protocols, as well as assess the utility of using ISCEV standard flashes as the basis for calculation of model parameters.

We originally used 8 flashes for calculation of model parameters: -1.6, -1.2, -0.8, -0.4, 0, 0.4, 0.86, and 1.4 log cd.s/$m^2$. Examination of different combinations of flashes with an emphasis on minimizing number of required flashes demonstrated that utilizing four stimuli - -0.4, 0, 0.4, and 0.86 log cd.s/$m^2$ – yielded extremely similar fits. Testing the ISCEV standard flashes of 0.48 and 1.0 provided similar fits, albeit with slight overestimation of both the time delay parameter $t_d$ and the sensitivity parameter log *S* compared to using additional dimmer stimuli (See Table 3.1).

Using the four stimuli established in the previous section, we calculated average model parameters for 14 eyes of 7 *CNGB1*$^{-/-}$ affected dogs and four eyes of *CNGB1*$^{-/-}$ affected dogs treated with AAV gene therapy (Figure 3.2). In the *CNGB1*$^{-/-}$ dogs, comparison of model parameters in untreated dogs to ERGs performed between 1- and 9-months post-treatment showed a significant increase in both $R_{max}$ and *S* parameters following treatment. Model parameters in these dogs were log $R_{max}$ (untreated = 0.881 ± 0.288 µV, treated = 1.539 ± 0.26 µV), $t_d$ (untreated = 2.169 ± 1.427 mSec, treated = 2.054 ± 0.89 mSec), and log *S* (untreated = 1.507 ± 0.297 1/(cd/$m^2$ $s^3$), treated = 1.939 ± 0.099 1/(cd/$m^2$ $s^3$)). Both log $R_{max}$ (2-tailed

independent t-test; t=8.95, p=1.3x10$^{-8}$) and log *S* (2-tailed independent t-test; t=5.75, p=1.04x10$^{-5}$) values were significantly smaller in *CNGB1*$^{-/-}$ affected dogs compared to normal dogs, and both log $R_{max}$ (LME F-test; F=6.04, p=1.54x10$^{-9}$) and log *S* (LME F-test; F=9.28, p=1.66x10$^{-20}$) values were significantly increased in the gene augmentation therapy treated eyes.

Similarly, average model parameters for 17 eyes of 11 *PDE6A*$^{-/-}$ untreated and 6 eyes of *PDE6A*$^{-/-}$ affected dogs treated with AAV gene therapy dogs were calculated (Figure 3.3). A comparison of model parameters in pre-treatment to ERGs performed between 1- and 24-months post-treatment showed a significant increase in both $R_{max}$ and S parameters following treatment. Model parameters were log $R_{max}$ (untreated = 0.471 ± 0.164 µV, treated = 1.02 ± 0.122 µV), $t_d$ (untreated = 1.784 ± 1.539 mSec, treated = 1.599 ± 1. 066) and log *S* (untreated = 1.547 ± 0.291 1/(cd/m$^2$ s$^3$), treated = 1.875 ± 0.284 1/(cd/m$^2$ s$^3$)). Both log $R_{max}$ (2-tailed independent t-test; t=11.70, p=7.3x10$^{-12}$) and log S (2-tailed independent t-test; t=5.79, p=4.25x10$^{-6}$) values were significantly smaller in *PDE6A*$^{-/-}$ affected dogs compared to normal dogs, and both log $R_{max}$ (LME F-test; F=8.70, p=3.35x10$^{-18}$) and log *S* (LME F-test; F=3.49, p=4.82x10$^{-4}$) values were significantly increased post-treatment.

**Cone-driven a-wave model (Figures 3.4-3.5).**

We first attempted to fit the simplified model presented by Birch & Hood (Eq. 4). Examination of different combinations of flashes with an emphasis on minimizing number of required flashes demonstrated that utilizing four stimuli - 0, 0.4, and 0.86, and 1.4 log cd.s/m$^2$ – yielded excellent fits, with log $R_{mp_3}$ = 1.039 ± 0.140 µV, $t_d$ = 0.062 ± 0.145 mSec, log $S_c$ = 3.510 ± 0.128 1/(cd/m$^2$ s$^3$). Using only ISCEV standard flashes of 0.48 and 1.0 log cd.s/m$^2$ yielded parameters of log $R_{mp_3}$ = 0.998 ± 0.157 µV, $t_d$ = 0.080 ± 0.158 mSec, log $S_c$ = 3.650 ± 0.196 1/(cd/m$^2$ s$^3$), suggesting that these flashes reasonably approximate model parameters, although

compared to using additional stimuli may slightly underestimate the log $R_{mp_3}$ parameter and overestimate the log $S_c$ parameter (Figure 3.4).

In 10 eyes of 6 young (< 3 months of age) *PDE6A*$^{-/-}$ affected dogs, parameters were log $R_{mp_3}$ = 0.744 ± 0.133 µV, $t_d$ = 0.233 ± 0.555 mSec, log $S_c$ = 3.548 ± 0.247 1/(cd/m$^2$ s$^3$). Similarly, in 14 eyes of 8 young (< 3 months of age) *CNGB1*$^{-/-}$ affected dogs, parameters were log $R_{mp_3}$ = 0.886 ± 0.236 µV, $t_d$ = 0.003 ± 0.012 mSec, log $S_c$ = 3.582 ± 0.183 1/(cd/m$^2$ s$^3$). The only significant difference between normal and affected dogs was a smaller log $R_{mp_3}$ value was in *PDE6A*$^{-/-}$ animals (2-tailed independent t-test; t=2.74, p=0.01) (Figure 3.5).

Whereas the simplified model provided good fits (*lsq* < 0.25) to the cone-driven a-wave in normal dogs in addition to young dogs with inherited retinal dystrophy, the original model (Eq. 3) was more difficult to fit and tended to provide worse fits to the waveforms. The model was sensitive to, and often distorted by, noisier signals and those with slight deviations from baseline. However, careful fitting enabled characterization of the photopic ERGs recorded in normal dogs. Using the three highest-strength stimuli determined for the simplified model, parameters were calculated as log $R_{mp_3}$ = 1.074 ± 0.213 µV, $t_d$ = 0.138 ± 0.236 mSec, log $S$ = 1.312 ± 0.154 1/(cd/m$^2$ s$^3$). These parameters agree with those determined by the simplified model (note that the log $S_c$ value is ~2 log units above the log $S$ value, similar to the difference reported in humans) [15].

**Naka-Rushton fits to b-wave amplitudes (Figures 3.6-3.7)**

After measurement of dark-adapted ERG b-wave amplitudes, the Naka-Rushton model was applied to luminance:response dark-adapted ERGs recorded in 6 normal adult dogs. The *lsq* and $R^2$ parameters both confirmed excellent fits of this equation, indicating that the first limb of the dark-adapted b-wave amplitudes in normal canine ERGs is well approximated by a semi-

saturation type function. Furthermore, calculation of model parameters provided normal data to compare against ERGs recorded from dogs with inherited retinal dystrophy. Model parameters were calculated as log $V_m$ = 2.159 ± 0.193 µV, log K = -2.4 ± 0.17 cd.s/m$^2$, n = 1.355 ± 0.194.

Following successful application of the Naka-Rushton function to dark-adapted ERGs in normal dogs, we calculated average model parameters 11 eyes of 7 *CNGB1*$^{-/-}$ affected dogs and four eyes of *CNGB1*$^{-/-}$ affected dogs treated with AAV gene therapy. Model parameters in these dogs were log $V_m$ (untreated = 1.869 ± 0.29 µV, treated = 1.820 ± 0.211 µV), log K (untreated = 0.063 ± 0.262 cd.s/m$^2$, treated = -2.184 ± 0.296 cd.s/m$^2$), and n (untreated = 1.162 ± 0.258, treated = 1.327 ± 0.213). All three parameters log $V_m$ (2-tailed independent t-test; t=2.63, p=0.016), log K (2-tailed independent t-test; t=7.06, p=5.7x10$^{-7}$), and n (2-tailed independent t-test; t=2.25, p=0.035) values were significantly different in affected dogs compared to normal controls. Comparing treated *CNGB1*$^{-/-}$ dogs to untreated controls, only the log K (LME F-test; t=13.0, p=1.24x10$^{-38}$) was significantly increased post-treatment.

Additionally, we successfully applied the model to 17 eyes of 10 *PDE6A*$^{-/-}$ untreated dogs and 6 eyes of *PDE6A*$^{-/-}$ affected dogs treated with AAV gene therapy. Model parameters in these dogs were log $V_m$ (untreated = 1.283 ± 0.21 µV, treated = 1.659 ± 0.211 µV), log K (untreated = -0.57 ± 0.591 cd.s/m$^2$, treated = -2.333 ± 0.419 cd.s/m$^2$), and n (untreated = 1.054 ± 0.232, treated = 1.475 ± 0.356). All three parameters log $V_m$ (2-tailed independent t-test; t=8.59, p=8.59x10$^{-9}$), log K (2-tailed independent t-test; t=4.48, p=1.33x10$^{-4}$), and n (2-tailed independent t-test; t=3.93, p=5.62x10$^{-4}$) values were significantly different in affected dogs compared to normal controls, with significantly decreased log $V_m$ and n values and a substantially increased log K parameter. Furthermore, significant increases in log $V_m$ and n and a decrease in log K were seen in treated *PDE6A* dogs compared to untreated dogs, with log $V_m$

(LME F-test; F=4.23, p=2.32x$10^{-5}$), log K (LME F-test; F-test; F=11.73, p=9.28x$10^{-32}$), and n (LME F-test; F t=2.0, p=0.046).

We attempted to correlate both amplitude and sensitivity parameters between the previously tested waveform-fitting mathematical models. The strongest, and only consistent, correlation was found between the rod-driven a-wave parameter $R_{max}$ and the Naka-Rushton value $V_m$ (Table 3.2). Given that these parameters reflect the healthy population of rod photoreceptors and rod bipolar cells, respectively, this finding is unsurprising in normal dogs.

When comparisons were made in *CNGB1*$^{-/-}$ and *PDE6A*$^{-/-}$ dogs, both untreated and post-gene therapy treatment, we observed a strong correlation in both groups between the log $V_m$ and log $R_{max}$ values. The linear fit is shifted right in the treated groups, which may reflect the increased population of functional rod photoreceptors. Additionally, the slope is somewhat increased in the *CNGB1*$^{-/-}$ treated dogs and substantially increased in the *PDE6A*$^{-/-}$ which may reflect improved signaling between rod photoreceptors and bipolar cells. Specifically, *CNGB1*$^{-/-}$ treated dogs showed the most significant improvement in rod sensitivity parameters, whereas *PDE6A*$^{-/-}$ treated dogs demonstrated substantial improvement in both rod amplitude and sensitivity parameters (Figure 3.7).

**Frequency-based approaches to the ERG (Figures 3.8-3.10 & Supplemental Figure 3.S1).**

One potential application of frequency domain transformation is the analysis of specific subsets of the ERG signal. To demonstrate this utility, we first applied the DFT to signals from a photopic ERG recorded from a normal dog. We then applied this method to a dark-adapted ERG recorded from a *CNGB1*$^{-/-}$ dog both pre- and 9 months post-gene augmentation therapy treatment (Figure 3.8). We then calculated the power in the OP band by integrating the transform over the frequency range as defined in the Methods. The total power contained in the signal was 5.564 log

$\mu V^2$ prior to treatment and 6.561 log $\mu V^2$ post-treatment, indicating the total signal power increased by an order of magnitude following treatment. Similarly, the power of the OP band was 3.565 log $\mu V^2$ prior to treatment and 4.558 log $\mu V^2$ post-treatment, which suggests that the power gain in this subset was similar to the overall gain. Moreover, the power contribution of the OP band to the overall signal is roughly 1% both pre- and post-treatment.

Another application of the DFT is analysis of signal quality, as defined by SNR. We demonstrate this utility by comparing recordings obtained in the same normal dog – one from a single sweep, and the other from the average of 25 sweeps. In the single sweep signal, calculated values were $P_{signal}$ = 181,315.5 $\mu V^2$, $P_{noise}$ = 1,706.89 $\mu V^2$, and SNR = 106.2. In the averaged signal, calculated values were $P_{signal}$ = 164,333.6 $\mu V^2$, $P_{noise}$ = 76.49 $\mu V^2$, and SNR = 2148.7. Thus, averaging multiple trials slightly reduced the signal power but substantially decreased noise power, resulting in a 20x improvement in SNR. This method provides a utility for quantification of signal quality, which can be used in determination of optimal sweeps needed for signal average (Figure 3.9).

Following the method outlined by Gauvin et al. in humans [148,149], we applied discrete wavelet transform (DWT) analysis to a normal adult dog and a *CNGB1*$^{-/-}$ dog treated with gene augmentation therapy (Figure 3.10). In the pre-treatment comparison, there were substantial differences in every frequency component, but a particularly striking difference in the a-wave 20Hz and 40Hz components. Similarly, the post-treatment ERGs demonstrated a sustained increase in every frequency component, with a notable increase in the a-wave components and the 40Hz b-wave component.

### 3.4. Discussion

In this study, we showed that mathematical models of the rod- and cone-driven a-waves, and the ON-bipolar cell driven b-wave, are suitable for use in fitting normal canine ERGs. Furthermore, we demonstrated that the parameters derived from normal dogs accurately characterize the dysfunction in two models of retinitis pigmentosa. We also quantified recovery of retinal function by comparing model parameters before and after gene augmentation therapy treatment. Finally, we showed that frequency-domain approaches of ERG analysis, including Fourier and wavelet transforms, can be used to investigate disease related abnormalities as well as showing recovery of response with gene therapy.

The rod a-wave model (Eq. 2) provides an excellent fit to normal dogs. We determined that the rod-driven a-wave can be fit optimally using 4 stimuli strengths. Both clinical and research ophthalmologists could easily add the two additional flashes at -0.4 and 0.0 log cd.s/$m^2$ into normal ISCEV protocols for the purpose of a-wave fitting. Furthermore, the model provides good fits when calculated solely with ISCEV standard flashes, although this method may overestimate the sensitivity parameter *S*. Thus, inclusion of the two weaker flash stimuli is recommended for optimal model fit.

Although reductions in rod function make it more technically challenging to fit the a-wave model to recordings from dogs with inherited retinal dystrophy, we successfully applied the model to multiple dogs with the *CNGB1*$^{-/-}$ and *PDE6A*$^{-/-}$gene mutations, respectively, at early stages in the disease process (< 3 months of age). In *PDE6A* dogs the model parameters for the rod-driven a-wave (following photopic subtraction) may reflect a difference in dark- and light-adapted cones, or possibly a very small rod response – however, the purpose of measuring parameters in these dogs was to provide a baseline for quantification of rod function following

gene augmentation therapy treatment. This model provides an additional method of quantifying rod-driven responses and may enhance diagnosis and characterization of retinal disease. These quantitative results enable a direct comparison with normal dogs, in addition to providing baseline values to assess disease progression. Furthermore, calculation of model parameters provides a succinct, accurate assessment of both disease progression as well as effects of gene therapy treatment.

Although more difficult to apply than the rod-driven a-wave model, we were able to successfully fit both the original (Eq. 3) and simplified (Eq. 4) versions of the cone-driven a-wave model to normal dogs and dogs with inherited retinal dystrophy. Given the technical difficulty in applying the original model, we recommend using the simplified function as it provides good fits and is easier to implement. Furthermore, the model can be reasonably approximated using only 0.48 and 1.0 log cd.s/$m^2$ flashes, potentially providing a useful tool for assessment of cone function when the number of different stimuli is limited. We were able to use the model to successfully characterize cone photoreceptor kinetics in normal dogs, as well as establish the presence of relatively normal cone photoreceptors in two established models of retinitis pigmentosa dystrophy in young dogs prior to the secondary loss of cones.

Several factors make a generalized model of the cone-driven a-wave difficult to implement, even in normal dogs. One of these are the generally low-amplitude responses recorded in normal dogs, especially compared to those recorded in other species such as humans [12,177]. Therefore, increased noise or large deviations from baseline can significantly alter low amplitude recordings and reduce model goodness-of-fit. Another consideration that complicates the application of a generalizable model to the cone-driven a-wave are substantial postreceptoral contributions to the photopic a-wave, although this is likely mitigated through the use of stronger

stimuli and using the initial slope of the a-wave in calculation of model parameters [40,66]. Nevertheless, these models reasonably approximate the cone-driven a-wave response and provide an additional tool in the analysis of the canine photopic ERG.

The Naka-Rushton b-wave model provides an excellent fit to dark-adapted ERG luminance:response plots of normal dogs. Furthermore, we successfully applied the model to lower amplitude recordings encountered in dogs with inherited retinal dystrophy. This well-established model provides a useful method for quantification of rod bipolar cell function, with assessment of sensitivity and health of the overall population of these second-order neurons. Moreover, calculation of model parameters enabled comparison of normal dogs with young dogs with inherited retinal dystrophy and demonstrated profound decrease in retinal sensitivity. Given the number of flashes required to appropriately fit the model, an expanded protocol must be planned beyond the additional flashes suggested for both a-wave models. However, the recommended flashes are at stimulus strengths that do not require large inter-stimulus gaps, and therefore can be added to any ERG protocol with relatively small time investment.

Although the presented models are valuable individually, we were interested in examining potential relationships between them as it may provide additional information about the interactions of different populations of retinal cells. In normal, untreated and gene therapy treated dog retinitis pigmentosa models, notable findings included significant relationships between the rod photoreceptor and bipolar cell amplitude parameters, with no correlations discovered between sensitivity parameters or between sensitivity and amplitude. Comparing these parameters also demonstrated the changes in relationships seen in specific populations of retinal cells, such as the increased correlation between rod photoreceptors and rod bipolar cells following gene augmentation therapy in *CNGB1*$^{-/-}$ and *PDE6A*$^{-/-}$ dogs. This increase was much

greater in the *PDE6A*$^{-/-}$ dogs, likely reflecting the substantial increases measured in maximal rod response. In the *CNGB1*$^{-/-}$ dogs the most significant increase was in rod sensitivity, and the less significant increase in the correlation of amplitude parameters mirrors the smaller increase we measured in maximal rod response.

The models of ERGs recorded from young untreated *PDE6A* dogs demonstrate a profound decrease in rod-driven log $R_{max}$ and log $S$ parameters and b-wave $V_m$ parameter, a slight decrease in the cone-driven log $R_{mp_3}$ parameter, and a substantial increase in the b-wave log K parameter. In contrast, the models of ERGs from *CNGB1* dogs also demonstrate a profound decrease in rod-driven log $S$ parameters and a substantial increase in the b-wave log K parameter, but less significant decreases in the rod-driven log $R_{max}$ and b-wave $V_m$ parameters, with no changes in the cone-driven a-wave parameters. In dogs treated with gene augmentation therapy, sensitivity was restored but amplitude did not fully return to normal.

The findings of the tested models corroborate physiological expectations – *PDE6A* dogs have early loss of rods and some shortening of cone outer segments, and absence of a critical enzyme of rod phototransduction are modeled by the severe changes in both amplitude and sensitivity parameters. In *CNGB1* dogs, there is evidence of residual desensitized rod function this is accurately modeled by the less severe decreases in amplitude parameters compared to sensitivity parameters [unpublished findings]. Furthermore, as gene augmentation therapy treats only a portion of the retina, our models support restoration of normal phototransduction in the treated retina. Future investigation should examine the percentage of treated retina using changes in amplitude parameters [152,159].

There are several limitations to the mathematical models of the ERG. In pathological, low-amplitude ERGs, it may be difficult to accurately assess sensitivity of responses as

responses are difficult to detect above background noise. There may be utility for frequency-based approaches in such instances. Additionally, in this study gene augmentation treated dogs were not age-matched with untreated dogs for comparison due to difficulty in measuring parameters in older dogs with marked decline in ERG responses. Thus, the comparisons made were against young untreated dogs, and the improvements in amplitude parameters would likely have been even greater if age matched. Additionally, although we allowed the time delay parameter $t_d$ to vary in both rod- and cone-driven a-wave models to determine optimal model fits in individual dogs, there were no statistically significant differences in model parameters between normal dogs and dog models of retinitis pigmentosa, both treated and untreated. Thus, in the dog the $t_d$ parameter could be fixed at 1.5 mSec for the rod-driven a-wave model and 0 mSec for the cone-driven a-wave model.

In characterizing frequency components of the ERG, the DFT is useful in comparing frequency components of normal dogs and dogs with inherited retinal dystrophy. Additionally, it can be used to calculate and compare SNR in different ERG signals. A major drawback in the use of the DFT is that it calculates the frequency content from the entire signal, and thus it fails to capture the frequency content of specific ERG components, such as the a- and b-waves. The relatively recent development of wavelet analysis in signal processing provides a useful tool for examination of time-sensitive components of the ERG signal. Specifically, the DWT has recently been applied to the study of human ERG waveforms, sacrificing some of the frequency resolution of the DFT to better characterize how frequency contributions to the overall signal vary over time. Considering different frequency components may differentiate contributions from ON and OFF pathways, this novel method may enable better characterization of normal

ERGs as well as detection and determination of abnormalities in dogs with retinal dysfunction [148,149].

In this study, we have demonstrated the potential of several mathematical models to accurately characterize different waveforms in the scotopic and photopic ERG in both normal dogs and those with inherited retinal dystrophy as models of retinitis pigmentosa in humans. In normal dogs, excellent fits were possible with models of the rod- and cone-driven a-waves, as well as Naka-Rushton fitting of the dark-adapted b-wave. In young dogs with inherited retinal dystrophy, models were more technically challenging to fit to recordings but demonstrated profound alterations in model parameters. We further presented recent advances in signal processing analysis, such as the wavelet transform, and demonstrated how that can potentially be applied to normal and abnormal ERG signals. Although some of the methods presented require addition of flashes to the ISCEV standard protocol, particularly the Naka-Rushton fit of the dark-adapted b-wave, we have shown how these models can be reasonably applied even with limited protocol alterations.

# APPENDIX

| # of flash strengths used | Log $R_{max}$ (µV) | $t_d$ (mSec) | Log $S$ 1/(cd/m$^2$ s$^3$) |
|---|---|---|---|
| 8 | 1.968 ± 0.136 | 1.526 ± 0.135 | 1.975 ± 0.097 |
| 4 | 1.969 ± 0.139 | 1.46 ± 0.317 | 1.972 ± 0.105 |
| 2 (ISCEV standard) | 1.969 ± 0.132 | 1.81 ± 0.101 | 2.052 ± 0.106 |

**Table 3.1. Rod-driven a-wave model parameters in normal dogs by number of stimuli used.**

| Group | Slope | Intercept | Pearson *r* | *p-value* |
|---|---|---|---|---|
| Normal | 1.188±0.189 | -0.182±0.371 | 0.902 | $1.44x10^{-4}$ |
| *CNGB1*$^{-/-}$ Untreated | 0.772±0.217 | 1.189±0.200 | 0.765 | $6.11x10^{-3}$ |
| *CNGB1*$^{-/-}$ Treated | 0.808±0.122 | 0.403±0.194 | 0.797 | $6.36x10^{-7}$ |
| *PDE6A*$^{-/-}$ Untreated | 0.570±0.226 | 1.014±0.115 | 0.546 | 0.023 |
| *PDE6A*$^{-/-}$ Treated | 1.353±0.140 | 0.191±0.144 | 0.915 | $1.56x10^{-8}$ |

**Table 3.2. Correlation (*r*) values of log $V_m$ vs log $R_{max}$ comparisons, along with linear slope parameters for the independent variable and their associated *p*-values.**

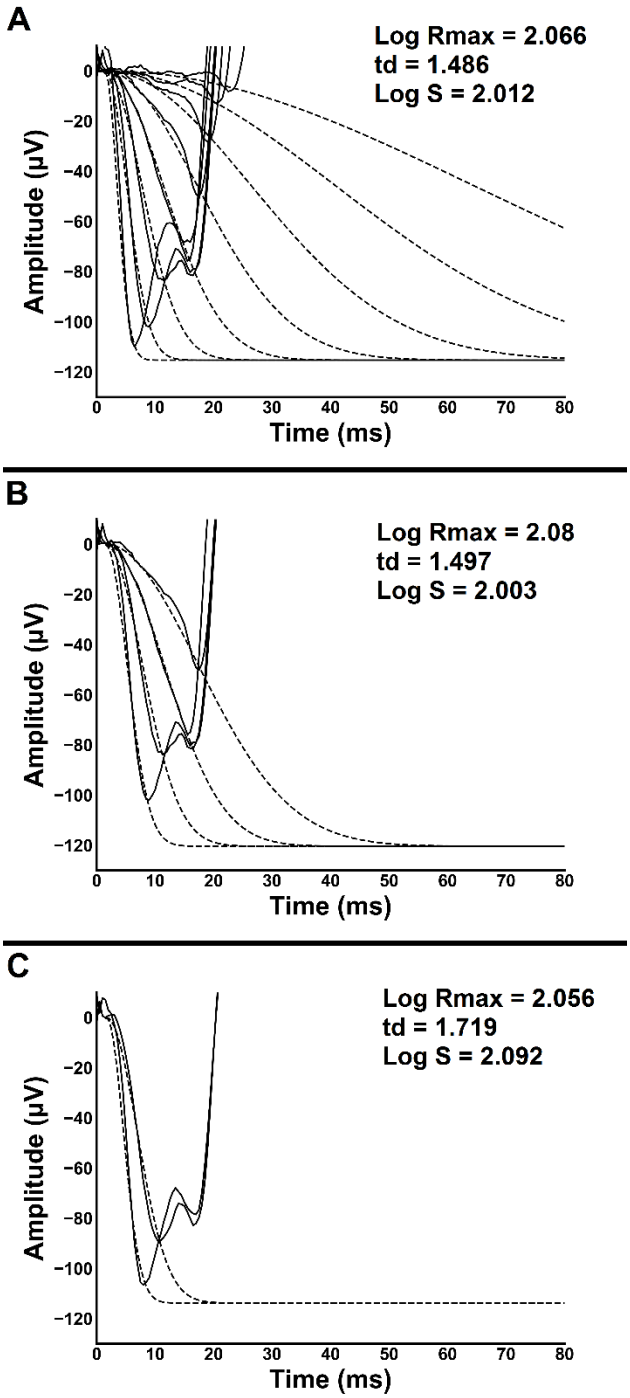


**Figure 3.1. Birch & Hood a-wave modeling of a normal canine scotopic ERG**

A. Rod-driven a-wave modeling of a normal dog using 8 different flash stimuli, ranging in strength from -1.6 to 1.4 log cd.s/$m^2$. Model parameters are provided in the inset.

**Figure 3.1. (cont'd)**

B. Rod-driven a-wave modeling of the same dog using 4 different flash stimuli, ranging in strength from -0.4 to 0.86 log cd.s/$m^2$. Model parameters are provided in the inset.

C. Rod-driven a-wave modeling of the same dog using 0.48 and 1.0 log cd.s/$m^2$ ISCEV standard flash stimuli. Model parameters are provided in the inset.

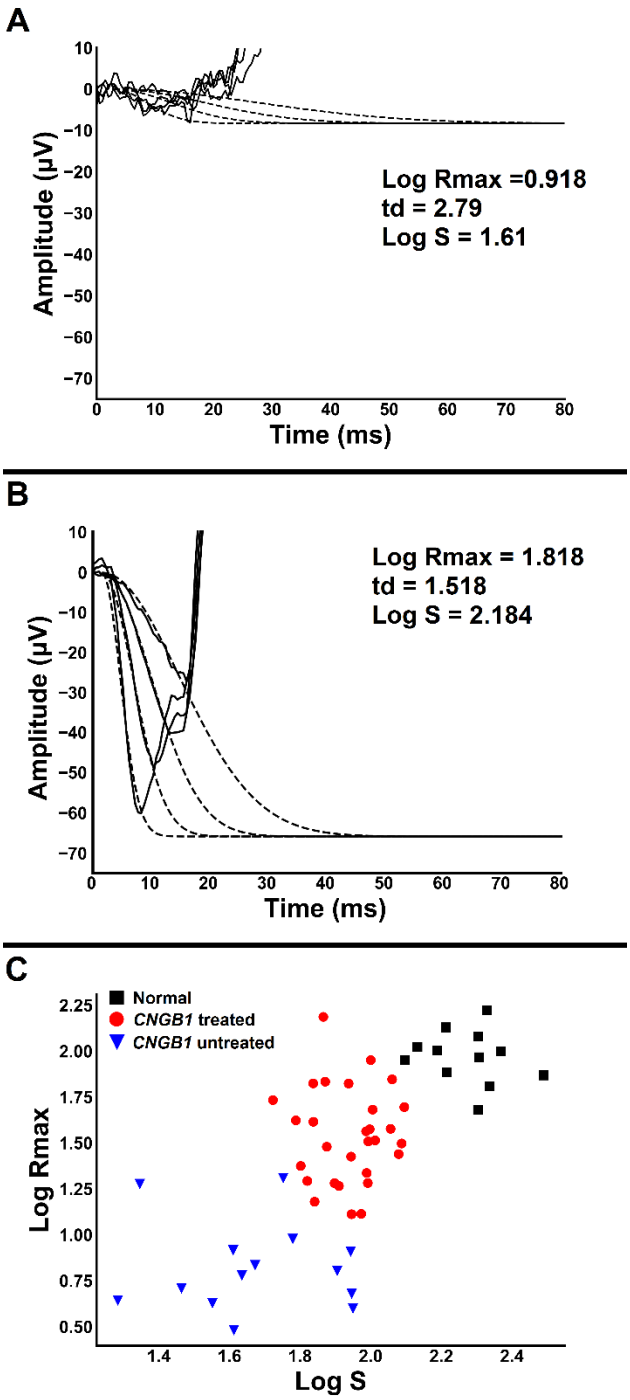


**Figure 3.2. Birch & Hood scotopic a-wave modeling of a *CNGB1* affected dog pre-treatment and post-gene augmentation therapy**

**Figure 3.2. (cont'd)**

A. Rod-driven a-wave modeling of a *CNGB1*$^{-/-}$ dog before treatment using 4 different flash stimuli, ranging in strength from -0.4 to 0.86 log cd.s/m$^2$. Model parameters are provided in the inset.

B. Rod-driven a-wave modeling of the same *CNGB1*$^{-/-}$ dog 9 months after treatment with gene augmentation therapy using 4 different flash stimuli, ranging in strength from -0.4 to 0.86 log cd.s/m$^2$. Model parameters are provided in the inset.

C. Log $R_{max}$ (amplitude) vs. log $S$ (sensitivity) of untreated *CNGB1*$^{-/-}$ dogs ($n$ = 14), *CNGB1*$^{-/-}$ dogs treated with gene augmentation therapy ($n$ = 4), and normal dogs ($n$ = 12). This demonstrated a significant reduction in both parameters in the affected dogs and a significant increase in all treated eyes following gene augmentation therapy.

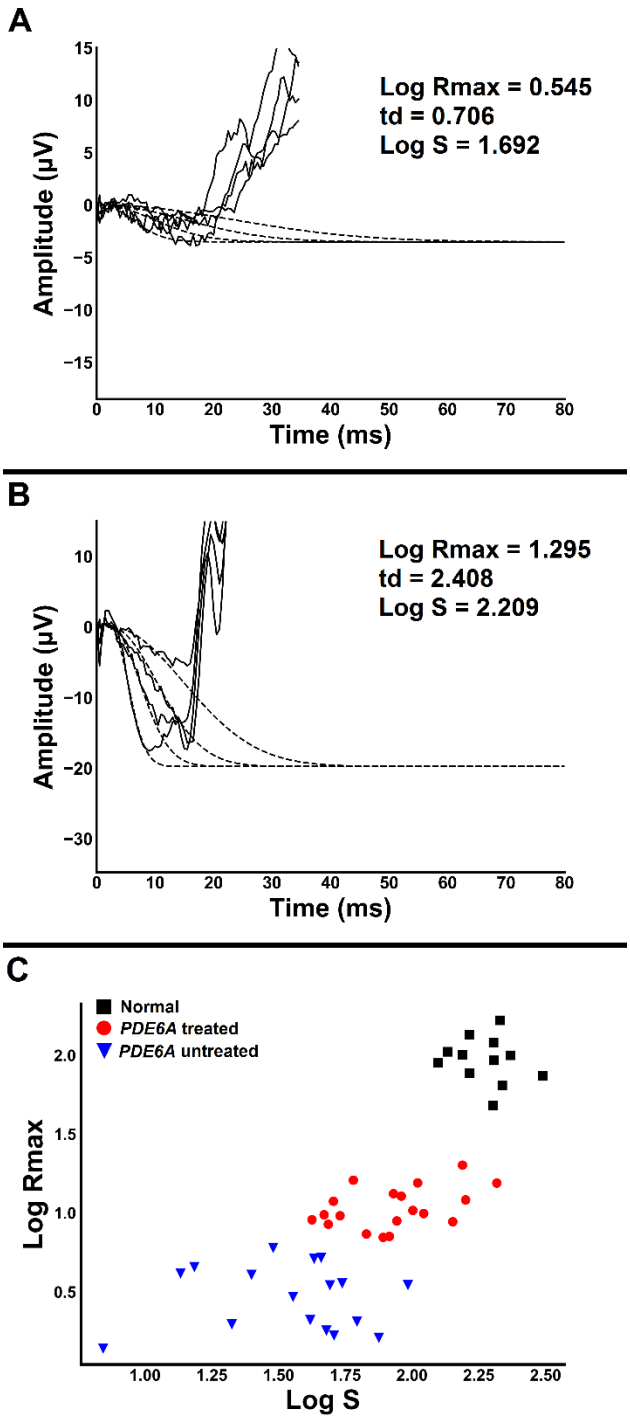


**Figure 3.3. Birch & Hood scotopic a-wave modeling of a *PDE6A* affected dog pre-treatment and post-gene augmentation therapy**

**Figure 3.3. (cont'd)**

A. Rod-driven a-wave modeling of a *PDE6A*$^{-/-}$ dog before treatment using 4 different flash stimuli, ranging in strength from -0.4 to 0.86 log cd.s/m$^2$. Model parameters are provided in the inset.

B. Rod-driven a-wave modeling of the same *PDE6A*$^{-/-}$ dog 3 months after treatment with gene augmentation therapy using 4 different flash stimuli, ranging in strength from -0.4 to 0.86 log cd.s/m$^2$. Model parameters are provided in the inset.

C. Log $R_{max}$ (amplitude) vs. log $S$ (sensitivity) of untreated *PDE6A*$^{-/-}$ dogs ($n$ = 17), *PDE6A*$^{-/-}$ dogs treated with gene augmentation therapy ($n$ = 6), and normal dogs ($n$ = 12). This demonstrated a significant reduction in both parameters in the affected dogs and a significant increase in all treated eyes following gene augmentation therapy.

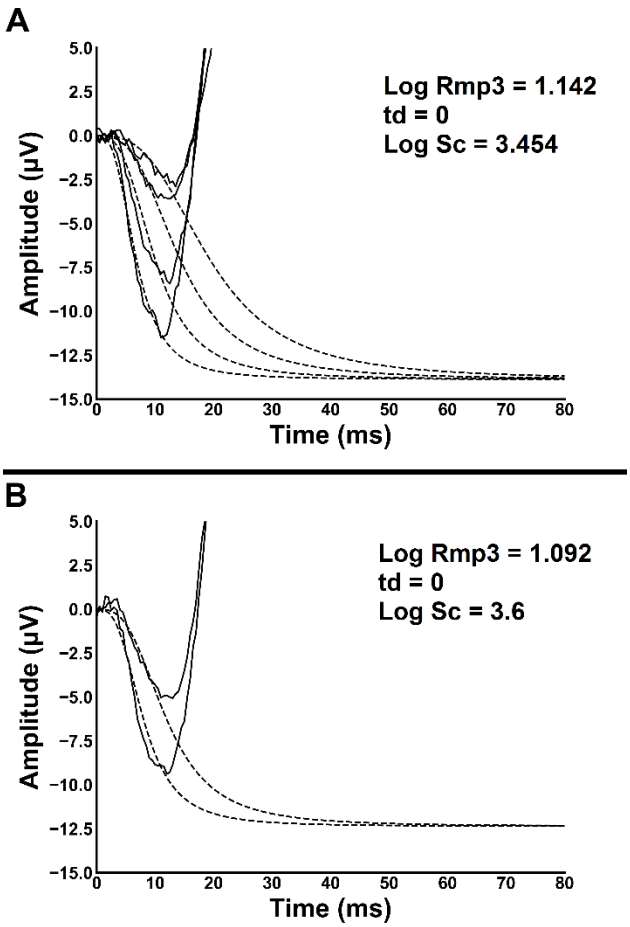


**Figure 3.4. Simplified cone a-wave model applied to normal dogs and those with inherited retinal disease**

A. Cone-driven a-wave modeling of the same dog using 4 different flash stimuli, ranging in strength from 0 to 1.4 log cd.s/$m^2$. Model parameters are provided in the inset.

B. Cone-driven a-wave modeling of the same dog using 0.48 and 1.0 log cd.s/$m^2$ ISCEV standard flash stimuli. Model parameters are provided in the inset.

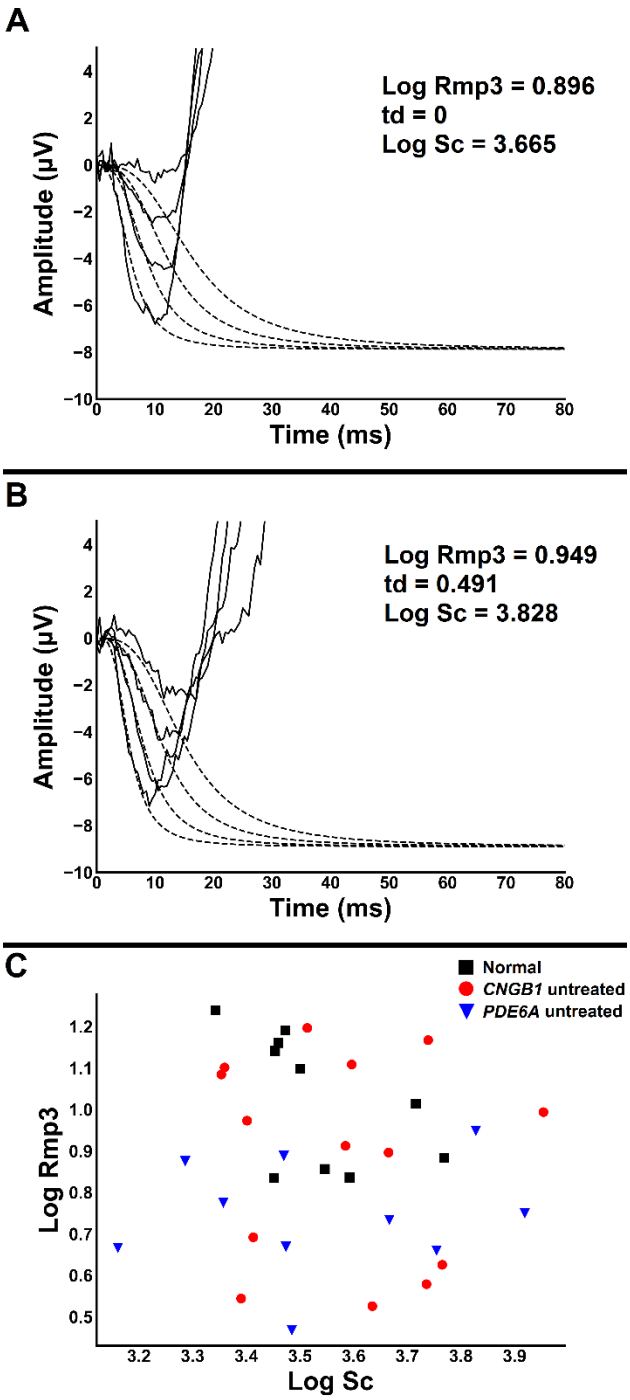


**Figure 3.5. Simplified cone a-wave model applied to normal dogs and those with inherited retinal disease**

**Figure 3.5. (cont'd)**

A. Cone-driven a-wave modeling of an untreated *CNGB1*$^{-/-}$ dog using 4 different flash stimuli, ranging in strength from 0 to 1.4 log cd.s/m$^2$. Model parameters are provided in the inset. Model parameters were similar in both affected and normal dogs.

B. Cone-driven a-wave modeling of an untreated *PDE6A*$^{-/-}$ dog using 4 different flash stimuli, ranging in strength from 0 to 1.4 log cd.s/m$^2$. Model parameters are provided in the inset. Model parameters were similar in both affected and normal dogs, albeit with a slight reduction in the amplitude parameter log $R_{mp3}$.

C. Log $R_{mp3}$ (amplitude) vs. log $S_c$ (sensitivity) of normal ($n$ = 10), *CNGB1*$^{-/-}$ ($n$ = 8), and *PDE6A*$^{-/-}$ ($n$ = 10) dogs.

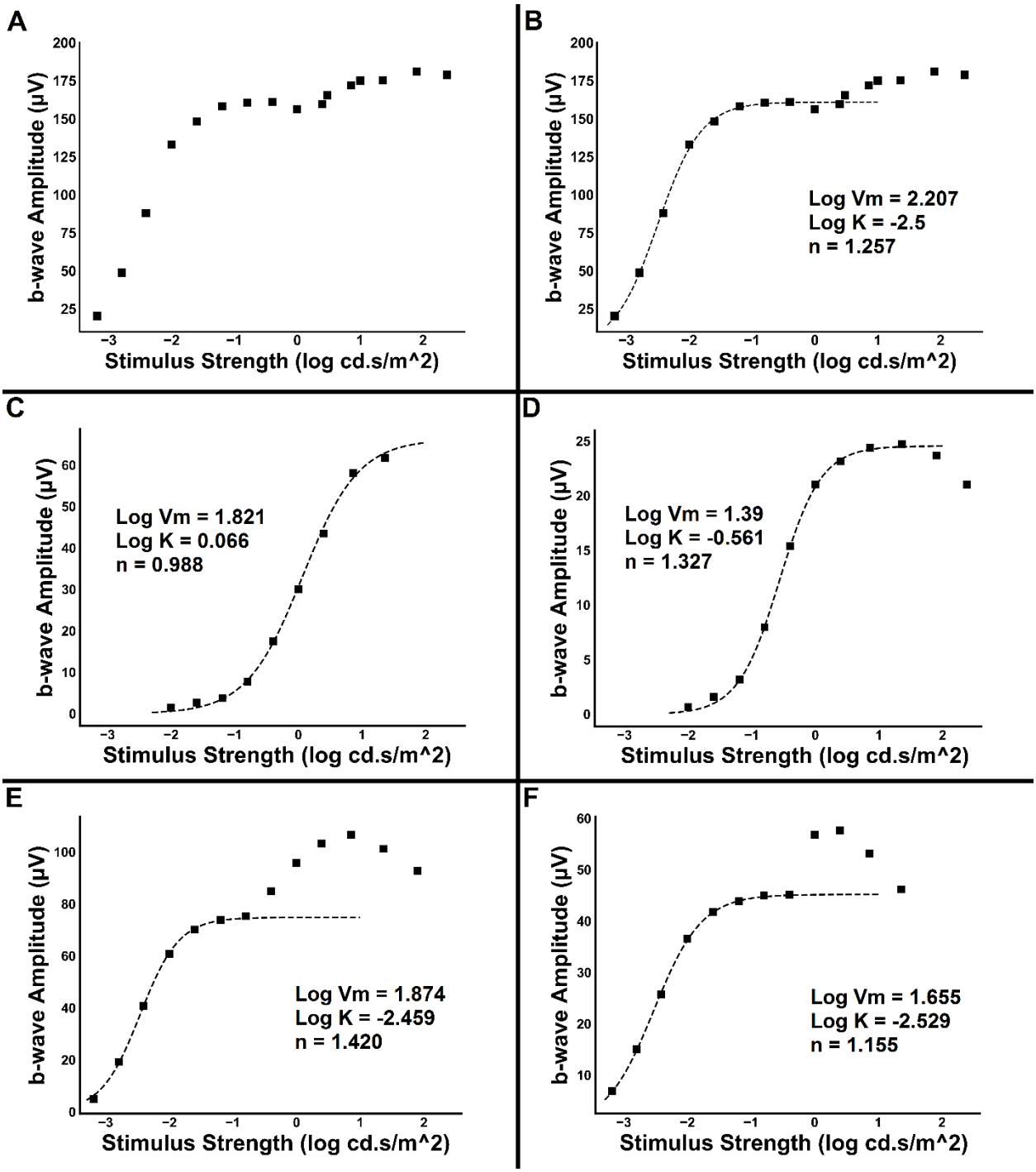


**Figure 3.6. Naka-Rushton fitting of the luminance:response curves of the dark-adapted b-wave**

A. Luminance:response curve of the dark-adapted b-wave of a normal dog. Note the two ascending limbs, separated by an inflection point, which follow semi-saturation kinetics.

**Figure 3.6. (cont'd)**

B. Naka-Rushton (Michaelis-Menten) modeling of the luminance:response curve of the dark-adapted b-wave of the same normal dog. Model parameters are provided in the inset.

C. Naka-Rushton (Michaelis-Menten) modeling of the luminance:response curve of the dark-adapted b-wave of an untreated *CNGB1*$^{-/-}$ dog. Model parameters are provided in the inset. The reduced amplitude and sensitivity are reflected in a reduction in the $V_m$ parameter and an increase in the K parameter, respectively.

D. Naka-Rushton (Michaelis-Menten) modeling of the luminance:response curve of the dark-adapted b-wave of an untreated *PDE6A*$^{-/-}$ dog. Model parameters are provided in the inset. The reduced amplitude and sensitivity are reflected in a reduction in the $V_m$ parameter and an increase in the K parameter, respectively.

E. Naka-Rushton (Michaelis-Menten) modeling of the luminance:response curve of the dark-adapted b-wave of a *CNGB1*$^{-/-}$ dog 3 months following treatment with gene augmentation therapy. Model parameters are provided in the inset.

F. Naka-Rushton (Michaelis-Menten) modeling of the luminance:response curve of the dark-adapted b-wave of a *PDE6A*$^{-/-}$ dog 4 months following treatment with gene augmentation therapy. Model parameters are provided in the inset.

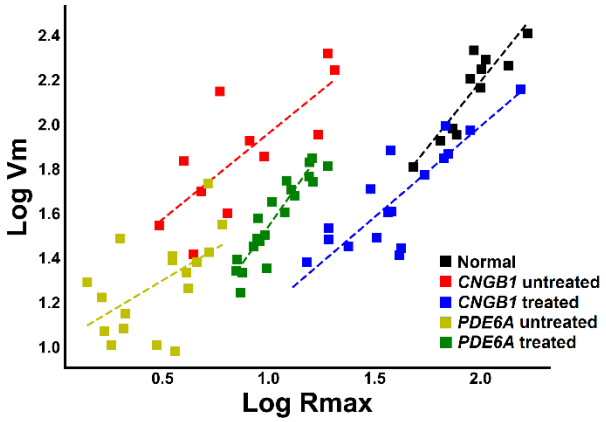


**Figure 3.7. Correlations of amplitude parameters in normal dogs, untreated dogs with PRA, and dogs treated with gene augmentation therapy**

Correlation of rod-driven b-wave amplitude parameter log $V_m$ and rod-driven a-wave amplitude parameter log $R_{max}$. Inset key indicates genotype and treatment status.

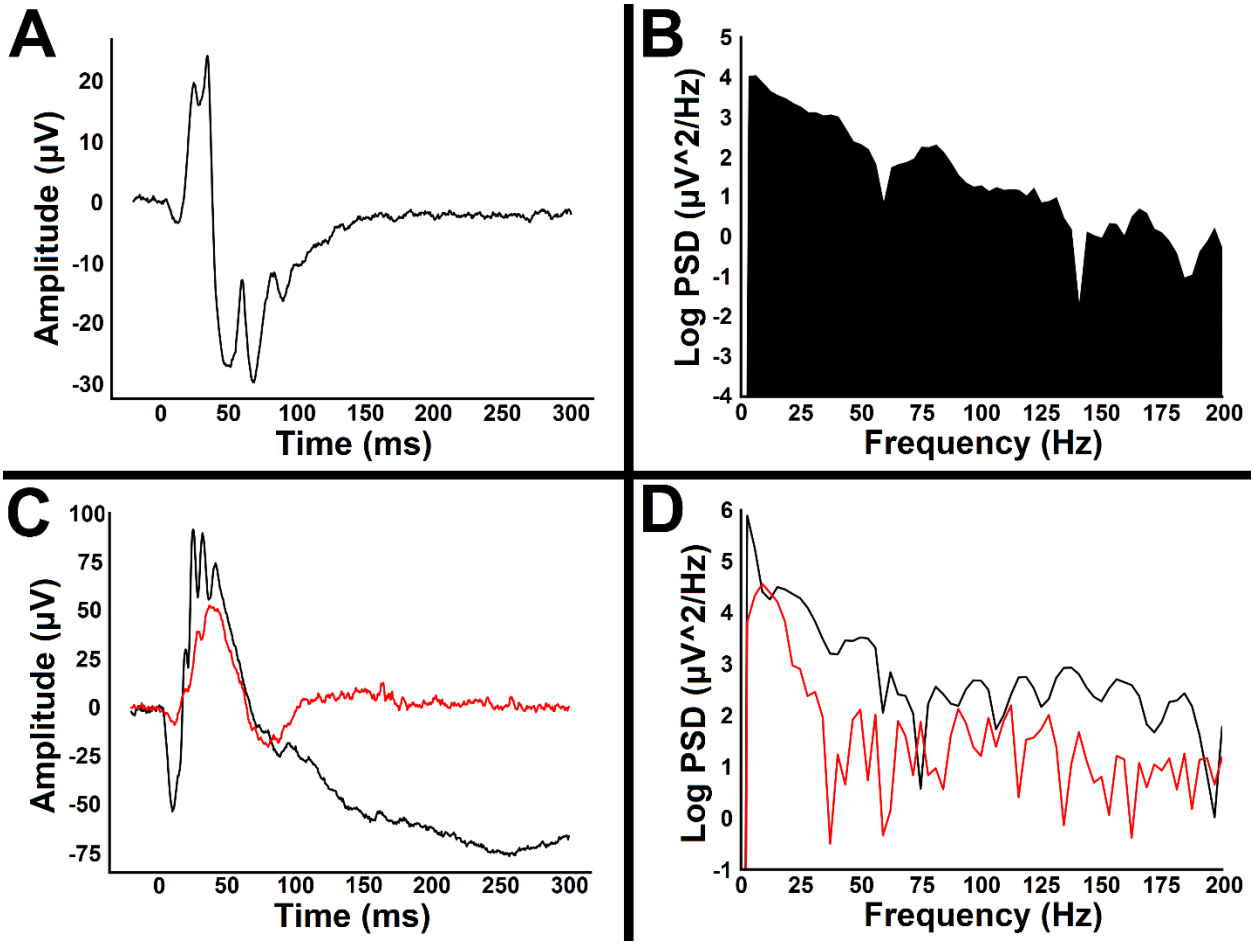


**Figure 3.8. PSD analysis of the canine ERG**

A. Standard light-adapted ERG of a normal dog with 0.39 log cd.s/$m^2$ stimulus strength.

B. Corresponding DFT power spectrum of the tracing shown in A. The PSD demonstrates the relative contribution of different frequencies to the overall ERG signal.

C. Standard dark-adapted ERG of a *CNGB1*$^{-/-}$ dog before (red tracing) and 9 months after treatment (black tracing) with gene augmentation therapy normal dog with 0.39 log cd.s/$m^2$ stimulus strength.

D. Corresponding DFT power spectrum of the tracings shown in C.

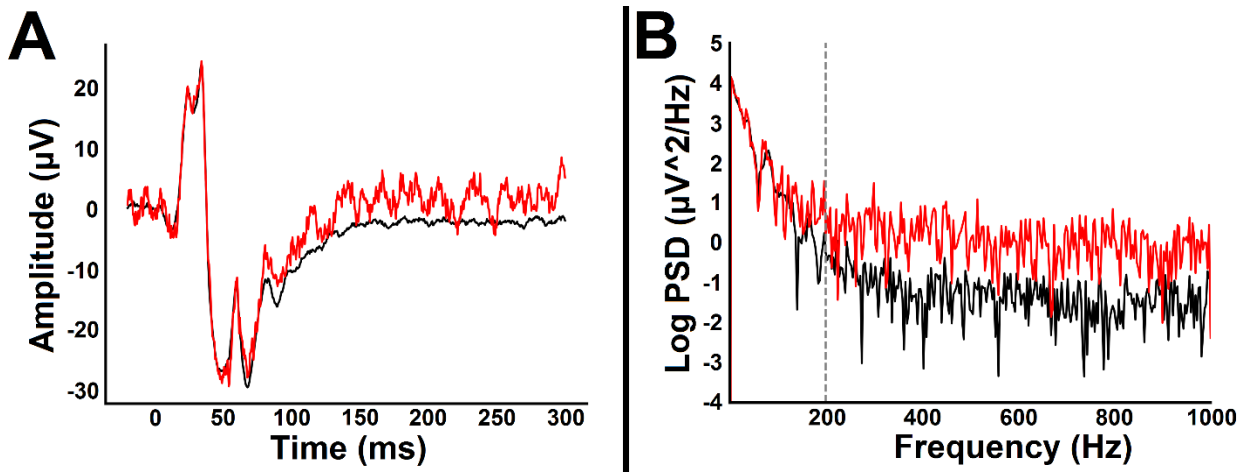


**Figure 3.9. SNR analysis of the canine ERG**

A. Standard light-adapted ERG of a normal dog with 0.39 log cd.s/$m^2$ stimulus strength showing a single sweep (red tracing) and average of ten sweeps (black tracing).

B. Corresponding DFT power spectrum of the tracings shown in A.

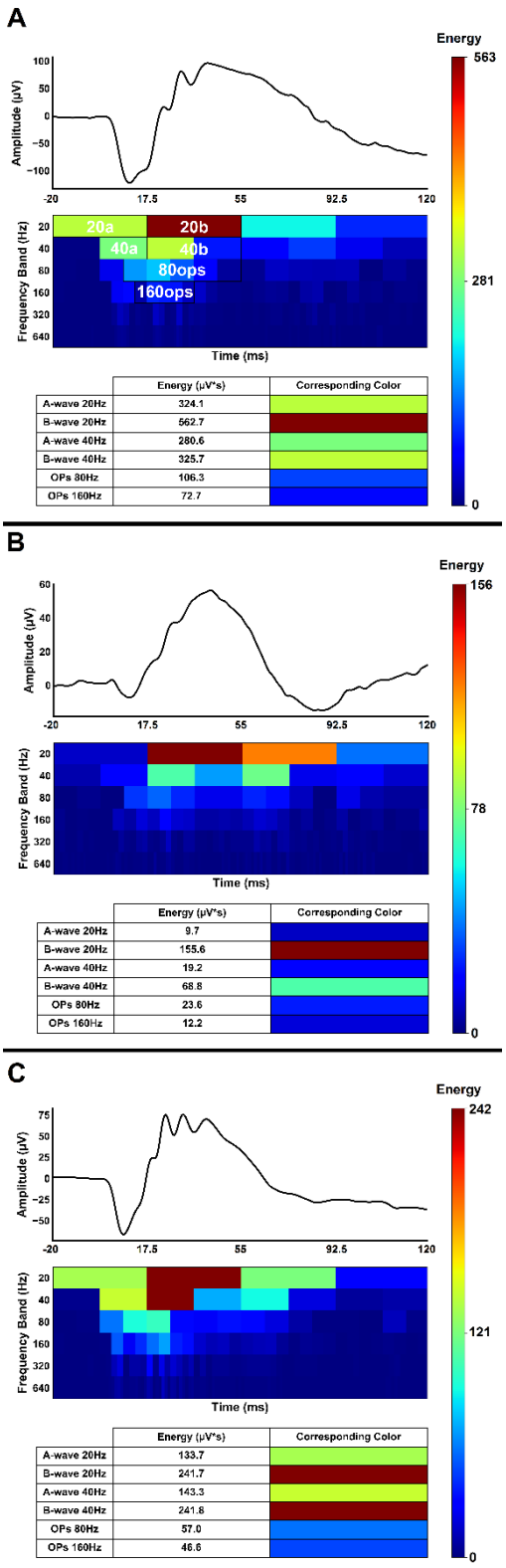


**Figure 3.10. DWT analysis of a normal dog and *CNGB1* dog treated with gene augmentation therapy**

**Figure 3.10. (cont'd)**

In each figure, the tracing at the top of the figure demonstrates a standard dark-adapted ERG with 0.86 log cd.s/$m^2$ stimulus strength, shown in the time-domain. Utilizing the method outlined by Gauvin et al (2015), a discrete wavelet transform (DWT) was applied to the waveform. In the figure below the ERG tracing, the color of each box denotes its energy contribution to the overall response, with warmer colors indicating a larger contribution and cooler colors a smaller one. The central frequencies are shown to the left of each band. The x-axis is time (ms) and is shown with the same scale as the above tracing. In the 20Hz band, each bin is 37.5 ms long, and each subsequent doubling of frequency bands halves the time duration (eg. the 40Hz band has bins with 18.75ms length). The white text overlay denotes the frequency and time resolution of the components and their contributions to the ERG. The inset to the right of the main figures denotes the scale of the color heat map. A table of absolute energy contribution of each frequency contribution (μV·s), with corresponding ERG component and heat map color, is shown at the bottom of the figure.

A. DWT analysis of 0.86 log cd.s/$m^2$ dark-adapted ERG of a normal dog.

B. DWT analysis of 0.86 log cd.s/$m^2$ dark-adapted ERG of a *CNGB1*$^{-/-}$ dog before treatment with gene augmentation therapy.

C. DWT analysis of 0.86 log cd.s/$m^2$ dark-adapted ERG of the same *CNGB1*$^{-/-}$ dog 9 months after treatment with gene augmentation therapy.

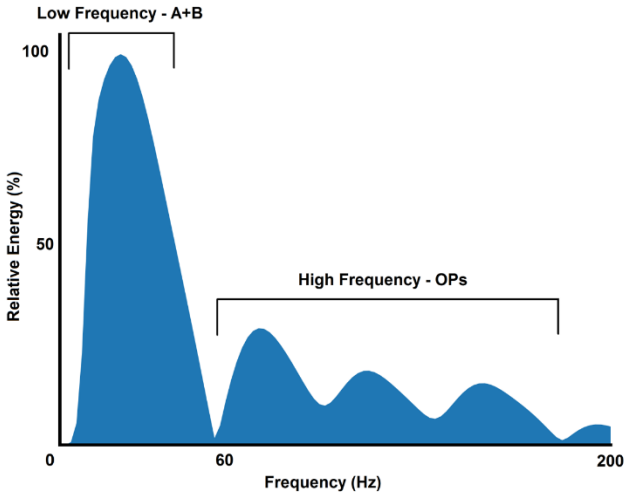


**Figure 3.S1. DFT reference Standard DFT of a normal dark-adapted ERG, denoting relative energy of the signal (%) vs the frequency (Hz). The frequency ranges that contribute to different ERG waveforms are shown**

# CHAPTER 4.

# USE OF EXPANDED ERG PROTOCOLS TO CHARACTERIZE ROD AND CONE CONTRIBUTIONS TO THE CANINE ERG

## 4.1. Introduction

Electroretinography is an invaluable tool in ophthalmology. The electroretinogram (ERG) has been used in dogs for decades for clinical assessment and research into retinal function and dysfunction. However, assessment of canine ERGs is often restricted to responses elicited by a limited number of stimuli [1,13]. While these short protocols provide a general overview of retinal function and aid in the diagnosis of retinal disease, they are somewhat limited in the information that they can provide. For example, receptor response threshold is not obtained by the standard protocols. However, additional protocols provided for flash ERG by the International Society for Clinical Electrophysiology of Vision (ISCEV) include the dark-adapted red flash, a strong flash to saturate the rod a-wave, a dark- and light-adapted luminance-response series, photopic ON-OFF with long duration flashes, photopic negative response (PhNR), and S-cone [124,151,178–182].

Standard ERG protocols typically feature white light flashes (which consists of wavelengths comprising the visible spectrum) presented in the dark (scotopic) to a dark-adapted eye or to a light-adapted eye superimposed on a constant white backgound light (photopic) [1,13]. Chromatic flashes utilize stimuli of specific wavelengths in order to preferentially stimulate different photoreceptors. These protocols typically feature long wavelength red flashes, which target M/L-cone function, and may also include short wavelength blue flashes, which target rod and S-cone function [113,183–185]. In humans, dark-adapted red flashes elicit a cornea-positive cone-driven response, known as the x-wave, that precedes the rod-driven b-wave. Chromatic flashes have also been utilized in investigation of disease processes such as glaucoma [186–189].

Several studies in dogs have demonstrated separation of dark-adapted rod- and cone-driven responses [138,190–194]. Dogs have two type types of cones - M/L-cones, which are mainly stimulated by longer wavelength light (peak sensitivity at 555 nm) and S-cones, which are

mainly stimulated by shorter wavelength light (peak sensitivity at 430-435 nm). Additionally, rods have a peak sensitivity at 508 nm [136]. Chromatic stimuli have also been used in analysis of retinal dysfunction, such as evaluation of drug-induced retinal toxicity [195]. However, chromatic stimuli are used less frequently in current canine ERG studies [13]. Our aim was to expand understanding of differential responses to red and blue light flashes in dogs as well as to develop a short chromatic protocol that could be easily incorporated into current guidelines for ERGs in dogs.

Just as photoresponsive retinal cells (photoreceptors and melanopsin containing ganglion cells – the latter do not make a major contribution to the ERG) are preferentially stimulated by specific stimulus wavelengths, photoreceptors are also differentially affected by the strength of background light. Cones have faster response and recovery time but are less sensitive to light, and thus are the primary drivers of the light-adapted visual response (as well as significant contributors to responses to higher strength light flashes in dark-adapted conditions). Conversely, rod photoreceptors have slower response and recovery time but are more sensitive, and therefore the primary driver of responses to dimmer light stimuli in the dark-adapted retina [196–201]. Cones signal through ON and OFF pathways to depolarizing and hyperpolarizing bipolar cells, and the relative and opposing contributions of these pathways exhibit what has been described as a 'push-pull' mechanism that that leads to the resulting shape and amplitude of the b-wave response [73,202,203]. The primary rod pathway is through rod bipolar cells; however, studies in mice and primates indicate that rods also signal through gap junctions with cones as well as via direct synapses with cone OFF-bipolar cells, with the relative contribution of each pathway influenced by ambient light levels [204–208]. A putative direct connection between rod photoreceptors and cone

ON-bipolar cells has also been shown in mice lacking metabotropic glutatmate receptor 6 (mGluR6), although this has not yet been demonstrated in primates [209,210].

There are further differences between other populations of retinal cells. In humans, both the degree and length of light adaptation have been shown to differentially affect responses originating from different classes of bipolar cells and photoreceptors [17,74,105,202,211]. Studies of brightness discrimination (which provide a behavioral measure analogous to contrast sensitivity) in the dog show that human brightness discrimination is roughly twice as good as that of dogs [212]. However, the electroretinographic responses to different background lighting conditions have not been quantified or modeled in the dog.

Both ISCEV and European College of Veterinary Ophthalmologists (ECVO) guidelines recommend the inclusion of a 30Hz photopic flicker as part of a standard ERG recording [1,13]. Expanded flicker protocols have additionally been used to separate rod- and cone-driven signaling pathways in both human and rodent ERG recordings. As would be anticipated, these studies show that rods drive responses to low frequency flickers in dark-adapted conditions, while cones contribute more to higher frequency flickers as well as those in light-adapted conditions [20,213]. Further differences have been found between flickers presented in dark- and light-adapted conditions, as well as changes in the shape and amplitude of responses to flickers of increasing stimulus strength [213,214]. Moreover, a study in mice demonstrated differential responses of second order neurons to flicker stimuli, with ON-bipolar cells driving responses to lower frequency flickers and OFF-bipolar cells driving responses to higher frequency flickers [22]. Although both ERG and behavioral studies have examined the critical flicker fusion frequency in dogs, there are limited reported investigations of responses to flickers at different frequency or stimulus strength [135,191,192].

A major aim of these studies is the analysis of rod and cone contributions to the canine ERG using expanded protocols tested in both phenotypically normal dogs as well as identified canine models of specific retinal dysfunction. Animals with gene mutations are often utilized to investigate rod and cone contributions; in this study we used a retinitis pigmentosa dog model with non-functional rods and an achromatopsia model with non-functional cones. For a model with nonfunctional rods we used dogs homozygous for a *PDE6A* null mutation [161]. This allowed us to assess cone only responses with the presence of little or no active rod interaction. In young *PDE6A*$^{-/-}$ dogs, cone b-waves are of normal amplitude but of slightly delayed peak time while cone a-waves are slightly reduced. They do progressively lose remaining cone function over the first 12 months of age [215]. We additionally tested an abbreviated protocol on a dog with compound heterozygous mutations in the *CNGB3* gene (a *CNGB3*$^{*/del}$ dog with a D262N missense mutation and genomic deletion), who have almost no cone responses by 12 weeks of age and serve as a model of rod-driven function [154(p3)].

In designing this current study, we considered multiple approaches to characterize rod and cone pathways in the dog. We were particularly interested in methods that have enabled separation of these pathways with different states of retinal adaptation. We ultimately tested three different types of protocols. We assessed temporal separation of dark-adapted rod and cone responses using red and blue chromatic flashes, an older technique that has been infrequently used in recent canine ERG studies. Additionally, we considered the effect of light adaptation on the individual contributions of rod and cone pathways using a luminance:response protocol with progressively increasing background luminance. Finally, we examined the temporal differences in rod- and cone-driven responses using expanded dark- and light-adapted flicker protocols which varied in either flash frequency or stimulus strength. Not only do these protocols have

potential utility in routine ERG recordings, but it may be possible to develop mathematical models for these protocols, similar to the Naka-Rushton b-wave fitting, to quantify normal response ranges as well as parameterize pathological ERG recordings [15,18,166]. Although some of these models have been researched and utilized in humans, less is known about their capacity to characterize retinal function in normal dogs as well as dog models of retinal disease.

**4.2. Materials and Methods**

Animals

Purpose bred *PDE6A*$^{-/-}$, *CNGB3*$^{*/del}$, and phenotypically normal control dogs maintained in a colony at Michigan State University were investigated in this study. They were housed under 12hr:12hr light:dark cycles. The *PDE6A* mutation arose in the Cardigan Welsh Corgi breed but has been bred onto a laboratory beagle background. The *CNGB3* mutations arose in the Alaskan Malamute (genomic deletion) and Germain Shorthaired Pointer (missense mutation) breeds but has been bred onto a laboratory beagle background.

Anesthesia

General anesthesia was induced by isoflurane mask for puppies and by IV propofol for older animals (4-6 mg/kg, PropoFlo, Abbott Laboratories, North Chicago, IL, USA). The animals were intubated, and subsequently maintained under anesthesia with isoflurane (IsoFlo, Abbott Laboratories, North Chicago, IL, USA) [between 2-3.5% in a 1-2 L/min oxygen flow via a rebreathing circle system for dogs over 10 kg and via a Bain system for dogs under 10 kg].

Electroretinography (ERG)

General procedures for ERGs were described previously [168]. Differences in apparatuses and protocols are noted below. Briefly, prior to anesthesia dogs were dark-adapted for one hour

and pupils dilated with tropicamide (Tropicamide Ophthalmic Solution UPS 1%, Falcon Pharmaceuticals Ltd., Fort Worth, TX, USA). A monopolar gold-ringed electrode contact lens (ERG-Jet electrode, Fabrinal Eye Care, La Chaux-De-Fonds, Switzerland) was used and for reference and grounding platinum needle skin electrodes (Grass Technologies, Warwick, RI, USA) were placed 5 mm lateral to the lateral canthus and over the occiput, respectively. ERGs were recorded using an Espion $E^2$ Electrophysiology system with ColorDome Ganzfeld (Diagnosys LLC, Lowell, MA, USA).

*Chromatic ERG*

Flashes were presented at 1Hz for a dark-adapted eye and averaged as needed depending on the signal to noise ratio. Red flash stimuli, with a wavelength centered at 630 nm and half-bandwidth of 20 nm, ranged from 0.05 to 2.5 cd.s/$m^2$. Blue flash stimuli, with a wavelength centered at 445 nm and half-bandwidth of 20 nm, ranged from 0.00005 to 0.05 cd.s/$m^2$.
For the purpose of matching of red and blue flashes in control dogs, we performed Naka-Rushton fitting of b-wave amplitudes. Amplitudes were measured from the trough of the preceding a-wave to the peak of the following b-wave, accounting for oscillatory potential (OP) intrusion along the leading edge of the b-wave. Model parameters were calculated by fitting the Naka-Rushton function to the first limb of the b-wave luminance-response plot. The Naka-Rushton function and parameters are as follows:

$$R/V_m = L^n/(L^n+K^n)$$

$V_m$ represents the maximum response amplitude of the first limb of the b-wave luminance:response plot, *k* is a semi-saturation constant considered a measure of retinal sensitivity, and *n* is dependent on of the slope of the plot at the position of *k*, which may reflect retinal homogeneity [139,166,167].

For this study, subjects included 10 phenotypically normal control dogs (4 male and 6 female) and 5 *PDE6A*$^{-/-}$ dogs (2 male and 3 female). Control subjects were all 2 months of age (dogs have a measurable ERG by 3 weeks of age, which grows in amplitude to reach adult ERG amplitudes by 8 weeks of age [216]), while *PDE6A*$^{-/-}$ dogs ranged from 1-2 months of age (younger dogs were used for this study to preclude significant cone loss in *PDE6A*$^{-/-}$ subjects). We also tested the short chromatic matching protocol on one adult *CNGB3*$^{*/del}$ dog (additional dogs were not available for inclusion in statistical analyses).

*Blue Background ERG*

Each flash was presented at one second intervals on a dark background and repeated to generate an averaged response detectable against background electrical noise. White flash stimuli ranged from 0.01 to 2.5 cd.s/m$^2$, and were presented on no background, as well as blue backgrounds of 0.01, 0.1, 1.0, and 10 cd/m$^2$ for gradual suppression of rod responses. Dogs were dark-adapted for one hour prior to recording and were adapted for five minutes to each background luminance.

For this study, subjects included 10 phenotypically normal control dogs (4 male and 6 female) and 5 *PDE6A*$^{-/-}$ dogs (2 male and 3 female). Control subjects were all 2 months of age, while *PDE6A*$^{-/-}$ dogs ranged in age from 1-2 months of age.

*Flicker ERG*

Two different protocols, adapted from previous work by Seeliger et al. [217], were tested – one with a stimulus of 3.2 cd.s/m$^2$ white light with flickers of increasing frequency from 0.5-30 Hz, and the other with a frequency of 6Hz and stimuli luminance ranging from 1x10$^{-5}$ to 32.0 cd.s/m$^2$. The flickers were presented in both scotopic (in the dark) and photopic (30 cd/m$^2$ white

background) conditions. Dogs were dark-adapted for 1 hour prior to the scotopic flickers, and light-adapted for 10 minutes on a 30 cd/m$^2$ white background prior to photopic flickers.

For this study, subjects included 11 phenotypically normal control dogs (4 male and 7 female) and 3 *PDE6A*$^{-/-}$ dogs (3 female). Subjects ranged in age from 3-7 months (all *PDE6A*$^{-/-}$ dogs were tested at 3 months of age).

Statistical analysis

All statistical tests were performed in Python with the Statsmodels package [173]. ANCOVA testing was used to compare statistical significance between the means of different groups when modeled with linear regression:

$$y_{ij} = \mu + \tau_i + B\left(x_{ij} - \bar{x}\right) + \varepsilon_{ij}$$

The variables *i* and *j* are the *j*th observation of the *i*th categorical group, the dependent variable *y* is modeled as a function of independent variable *x*, μ and $\bar{x}$ are mean parameters derived from the data, and the fitted variables are the effect parameter τ, slope parameter B and error term ε. After assessment of linearity of regression, homogeneity of error variances, independence and normality of error terms, and homogeneity of regression slopes, mean group differences were assessed using the F-test [218].

**4.3. Results**

Rod and cone contributions to the chromatic ERG in the dark-adapted eye in control dogs and dogs lacking rod function (Figures 4.1-4.3).

Red and blue flash dark-adapted ERG series were performed in control dogs and young *PDE6A*$^{-/-}$ dogs (Fig. 1). Naka-Rushton fitting (Supplemental Figure 4.S1) was performed to match stimulus strengths based on the constant K in control dogs in determination of the ½ saturation parameter K, with model parameters as follows:

Blue: $V_m$ = 162.68±30.26 µV, K = 0.0012±3.6 cd.s/$m^2$, n = 1.019±0.232

Red: $V_m$ = 151.25±24.36 µV, K = 0.257±0.047 cd.s/$m^2$, n = 1.064±0.103

Comparison of model parameters indicates that the semi-saturation parameter $V_m$ was similar across both tested flash colors, as was the slope parameter n. However, the greatest differences were revealed in comparison of the K parameter, reflecting the differences in spectral sensitivity with different flash colors. The b-wave response was over 200 times more sensitive to blue flashes than red (Supplemental Figure 4.S1).

In control dogs specifically, this chromatic matching revealed a small positive deflection preceding the larger rod-driven b-wave in response to the red stimulus. Overlaying dark-adapted responses to red and blue flashes (with -1.0 and -3.3 log cd.s/$m^2$ flash strengths, respectively) suggests that this difference may reflect the cone contribution to the dark-adapted ERG (the x-wave). Although this positive deflection was present in all ERGs recorded in control dogs, there was great variability in both the amplitude and appearance of the deflection (Figure 4.2). This x-wave response is small even in control dogs, which is not unexpected given the relatively low-amplitude responses seen in the white-flash photopic ERG series.

Using the results of chromatic matching in control dogs, we devised a short protocol consisting of a single red and blue flash with -1.0 and -3.3 log cd.s/$m^2$ stimulus strengths, respectively. Overlaying these responses in a *PDE6A*$^{-/-}$ dog, a model of cone-driven function, demonstrated a small response to the red flash stimulus and no response to the blue flash. In the *CNGB*$^{*/del}$ dog, a model of rod-driven function, the red flash b-wave had a substantially lower amplitude than that of the blue flash and had no discernible x-wave response (Supplemental Figure 4.S2).

Comparison of control to *PDE6A*$^{-/-}$ dog responses in the red-flash ERG further supports the presence of a small x-wave in control dogs. Overlaying responses between control and *PDE6A*$^{-/-}$ dogs shows that the leading edge of the cone-mediated b-wave in the *PDE6A*$^{-/-}$ dogs closely aligns with the positive deflection preceding the rod-mediated b-wave seen in control dogs (Figure 4.3). This similarity was particularly noticeable in response to dimmer red flash stimuli, such as -1.0 log cd.s/m$^2$, when there was greater separation between the cone-driven x-wave and rod-driven b-wave (Figure 4.3A). Note that both the a- and b-waves of the *PDE6A*$^{-/-}$ dogs are somewhat slower than those of controls. This is consistent with the timing differences seen when comparing both dark- and light-adapted ERGs recorded from young *PDE6A*$^{-/-}$ dogs with those from light-adapted young control dogs [unpublished findings].

Using ANCOVA to compare linear regressions of the matched red and blue flash parameters in control dogs, there was a small but statistically significant difference between the peak time of the b-waves, with the red having a shorter peak time (Figure 4.3E blue and red tracings) (ANCOVA F-test: $\tau$=5.67±1.994; F=2.84, *p*-value=0.016). The peak time of the a-wave was not assessed due to intrusion of the cone-driven response. We performed further analysis of the latency, peak time, slope, and amplitude of the rod- and cone-driven recordings in the control dogs and the responses (predominantly cone-driven) in the *PDE6A*$^{-/-}$ dogs (Figure 4.3C-F). In the *PDE6A*$^{-/-}$ dogs, weak flash stimuli elicited a cone-driven component with a single peak, but with stronger flashes additional peaks were visualized (red tracings, Figure 4.3A-B). In control dogs, the cone-driven components became overwhelmed by the growth of the rod-driven a-wave and earlier onset of the rod-driven b-wave with increasing luminance (Figure 4.3A-B). For accurate analysis, we restricted direct comparisons to the leading slope of the cone-driven x-wave. Using ANCOVA to compare the slope, amplitude, and peak time of this first limb between control and

*PDE6A*$^{-/-}$ dogs demonstrated no significant differences in the means of tested parameters (Figure 4.3C-F).

A- and b-wave amplitudes change at different rates depending on background luminance (Figures 4.4-4.5).

The stimuli in this protocol were chosen so in the dark-adapted eye the weakest flashes result in rod responses and with increasing flash strength mixed rod and cone responses are obtained. This protocol was performed in both control and *PDE6A*$^{-/-}$ dogs (Figure 4.5). In dark-adapted recordings, the Naka-Rushton function models the first leg of the increase in b-wave amplitudes with increasing stimulus strength, up to a semi-saturation parameter $V_m$. A second leg of the response, also characterized by semi-saturation kinetics, follows this inflection point. Our previous studies of normal dogs have suggested that this inflection point is typically reached between 0.1 and 0.5 cd.s/m$^2$ with white flashes and no background light. Given the choice of stimuli near the inflection point, the b-wave responses were well-approximated as a linear function of amplitude vs log stimulus (Supplemental Figure 4.S3).

The approximation of a- and b-wave responses with a linear function (of the form amplitude = slope * stimulus strength + intercept) provided a good fit across all the tested background conditions in control dogs (Figure 4.5A-B). This enabled a comparison of both slope and intercept parameters, with the slope (with units of μV per log cd.s/m$^2$) representing the gain in amplitude relative to log-stimulus and the intercept (the response to flash strength of 0 log cd.s/m$^2$, with units of μV) the vertical shift in response for each background (Tables 4.1-4.2).

The intercept value sets the baseline for a- and b-wave amplitudes (the difference between a- and b-wave intercepts is the 'gain' with stimulus strength 0 log cd.s/m$^2$), while the slope value establishes the gain in amplitude with increasing stimulus strength. There were

significant differences in both parameters across all background luminance, most notably in the intercept parameter. These changes were particularly striking across the three dimmest luminance and will be discussed in more detail below. The responses of the *PDE6A*$^{-/-}$ dogs did not follow the same approximate linear relationship and could not be modeled in the same way as controls.

Another area of investigation with this protocol was the relative changes in cone-driven responses to increasing background luminance. These changes were studied by examining the responses in *PDE6A*$^{-/-}$ dogs which have no rod function. Although analysis of these responses could not compare direct interactions between rods and cones, it did enable characterization of saturation kinetics of isolated cone photoreceptors and postreceptoral pathways. In these dogs, a- and b-wave amplitudes were remarkably consistent across all background luminances, albeit with a slight decrease in b-wave amplitude for stronger flashes on the strongest background Figure 4.5A2). As such, the b:a ratio in these dogs remained largely similar, in contrast to control dogs who exhibited substantial decreases in gain from a-wave to b-wave increasing from 0 to 1 cd/m$^2$ background luminance (Figure 4.5C). The b:a ratio was flat in the control group at 10 cd/m$^2$ and the response is likely driven predominately by cones. However, in control dogs with stronger flashes (above -0.5 log cd.s/m$^2$) on the 1 cd/m$^2$ background the b:a ratio declined similarly to the weaker backgrounds, which may reflect remaining rod contributions.
The constant luminance, increasing frequency flicker ERG demonstrates the transition from rod to cone-driven responses. Measured amplitudes of both flicker protocols were well-approximated with nonlinear equations. (Figures 4.6-4.9).

We recorded ERGs in responses to a constant stimulus strength (3.2 cd.s/m$^2$), delivered at increasing frequency in both control and *PDE6A*$^{-/-}$ dogs (Figure 4.6). The dark-adapted response

in the control dogs (that have both rod and cone function) had high amplitudes at low frequencies. Response amplitudes decreased with progressively higher frequency, reaching a plateau after about 7 Hz. The plateau in amplitude reduction with increasing frequency suggest that rods were no longer able to recover between flashes or had become light-adapted (Figures 4.6A1, 4.7A, black tracing). However, even after the plateau the dark-adapted amplitudes were slightly higher than those in the light-adapted series (compare Figure 4.6A1 and 4.6B1 – noting the scale difference - and see Figure 4.7A inset). The response amplitude in the photopic flicker series in normal dogs were similar across the range of frequencies tested (Figures 4.6B1, 4.7A red tracing). In contrast to the normal dogs the response amplitude of *PDE6A*$^{-/-}$ dogs (cone only responses) in the dark-adapted series was similar across the range of flickers used (Figures 4.6A2, 4.7B). Similar to the light-adapted normal dogs, the amplitude in the light-adapted flicker series of *PDE6A*$^{-/-}$ dogs was similar across all tested frequencies. However, the light-adapted series amplitudes were slightly lower than the dark-adapted series (compare Figures 4.6A2 and 4.6B2 – noting the scale difference - and Figure 4.7B). The small but persistent difference in amplitudes between dark- and light-adapted cone responses in the *PDE6A*$^{-/-}$ dogs as well as the control dogs above 7Hz, may reflect a reduction of the dark current in cones due to the 30 cd/m$^2$ background luminance in light-adapted conditions (Figure 4.7A-B). We also noted a difference in the shape of the light-adapted series waveforms between controls and *PDE6A*$^{-/-}$ dogs, with the latter showing broader peaks and absent post-peak negativity (Figure 4.6B1-2).

The decline in amplitude of the dark-adapted ERG of control dogs (Figure 4.7A) is well-approximated by a negative exponential function of the form a*e^bx+c. The a parameter scales the response to its maximal value and reflects the b-wave amplitude with 0.5 Hz flashes and b is a function of the rate of change and reflects the decline in amplitude with progressively higher

frequency flashes. The c is parameter is likely driven by dark-adapted cones and shifts the model upward by the constant amplitude seen in the light-adapted ERG as well as the difference between dark- and light-adapted cones (Figure 4.7C). For this model, parameters were: a = 189.3 µV; b = -0.537 $Hz^{-1}$; c = 32.9 µV

We additionally recorded ERGs in control and *PDE6A*$^{-/-}$ dogs using a constant flash frequency (6 Hz) and increasing stimulus strength (Figure 4.8). In control dogs, both the initial increase and subsequent decrease in flicker amplitude with increasing luminance (Figure 4.8A1) can be modeled by semi-saturation kinetics. Both of these findings are interesting, as they suggest that the Naka-Rushton equation traditionally fit to the first limb of the single flash dark-adapted ERG ERG b-wave luminance:response series is also suitable for the rod component of the luminance:response plot dark-adapted ERG b-wave from a slow flicker series. Furthermore, this suggests that the initial increase in rod-mediated amplitude and, with progressive light-adaptation, decrease in the dark-adapted ERG 6 Hz ERG series, follows semi-saturation kinetics. The *PDE6A*$^{-/-}$ dog 6 Hz luminance:response series indicates that cone responses are similar in both dark- and light-adapted conditions (Figure 4.9B), with the light-adapted responses tending to have a lower amplitude as found with the responses of increased flicker frequency with a set luminance described above.

At 6 Hz frequency, the peak dark-adapted ERG amplitude occurred between -2 and -1 log cd.s/$m^2$ flash stimulus (Figure 4.9A). The increase in amplitude was approximated with model parameters $V_m$ = 99.13 µV, K = 0.0043 cd.s/$m^2$, and n = 0.888, while the decrease in amplitude was approximated with model parameters $V_m$ = 72.21 µV, K = 0.271 cd.s/$m^2$, and n = -0.693 (with an additional additive vertical shift of 26 µV, reflecting the amplitude of cone-driven responses with higher stimulus strength) (Figure 4.9C). Furthermore, the light-adapted ERG

amplitude increase could be modeled with parameters $V_m$ = 21.21 µV, K = 1.592 cd.s/$m^2$, and n = 1.138 (Figure 4.9D). These results suggest that the decline in dark-adapted ERG amplitudes (driven by rod saturation with progressively stronger flashes) is somewhat offset by an increase in the cone-driven response.

**4.4. Discussion**

In this study, we tested three different ERG techniques to further assess canine retinal function. We showed that selection of matched red and blue flashes can be achieved through Naka-Rushton fitting of the b-waves. We used this method in addition to comparison to dogs with no detectable rod function (*PDE6A*$^{-/-}$) to demonstrate that rod- and cone-driven contributions to the dark-adapted b-wave can be temporally separated and assessed by comparing responses from one red flash and blue flash. We also showed that blue-background ERGs can be used to quantify the differential effects of background light on the response and saturation of rod photoreceptors and rod bipolar cells. We used expanded flicker protocols to demonstrate that cone response amplitudes are similar with flash frequency under 30 Hz whereas rod responses predominate up to about 7 Hz. Finally, we fit models to the amplitude of flicker responses in control dogs; the response to constant luminance, increasing frequency dark-adapted ERG can be modeled with a negative exponential function, whereas the constant frequency, increasing luminance dark- and light-adapted ERG follow Michaelis-Menten type saturation kinetics.

The selective use of red and blue flashes reveals a dark-adapted cone-driven response known as the x-wave. The x-wave is elicited by red flash stimuli and has been demonstrated in humans and other species such as rats and monkeys. It is used to characterize the dark-adapted ERG, with normal x-waves and absent b-waves in diseases such as Oguchi disease, and normal b-waves and absent x-waves in diseases such as protanopia and complete achromatopsia

[187,219,220]. The x-wave has also been described in the past in ERG studies of dogs and used to characterize dogs with either rod or cone dystrophy. However, these studies either measured the x-wave early during dark-adaptation [191,192,194] or did not demonstrate complete temporal separation of rod- and cone-driven components in the fully dark-adapted dog [193].

We demonstrated that identification and isolation of the dark-adapted cone-driven x-wave is possible in dogs using sufficiently dim red stimuli. We found significantly earlier peak times in the b-waves with red stimuli compared to blue, which may reflect cone-driven contributions to the dim red flash response. Additionally, we found that using a single red flash with strength -1.0 log cd.s/$m^2$ and blue flash with strength -3.2 log cd.s/$m^2$ is sufficient to elicit the x-wave and temporally separate dark-adapted rod and cone responses in dogs and could be easily incorporated into any dark-adapted ERG protocol for assessment of dark-adapted cone function (Supplemental Figure 4.S2).

Psychophysical studies of human vision show that humans have similar ability to discriminate across multiple magnitudes of background illumination. The remarkable adaptability of the visual response depends on a gain control mechanism, which prevents saturation of post-receptoral responses to rod-mediated signaling [221–224]. In dogs, we show that the photoreceptor-driven a-wave remains remarkably consistent across dim background lighting conditions (between 0 and 0.1 cd/$m^2$), while the bipolar cell-driven b-wave experiences a significant decrease in amplitude with the introduction of even dim background luminance (see Figure 4.5). These findings agree with those in humans and provide additional insight to the change in response characteristics of photoreceptors and second-order neurons when exposed to progressively brighter background light [17,74,105].

Linear regression models were used to fit the a- and b-wave amplitudes of the blue-background ERG of control dogs and enabled direct comparison between parameters (see Tables 4.1 and 4.2). The slope and intercept parameters for the b-wave declined more sharply than those of the a-wave for blue backgrounds between 0 and 0.1 cd/m$^2$ luminance. The relative difference in intercept parameter, which represents the overall sensitivity of the response, and the slope parameter, which reflects the increase in response amplitude with stronger flash stimuli, may reflect a gain-control mechanism from rods to bipolar cells to prevent response saturation. Additionally, the relationship between the linear regression models of the a- and b-wave amplitudes and their changes relative to background luminance provide a normative baseline for quantification and assessment of retinal responses to ERGs recorded with increasing background luminance with flash stimuli between 0.01 and 2.5 cd.s/m$^2$.

In the *PDE6A*$^{-/-}$ dogs, the absence of rod function enabled characterization of cone-driven responses to increasing background luminance. In these dogs, a-wave responses, although very small in amplitude, were remarkably consistent irrespective of background light. This indicates that cone photoreceptors adapt and respond similarly across a wide range of lighting conditions. Furthermore, there was no significant difference in the a-wave amplitudes in these dogs at any background luminance, and a slight decrease in b-wave amplitudes only with the brightest background luminance. These findings suggest that cone ON- and OFF- bipolar cells may experience similar saturation kinetics as rod bipolar cells, albeit with a higher threshold for changes to be seen. However, cone responses exhibit a ‘photopic hill’ effect whereby cone-driven b-wave amplitudes decrease with increasing stimulus strength, potentially reflecting a relative shift in signaling from the ON pathway to the OFF pathway (i.e. the ‘push-pull’

mechanism) or temporal separation of the ON and OFF responses, and this may contribute to these findings [73,202,203].

The use of flicker stimuli provides a better characterization of how rod- and cone-driven responses change as a function of altered temporal stimulation. As the interstimulus interval shortens with increasing flash frequency it reaches a stage that the slower responding rods cannot recover between flashes (and also likely lose their dark-adapted state). In our study, we found that rod responses in dogs predominate with stimuli up to about 7 Hz (Figure 4.8), in agreement with findings in other species such as mice [22]. Additionally, we found that cone-driven responses are similar across a wide range of frequencies, with comparable amplitudes in the photopic ERG between 0.5 and 30 Hz stimuli. We did note a difference in the shape of the waveforms in the photopic ERG (Figure 4.6B1-2). With lower frequency flashes, control dogs had a large cornea-negative deflection similar in appearance to the photopic negative response (PhNR), which is thought to derive from ganglion cells with possible amacrine cell contributions [109,225]. This negative component declined with higher frequency flickers, perhaps reflecting reduced ganglion cell recovery or masking of the response (due to shorter interstimulus interval). This negative response was not seen in *PDE6A*$^{-/-}$ dogs, which may be attributable to differences seen in the single flash photopic ERG (including a wider b-wave and attenuated a-wave).

Additionally, we provided baseline mathematical models of the amplitude changes seen in two flicker protocols in phenotypically normal dogs. In *PDE6A*$^{-/-}$ dogs, the amplitudes in the light-adapted compared to the dark-adapted ERG at all frequencies with higher flicker frequency (7-30 Hz) in control dogs. This may reflect a difference in basal activity of cone photoreceptors and bipolar cells, as well as differences in inner retinal contributions to the overall recorded waveform, but without a notable impact on the cone recovery [201,226,227].

In the future, detailed assessment of the relative contributions of different rod pathways (through rod bipolar cells, gap junctions with cones, and direct synapses with cone OFF-bipolar cells) with increasing background luminance could be performed through the use of long duration flashes to separate ON and OFF components, or with selective pharmacologic blockade of ON- or OFF-bipolar cell responses (using L-AP4 and PDA, respectively) [39,40]. The transition between cone ON- and OFF-bipolar cell contributions at different flicker frequencies could also be assessed with selective pharmacologic blockade. Additionally, analysis of the range at which cones can maintain similar amplitudes using frequencies higher than the 30 Hz used in this study would provide a further method for characterization of abnormal retinal function in dogs. Also of interest would be analysis of pure photoreceptor contributions to the flicker ERG responses, perhaps through the use of dog models of congenital stationary night blindness.

In this study, we designed protocols to separate and better characterize rod and cone contributions to the canine ERG. We measured responses to these protocols in both phenotypically normal control dogs and *PDE6A*$^{-/-}$ dogs as a model of cone-only function. Using these protocols, we preferentially stimulated isolated photoreceptor responses and provided further insight into the separate contributions of rods and cones in the dark- and light-adapted ERG. Additionally, we showed how rod and cone responses vary with stimulus frequency as well as background luminance. Finally, we showed how the inclusion of a single red and blue flash in the dark-adapted ERG could be of use in ophthalmological clinics to test dark-adapted cone function.

# APPENDIX

| Background ($cd/m^2$) | b-wave slope ($\mu V/log\ cd.s/m^2$) | b-wave intercept ($\mu V$) | a-wave slope ($\mu V/log\ cd.s/m^2$) | a-wave intercept ($\mu V$) |
|---|---|---|---|---|
| 0 | 31.77±2.04 | 181.37±1.92 | 49.17±1.92 | 67.66±1.27 |
| 0.01 | 24.78±1.06 | 90.83±0.99 | 45.85±2.67 | 58.68±1.77 |
| 0.1 | 11.45±0.92 | 30.27±0.86 | 31.00±2.10 | 39.35±1.39 |
| 1 | 4.07±0.48 | 9.82±0.45 | 6.11±1.36 | 7.41±0.90 |
| 10 | 8.08±0.87 | 14.06±0.82 | 1.86±0.28 | 3.30±0.19 |

**Table 4.1. Parameters of linear regression model of a- and b-wave amplitudes in control dogs by background luminance.**

| Background ($cd/m^2$) | b-wave slope | a-wave slope | b-wave intercept | a-wave intercept |
|---|---|---|---|---|
| 0 | 100±6.4 | 100±3.9 | 100±1.1 | 100±1.9 |
| 0.01 | 78±3.3 | 93.2±5.4 | 50.1±0.5 | 86.7±2.6 |
| 0.1 | 36±2.9 | 63±4.3 | 16.7±0.5 | 58.2±2.1 |
| 1 | 12.8±1.5 | 12.4±2.8 | 5.4±0.2 | 11±1.3 |
| 10 | 25.4±2.7 | 3.8±0.6 | 7.8±0.5 | 4.9±0.3 |

**Table 4.2. Percent change in parameters of linear regression model of a- and b-wave amplitudes in control dogs by background luminance, relative to values with no background light (0 $cd/m^2$).**

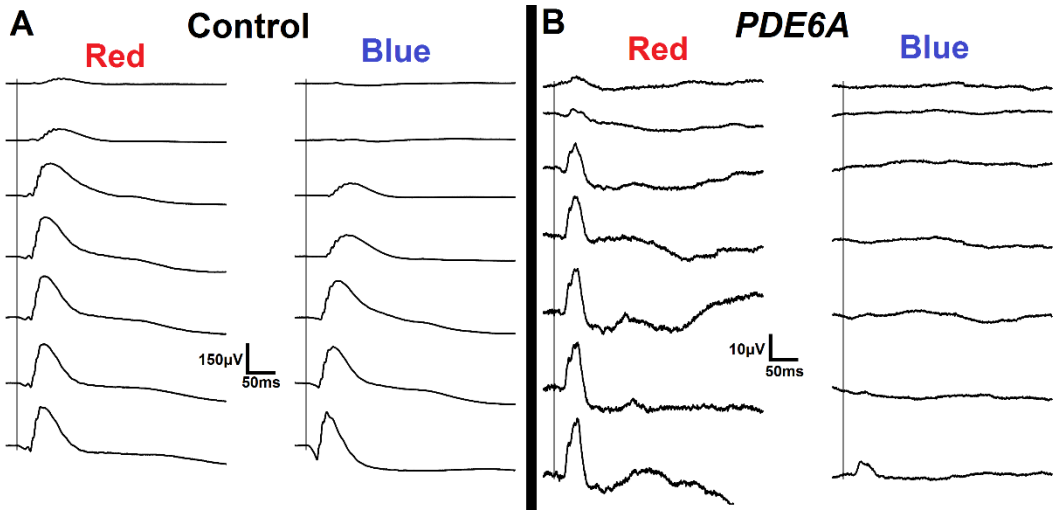


**Figure 4.1. Representative chromatic dark-adapted ERG tracings**

Red and blue flash dark-adapted ERG montage of a control dog (A) and *PDE6A*$^{-/-}$ dog (B). Red stimulus flash strengths ranged from -1.3 to 0.4 log cd.s/m$^2$ and blue stimulus flash strengths ranged from -4.3 to -1.3 log cd.s/m$^2$. Note the scale difference between A and B.

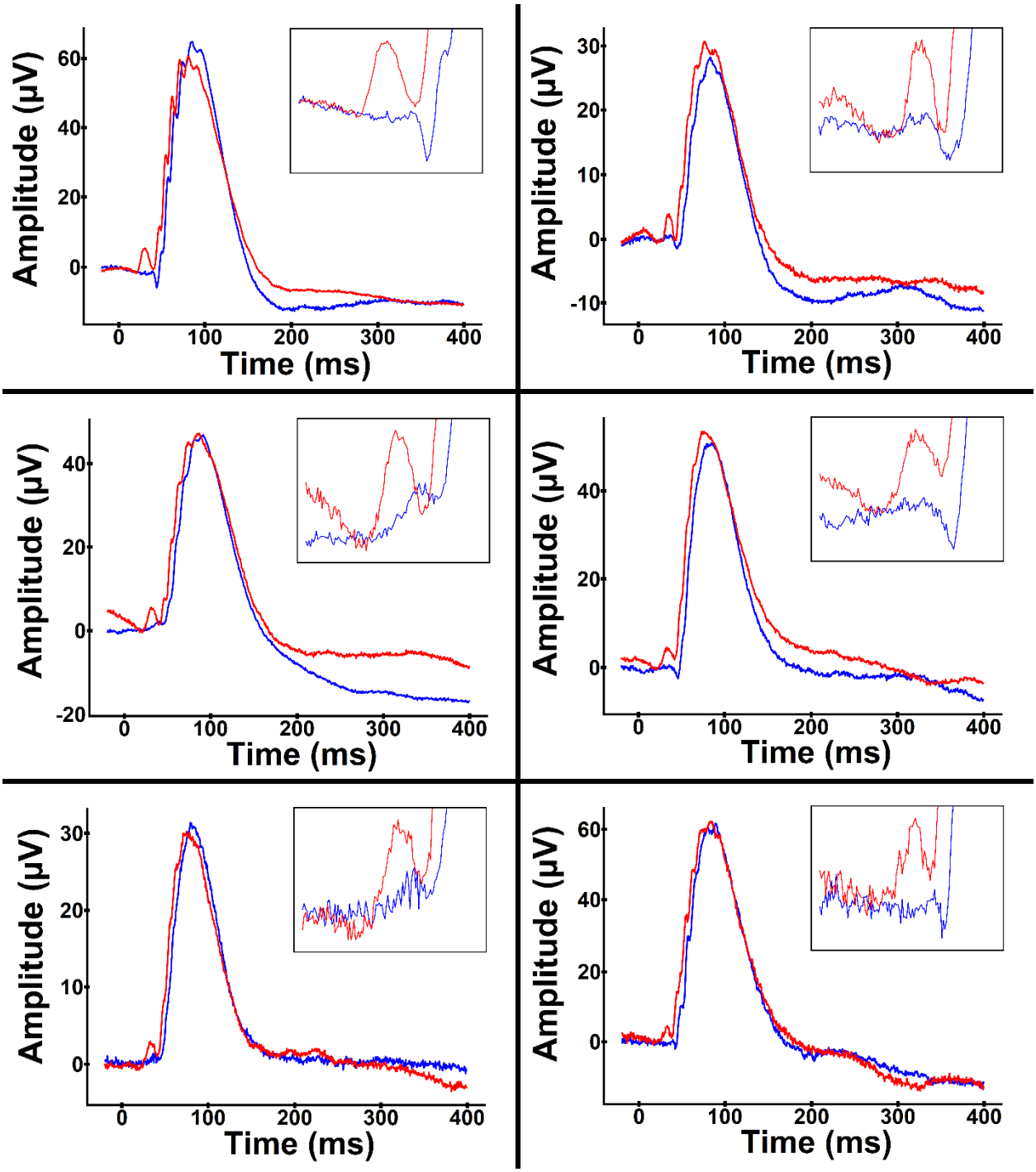


**Figure 4.2. Dark-adapted ERGs as a result of matched red and blue flashes in control dogs**

A single red flash with strength -1.0 log cd.s/$m^2$ and blue flash with strength -3.2 log cd.s/$m^2$ were used for comparison. Although the appearance differed between dogs, a small positive deflection was noted preceding the rod-driven b-wave in all dogs. This likely represents the dark-

**Figure 4.2. (cont'd)**

adapted cone-driven response to red flash stimulus known as the x-wave. Tracings recorded from six different dogs are shown, with magnification of the responses preceding the rod-driven b-wave shown in the inserts.

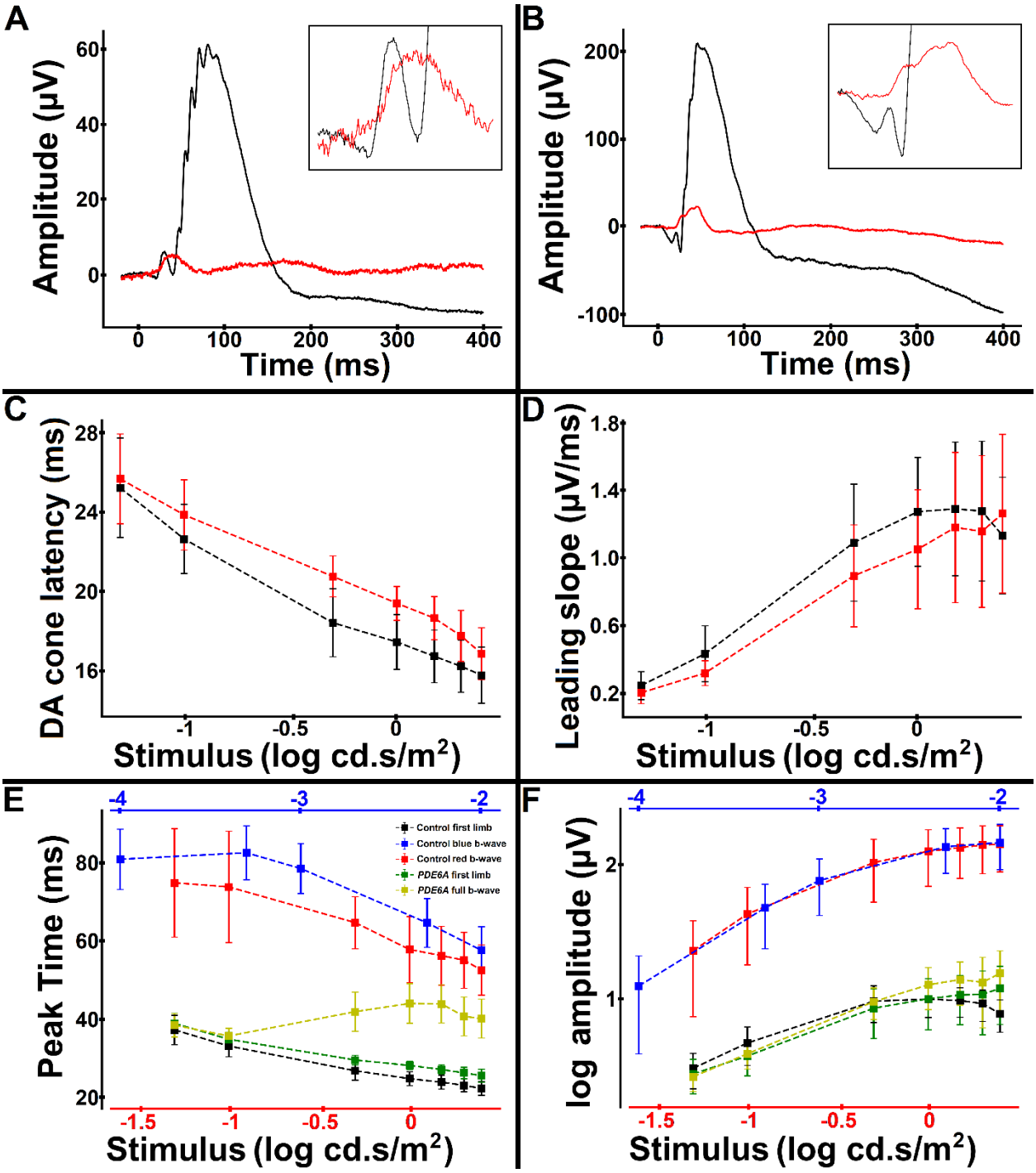


**Figure 4.3. Comparing red and blue flash ERG responses in control and *PDE6A* dogs**

Comparison of responses to a -1.0 (A) and 0.4 (B) log cd.s/m$^2$ red flash stimulus of a control dog (black) with a *PDE6A*$^{-/-}$ dog (red). With dimmer flashes, the slope, amplitude, and latency of the small deflection that appears before the leading edge of the rod b-wave in the control dog

**Figure 4.3. (cont'd)**

matches those of ascending limb of the b-wave in the *PDE6A*$^{-/-}$ dog. With stronger flashes, the leading edge of the positive deflection preceding the b-wave in the control dog (the x-wave) was somewhat masked by the growing a-wave, while the cone-driven b-wave response following the leading edge was masked by the rod-driven b-wave. Magnification of the cone-driven responses is shown in the insert.

Average latency (C) and slope (D) of the x-wave (control dogs, shown in black) and b-wave (*PDE6A*$^{-/-}$ dogs, shown in red) vs. stimulus strength with red flash stimulus.

Comparison of average peak time (E) and amplitude (F). The stimulus strength used for the blue flashes is shown above the graph, and those for the red flashes are below the graph. The comparisons between the two flashes were based on the difference of the Naka-Rushton K parameter. These figures denote the peak times (E) and amplitudes (F) of the rod-driven b-wave in control dogs in response to red and blue flashes (red and blue tracings, respectively), the leading edge of the cone-driven b-wave in control (black) and *PDE6A*$^{-/-}$ dogs (green), and the full cone-driven b-wave in *PDE6A*$^{-/-}$ dogs (yellow).

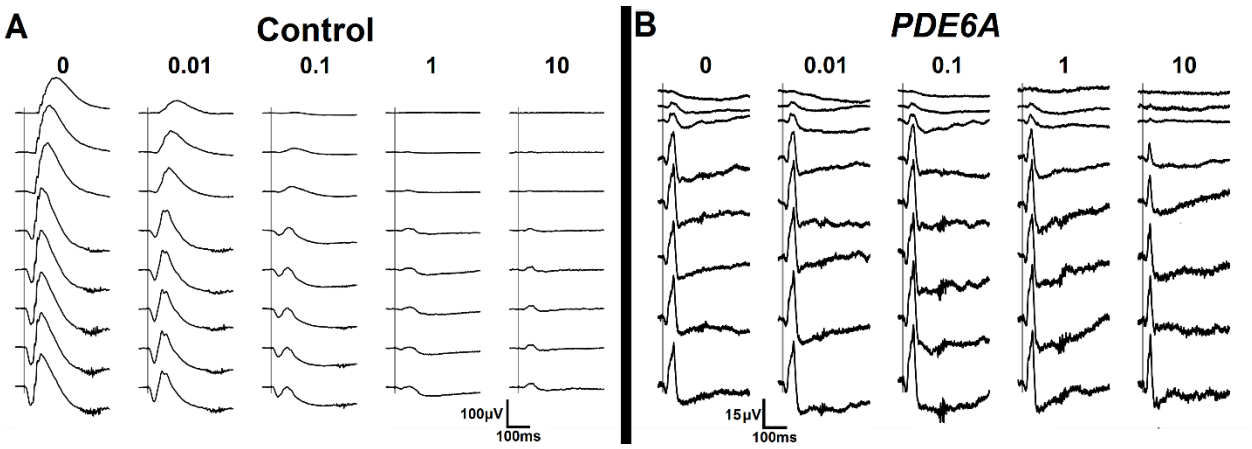


**Figure 4.4. Representative blue-background ERG tracings**

A. Blue background ERG montage of a control dog. White stimulus flash strengths ranged from -2 to 0.4 log cd.s/$m^2$. Background luminances, from left to right, were 0 cd/$m^2$ (dark-adapted), 0.01 cd/$m^2$, 0.1 cd/$m^2$, 1.0 cd/$m^2$, and 10 cd/$m^2$.

B. Blue background ERG montage of a *PDE6A*$^{-/-}$ dog. Note the smaller scale of response amplitude. A-wave amplitudes were similar for all background luminances, while b-wave amplitudes had a small decrease with the strongest background.

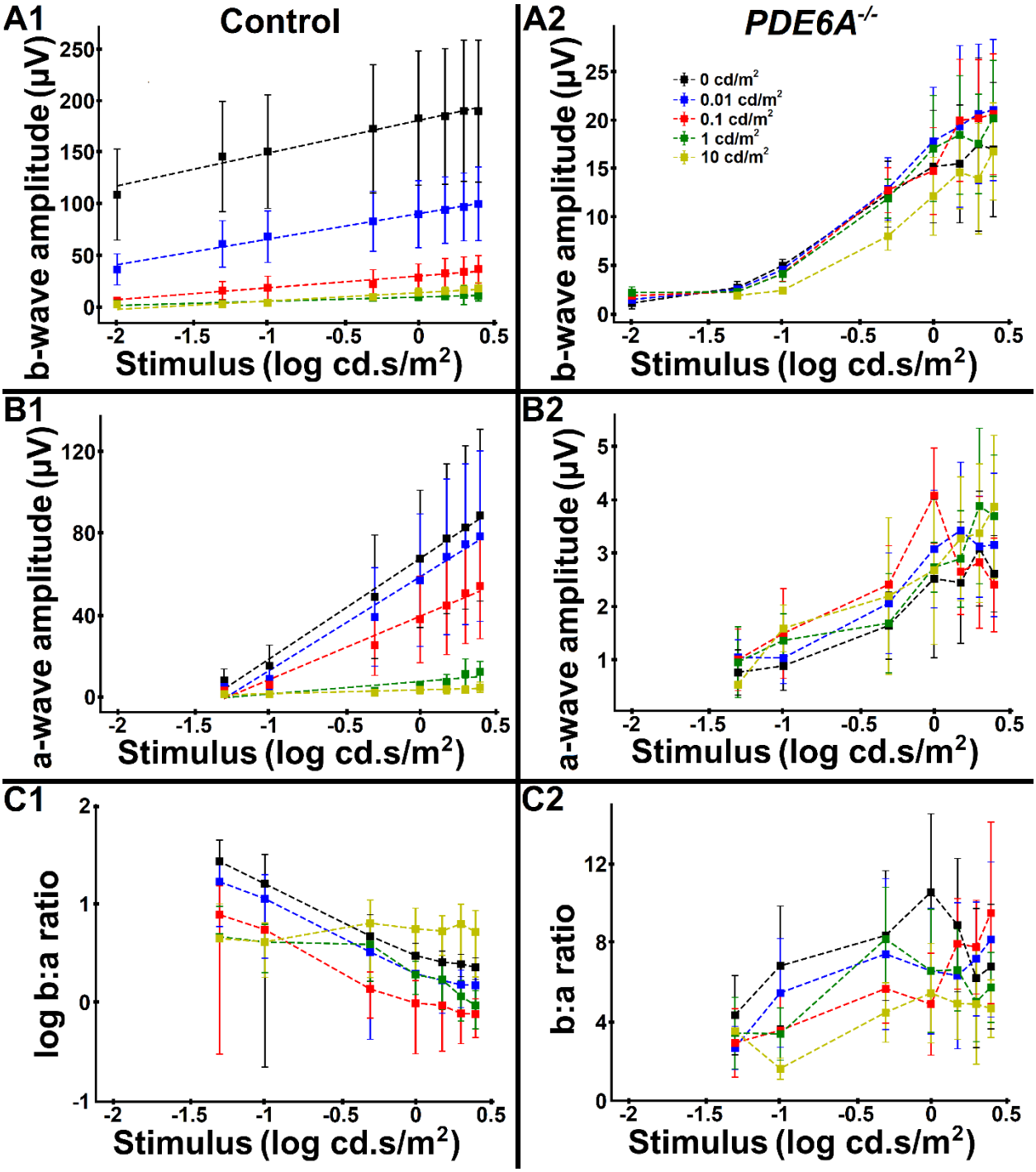


**Figure 4.5. Blue-background ERG measurements and models**

Responses for control dogs are shown in the first column (column 1) and responses for *PDE6A* dogs are shown in the second column (column 2).

**Figure 4.5. (cont'd)**

A. Mean b-wave amplitude vs. log stimulus strength by background luminance. In the control dog, the amplitude changes were well-modeled by a linear regression of b-wave amplitude vs. log stimulus strength.

B. Mean a-wave amplitude vs. log stimulus strength by background luminance. In the control dog, the amplitude changes were well-modeled by a linear regression of b-wave amplitude vs. log stimulus strength.

C. Mean b:a ratio vs. log stimulus strength by background luminance.

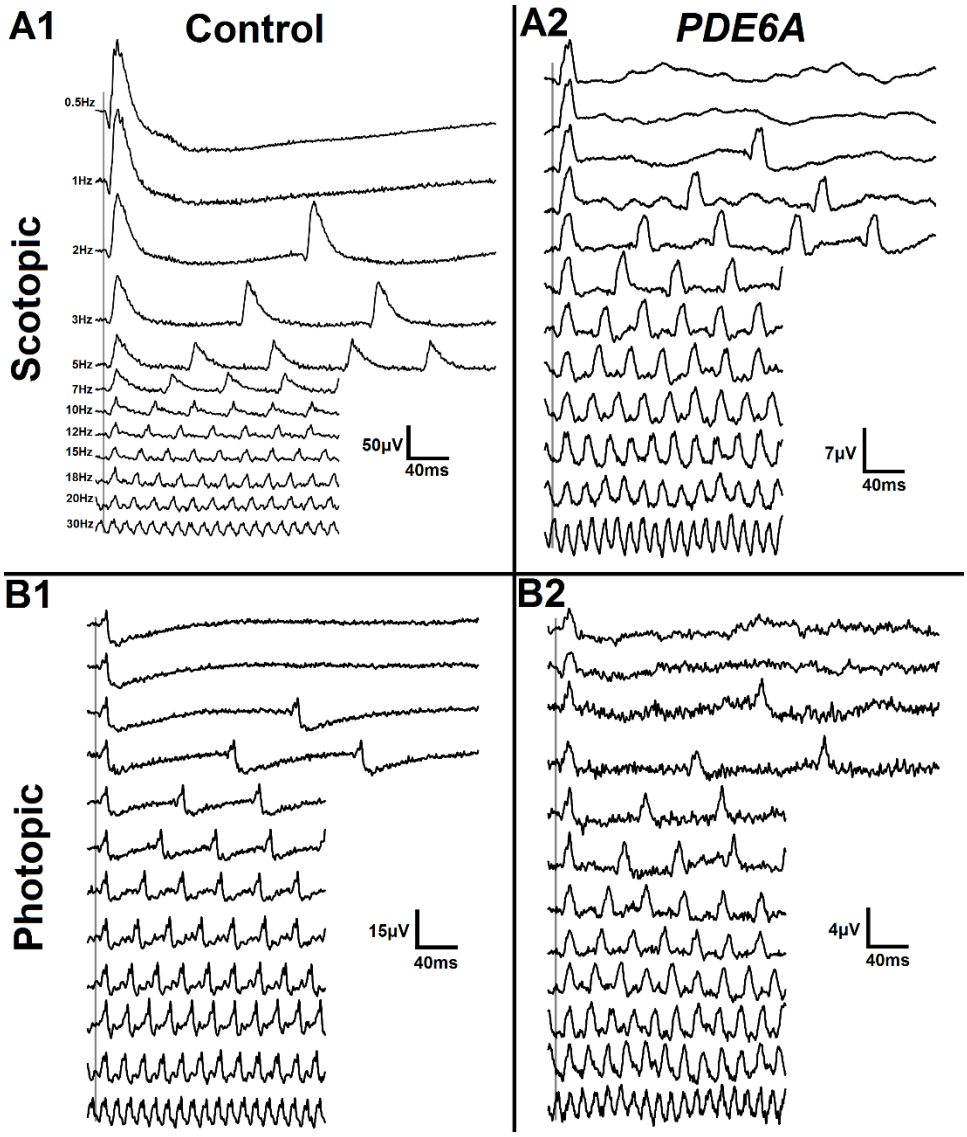


**Figure 4.6. Representative 3.2 cd.s/m$^2$ flicker ERG tracings**

Flash stimulus was held constant at 3.2 cd.s/m$^2$, and flash frequency varied from 0.5Hz to 30Hz. The first column (column 1) shows responses recorded from a control dog, and the second column (column 2) shows responses recorded from a *PDE6A* dog. The first row (row A) shows scotopic responses and the second row (row B) shows photopic responses.

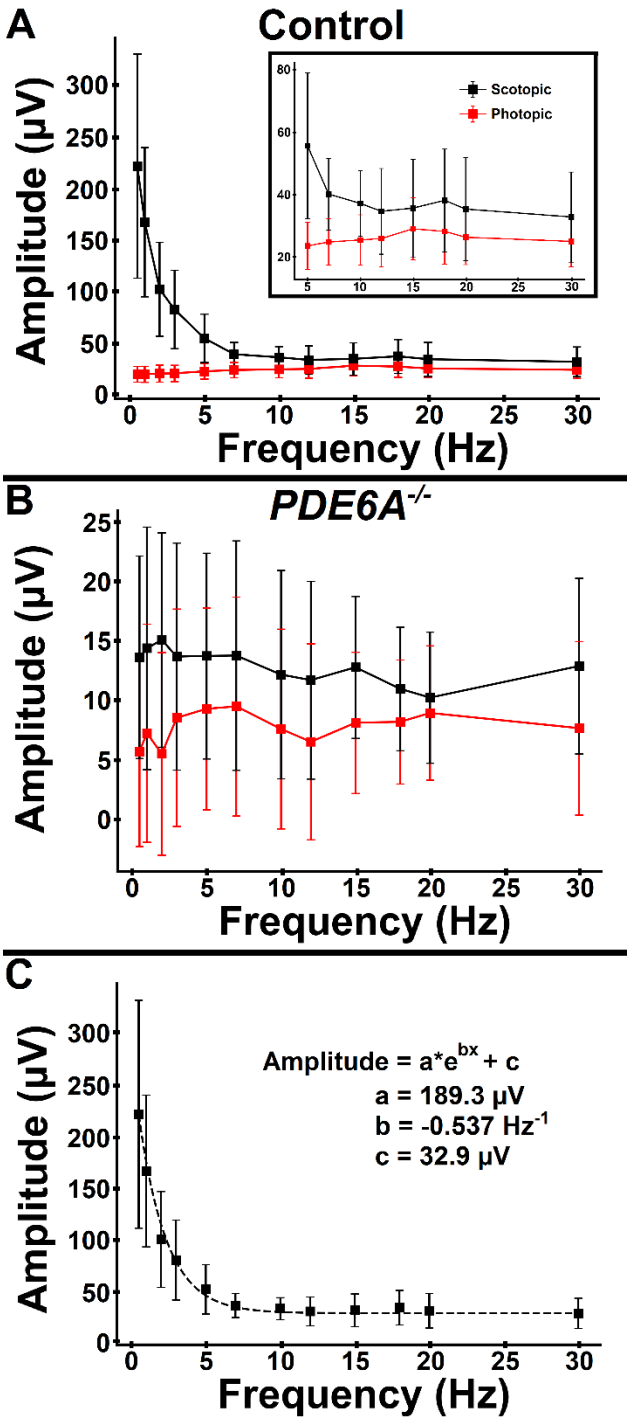


**Figure 4.7. 3.2 cd.s/m$^2$ flicker ERG measurements and models**

Comparison of dark- (black) and light-adapted (red) flicker amplitudes vs. flash frequency in the control (A) and *PDE6A* (B) dog. The inset in A shows the responses to frequencies between 5 and 30 Hz in the control dog. Above 7 Hz, the difference in amplitude was similar in both

**Figure 4.7. (cont'd)**

control and *PDE6A*$^{-/-}$ dogs.

C. The decline in amplitude of the dark-adapted flicker amplitude with increasing flash frequency in the control dog was well-modeled by a negative exponential function. The function and parameters are given in the inset.

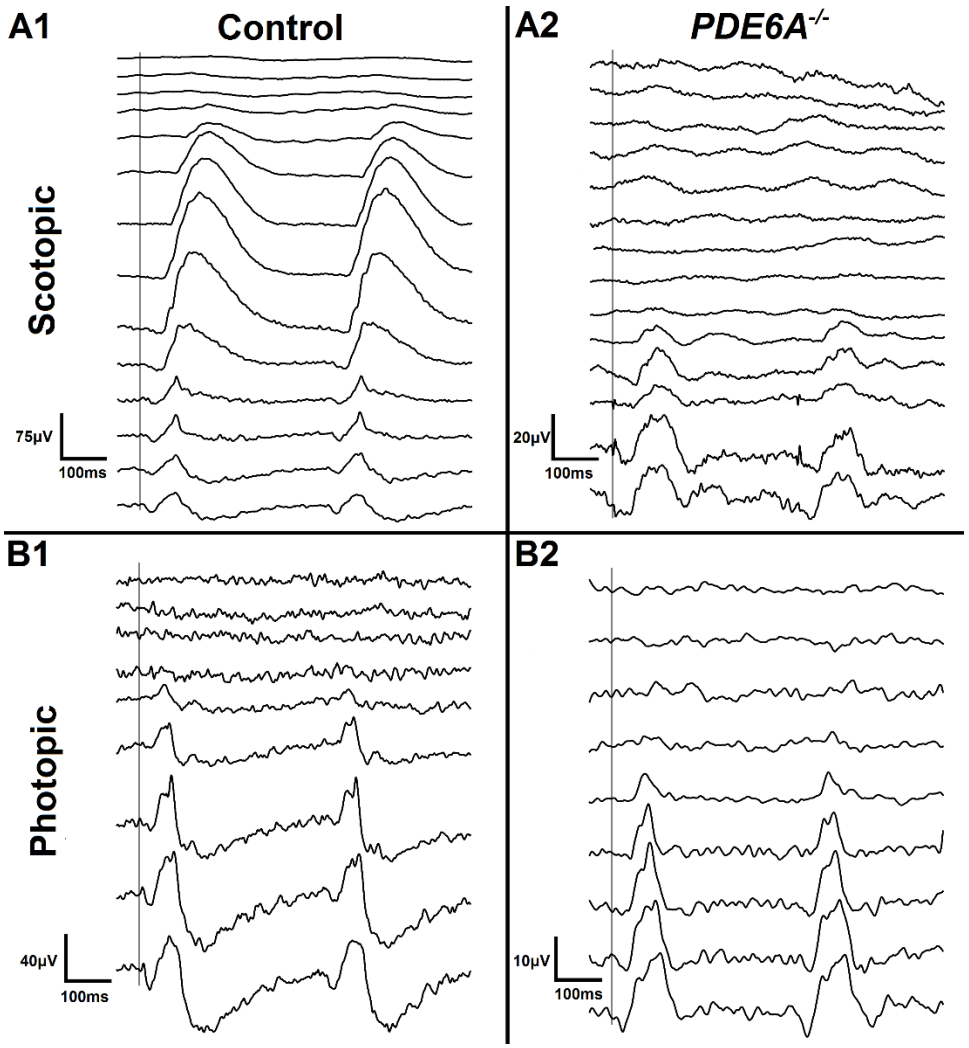


**Figure 4.8. Representative 6 Hz flicker ERG tracings**

Flash frequency was held constant at 6 Hz. The first column (column 1) shows responses recorded from a control dog, and the second column (column 2) shows responses recorded from a *PDE6A*$^{-/-}$ dog. The first row (row A) shows dark-adapted responses with stimulus strength varied from -4.9 to 1.5 log cd.s/m$^2$, and the second row (row B) shows light-adapted responses with stimulus strength varied from -2.5 to 1.5 log cd.s/m$^2$.

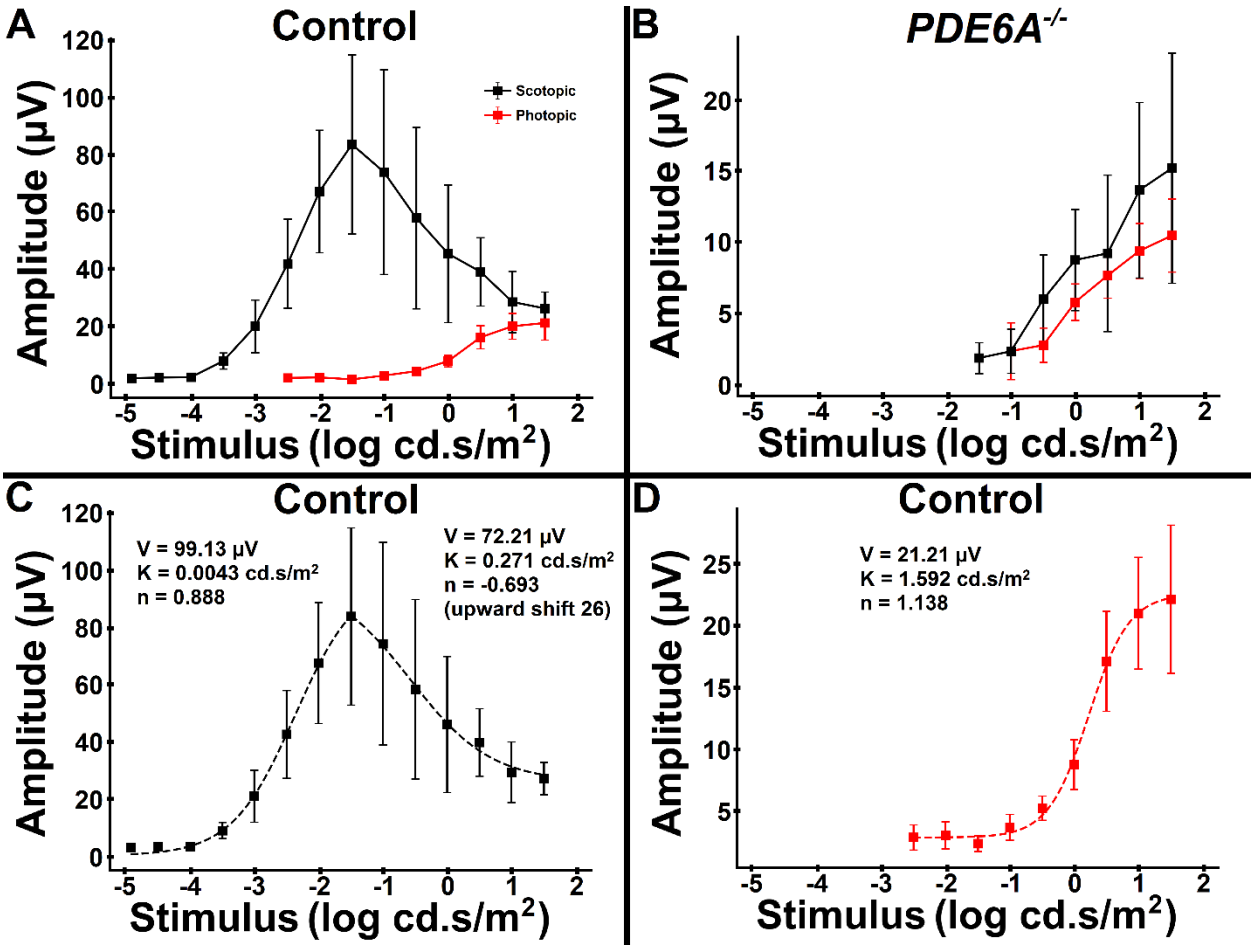


**Figure 4.9. 6Hz flicker ERG measurements and models**

A. Comparison of dark- (black) and light-adapted (red) flicker amplitudes vs. stimulus strength in the control dog.

B. Comparison of dark- (black) and light-adapted (red) flicker amplitudes vs. stimulus strength in the *PDE6A* dog.

C. The increase and subsequent decline in amplitude of the dark-adapted flicker amplitude with increasing stimulus strength in the control dog was well-modeled with a piecewise Michaelis-Menten equation. Parameters are given in the inset.

**Figure 4.9. (cont'd)**

D. The increase in amplitude of the light-adapted flicker amplitude with increasing stimulus strength in the control dog was well-modeled with a Michaelis-Menten equation. Parameters are given in the inset.

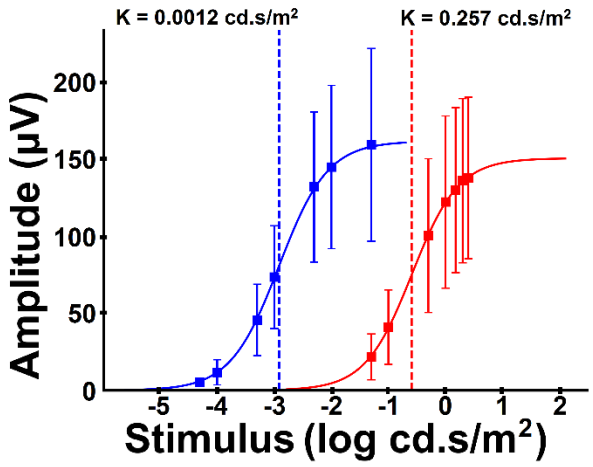


**Figure 4.S1. Matching of red and blue flash stimuli**

The figure demonstrates Naka-Rushton fitting of the red and blue flash b-wave amplitudes in control dogs. The half-saturation parameter K is given for each color and shown with the dashed lines.

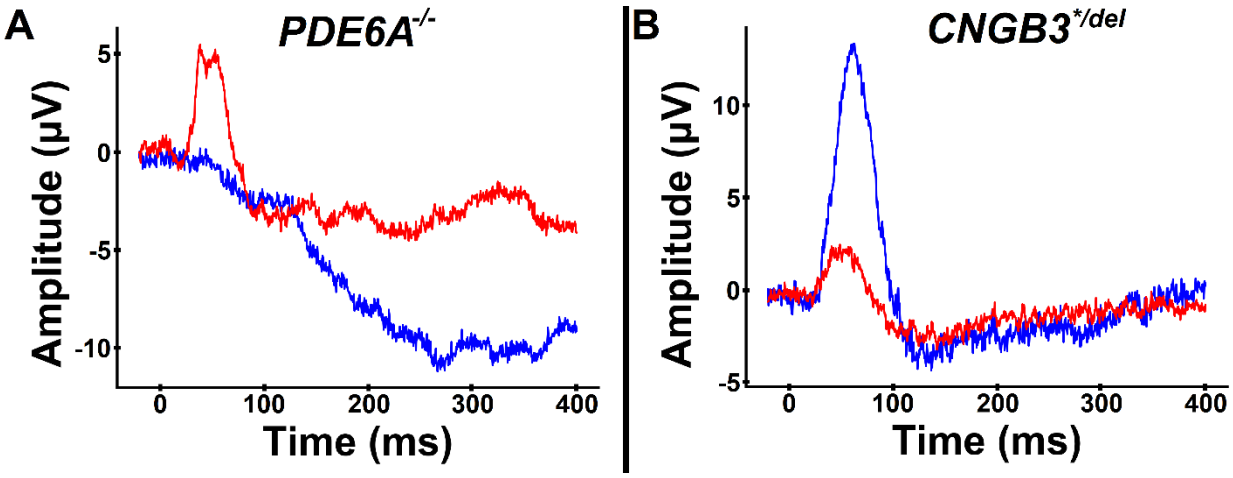


**Figure 4.S2. Representative chromatic dark-adapted ERG tracings in dogs with inherited retinal disease. A single red flash with strength -1.0 log cd.s/m$^2$ and blue flash with strength -3.2 log cd.s/m$^2$ were used for comparison**

A. Tracings from a *PDE6A* dog. There was no measurable response to the blue flash, as these dogs have little to no rod function and responses are cone-driven.

B. Tracings from a *CNGB3* dog, a model of complete achromatopsia. In these dogs, the amplitude of the red flash response is markedly reduced and there is no discernible x-wave, as these dogs have little to no cone function and responses are rod-driven.

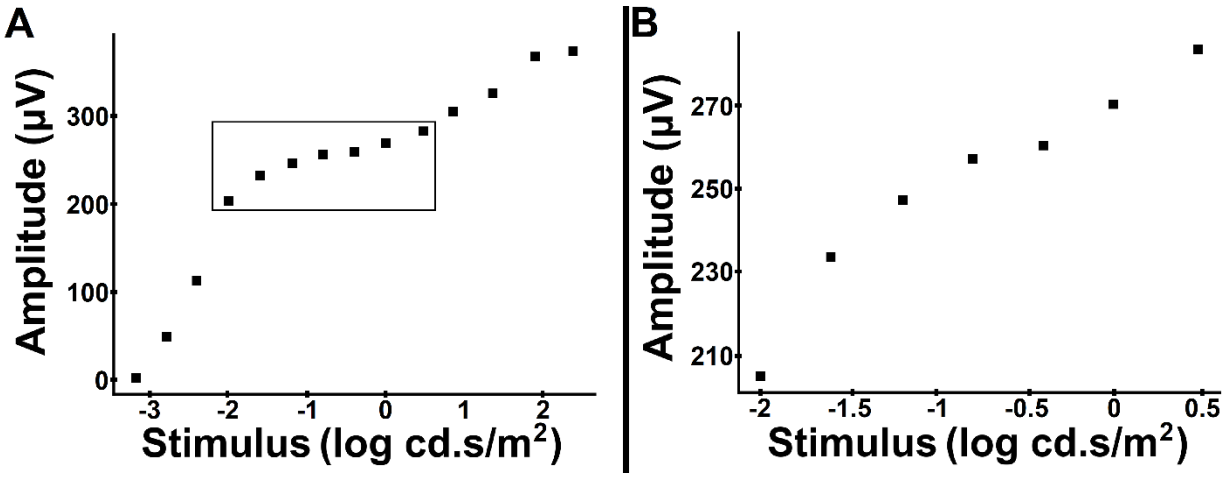


**Figure 4.S3. Luminance:response curve of b-wave amplitudes from a dark-adapted ERG recorded in a control dog**

White flash stimuli were presented on a dark background and repeated to generate an averaged response detectable against background electrical noise. The interstimulus interval was one second for weaker stimuli and progressively longer for stronger stimuli.

A. The typical luminance:response curve of the dark-adapted ERG demonstrates two separate ascending limbs to the left and right of an inflection point.

B. Magnification of the responses between -2.0 and 0.5 log cd.s/$m^2$. In this range, b-wave amplitude can be approximated as a linear function of log stimulus strength.

# CHAPTER 5.

# CHARACTERIZATION OF SCOTOPIC AND MESOPIC ROD SIGNALING PATHWAYS IN DOGS USING THE ON-OFF ELECTRORETINOGRAM

## 5.1. Introduction

The mammalian retina is uniquely equipped to process visual signals across a substantial range of luminances. In the dark, photoreceptors in the outer retina maintain a relatively depolarized state, with passive and active transport of cations in the outer segments causing an electrical current to flow along the length of the photoreceptor. In rods, this is known as the dark current [228–230]. In the dark-adapted retina, both rods and cones are able to respond to light stimulus; with weak light stimuli, the response is rod-driven – with stronger flashes, there is a mixed rod cone response. Progressive increases in background light desensitize and suppress the rod response, such that the light-adapted retinal response is cone-driven [15,231–233].

The visual signal is shaped by complex retinal processing that divides into two parallel pathways – ON and OFF. The separation of these pathways begins with ON and OFF bipolar cells, second order neurons in the retina that synapse with rod and cone photoreceptors [234–236]. Bipolar cells are classified based on their response to light stimulus of the photoreceptors – ON bipolar cells, including rod bipolar cells (RBCs), depolarize, whereas OFF bipolar cells hyperpolarize, in response to a light stimulus driven decrease in glutamate release from photoreceptor synaptic terminals [237,238]. The bipolar cell response is further shaped by photoreceptor pathways; cones synapse with both ON and OFF cone bipolar cells, whereas rods primarily interact with RBCs when responding to weak stimuli, but have additionally been shown to signal via gap junctions with cone photoreceptors as well as direct connections with OFF cone bipolar cells [239–243]. The alternative rod pathways are more prominent in mesopic conditions as well as in response to higher frequency flickering light stimuli [244–246].

The separation of flash On and Off responses with the full-field ERG provides a useful tool for the characterization of postreceptoral responses. The flash On and Off ‘responses’ are

separate from ON and OFF pathways. The On response is the retinal response to flash onset, beginning with photoreceptor hyperpolarization (generating the major portion of the a-wave) and leading to the depolarization of ON bipolar cells (which is the driver of the positive b-wave) as well as hyperpolarization of OFF bipolar cells (which has contributions to both the shape and amplitude of the a- and b-waves, particularly the early portion of the light-adapted a-wave in primates) [230,241,247–250]. In contrast, the Off response is the retinal response to stimulus offset, and is generated by several components – in humans, an initial rapid positive deflection (the d-wave) is generated primarily by OFF bipolar cells, but there are additional contributions from photoreceptors (return to a relatively depolarized state which results in a slow cornea-positive response) and ON bipolar cells (hyperpolarize, resulting in a fast cornea-negative response) [251–255]. With short-duration flashes these are merged in the ERG, and the recorded waveform reflect the combined contribution of these components. Additionally, short-duration flash cone responses exhibit a 'photopic hill' effect whereby cone-driven b-wave amplitudes reach a maximal level and then decrease and peak times lengthen with increasing stimulus strength. This occurs as the off pathway response slows and separates from that of the On pathway meaning the two responses are temporally separated rather than being superimposed [239–241].

The component waveforms of the ERG are shaped by 'processes' with contributions from different retinal cells (named PI/PII/PIII by Granit based on the order of disappearance under anesthesia) [256]. A major focus of this paper are the changes in response of PIII, which is driven by photoreceptors and is the primary contributor to the cornea-negative a-wave, and PII, driven mainly by ON bipolar cells (but additionally shaped by OFF bipolar cells) that heavily influences the cornea-positive b-wave. Note that PIII is present for the duration of a sustained flash and returns to baseline at flash offset, whereas PII differs at flash onset or offset based on the relative

contributions of the ON and OFF pathways [237,238,257]. These processes have been shown to further differ in humans and rats based on background luminance, with a greater decline in the amplitude of PII relative to the rod-driven PIII [249,258].

Interspecies differences have been shown in the ERG Off response (at flash offset). Two broadly different types of retinae have been identified in mammals based on the Off response and were first described by Granit and Therman in 1935 - the E-type retina in species such as the rat and mouse, and I-type retina of humans and other primates [251,253,259]. The I-type retina demonstrates relatively large photopic a-wave amplitude and a primarily positive d-wave (off response). In contrast, the E type retina demonstrates small photopic a-waves and a primarily negative d-wave (off response). Note that the aspartate-treated retina (which abolishes postreceptoral responses) demonstrates continued photoreceptor hyperpolarization, and a gradual return to baseline, in response to sustained flashes, and thus photoreceptors are unlikely to explain this difference in the Off response [260–263].

Few studies have addressed canine responses to the On-Off ERG, although they have been used in the study of some canine inherited retinal degenerations [264–267]. The dog exhibits the predominantly negative off response of the E-type retina [268]. Although the dog is frequently used as a model of inherited retinal disease in humans [269–271], normal canine responses to the On-Off ERG have not been studied in detail. The purpose of this study is to determine baseline features of the On and Off response in phenotypically normal dogs as well as to assess postreceptoral pathways and changes with increasing background luminance in the canine retina.

## 5.2. Materials and Methods

### Ethics Statement

All procedures were performed in accordance with the ARVO statement for the Use of Animals in Ophthalmic and Vision Research and approved by the Michigan State University Institutional Animal Care and Use Committee.

**Animals**

Six phenotypically normal control dogs that were laboratory beagle crossbreeds maintained as part of a colony of inherited retinal degeneration dogs at Michigan State University were utilized for this study. They were housed under 12hr:12hr light:dark cycles.

*Methods*

General anesthesia was induced by intravenous propofol (4-6 mg/kg, PropoFlo, Abbott Laboratories, North Chicago, IL, USA). The animals were intubated and subsequently maintained under anesthesia with isoflurane (IsoFlo, Abbott Laboratories, North Chicago, IL, USA) [between 2-3.5% in a 1-2L/min oxygen flow via a rebreathing circle system for dogs over 10 kg and via a Bain system for dogs under 10 kg].

**Electroretinography (ERG)**

General procedures for ERGs were described previously [168]. Briefly, prior to anesthesia dogs were dark-adapted for one hour and pupils dilated with tropicamide (Tropicamide Ophthalmic Solution UPS 1%, Falcon Pharmaceuticals Ltd., Fort Worth, TX, USA). A monopolar gold-ringed electrode contact lens (ERG-Jet electrode, Fabrinal Eye Care, La Chaux-De-Fonds, CH) was used, and for reference and grounding platinum needle skin electrodes (Grass Technologies, Warwick, RI, USA) were placed 5 mm lateral to the lateral canthus and over the occiput, respectively. ERGs were recorded using an Espion $E^2$ Electrophysiology system with ColorDome Ganzfeld (Diagnosys LLC, Lowell, MA).

**ERG Protocol**

A constant flash duration of 250 mSeconds was used with progressively stronger white light background luminance (0, or dark-adapted, 0.01, 0.1, 1, 10, and 42 cd/m$^2$), with 5 different white light stimuli tested at each background (0.01, 0.1, 0.7, 2.0, 5.0 cd.s/m$^2$) giving a total of 30 steps. Each flash was presented at one second intervals on a dark background and repeated to generate an averaged response detectable against background electrical noise. Dogs were dark adapted for 1 hour prior to initiating the protocol, and for 5 minutes to each subsequent increase in background luminance. A standard short-duration flash (< 4 mSec flashes) protocol was also performed on a separate day, with flash stimuli ranging from 0.0002 to 23 cd.s/m$^2$ in the dark-adapted ERG and 0.01 to 23 cd.s/m$^2$ in the light-adapted (42 cd/m$^2$) ERG – dogs were dark-adapted for 1 hour and light-adapted for 10 minutes, respectively.

**Rod-driven a-wave model**

We calculated parameters for the rod-driven a-wave after subtracting photopically matched ERG waveforms [272]. We fit the following equation described by Birch & Hood to the leading edge of the rod a-wave [164,273]:

$$R(I,t)=(1-\exp[-I\cdot S\cdot(t-t_d)^2])\cdot R_{max} \quad \text{for } t>t_d$$

The amplitude $R$ is a function of the retinal luminance $I$ and time $t$ after the flash onset and $t_d$ is a brief delay. $S$ is a sensitivity factor and $R_{max}$ is the maximum amplitude of the response.

**Curve fitting**

We calculated parameters using the *lmfit* curve-fitting program in the Python 3.6 environment [274], using the Levenberg-Marquardt algorithm to calculate optimal parameter values via least squares minimization [169]:

$$f(\boldsymbol{X}_i,\boldsymbol{\beta}+\boldsymbol{\delta}) \approx f(\boldsymbol{X}_i,\boldsymbol{\beta}) + \mathbf{J}_i\,\boldsymbol{\delta}$$

Where $\mathbf{J}_i$ is the gradient of $f$ with respect to $\boldsymbol{\beta}$. Successive calculation of the parameter $\boldsymbol{\delta}$ that minimizes the sum of square of the residuals $S$ is performed computationally until final model parameters are obtained [171,172].

We determined model goodness-of-fit with the least-squares parameter, with values less than 0.25 considered a good fit [164]:

$$lsq = \frac{\sum_{i=1}^{n}(y_i - f(X_I, \boldsymbol{\beta}))^2}{\sum_{i=1}^{n}(y_i - mean(y))^2}$$

**Isolating the rod-driven PII**

The parameters calculated from the a-wave model were used to define the rod-driven PIII. This modeled response was then subtracted from the photopically subtracted waveforms described above to isolate the postreceptoral PII process for responses with a measurable a-wave (0, 0.01, 0.1, and 1 cd/m$^2$ background light levels).

**5.3. Results**

**Characterization of the canine ON-OFF ERG**

Our protocol was designed to examine rod-only, cone-only, and mixed rod-cone contributions to the On-Off ERG using increasing background luminance. Representative tracings are shown in Figure 5.1. In the presence of none or low background light levels the ERG response was predominantly rod-driven – with increasing background luminance the rod contribution was sequentially decreased such that at 42 cd/m$^2$ the response was cone-driven. In the 10 cd/m$^2$ background there was an underlying negative component that suggested continued rod contributions. Although preceded by a small positive deflection, the off response in the dog was predominantly negative in all stimulus and background conditions.

The shape and amplitudes of the waveforms differed considerably with both stimulus strength and background luminance. Under none or low background light the b-wave was

prominent as was the a-wave in response to stronger stimuli. In response to weaker stimuli there was minimal change in waveform at the cessation of the flash and a slow return to baseline following the post b-wave negativity. With increased background light levels the b-wave was reduced, for example, in the presence of a 1 cd/$m^2$ background light the waveform in response to the weaker flashes had a large initial negative component with a small positive b-wave component superimposed on the down slope. With stronger stimuli and increasing background illuminance an Off response became more prominent. The Off response had a small positive component (which was most apparent for the three strongest flash stimuli in the 10 and 42 cd/$m^2$ background recordings likely reflecting more prominent cone-driven contributions) followed by a larger negative component. With increasing stimulus strength there was less of a negative post b-wave component.

A-wave amplitudes increased with increasing stimulus strength showing semi-saturation kinetics and declined with increasing background luminance (Figure 5.2A). In contrast, the b-wave amplitudes were relatively constant with increasing stimulus strength (Figure 5.2B). The b-wave amplitudes showed a substantially greater decline with increasing background luminance compared to the a-wave – this led to large decreases in the b:a ratio between 0 and 1 cd/$m^2$ background luminance (Figure 5.2C). This suggests that the postreceptoral components of the rod On pathway are suppressed at dimmer background luminances than the negative waveform (PIII response which originates directly from rod photoreceptors).

There was a similar phenomenon with change in the underlying negativity to the waveform. We measured the 'drift' amplitude, which we defined as the absolute change between the peak of the b-wave and amplitude at flash cessation prior to the d-wave (see Figure 5.3A). The increase in drift amplitudes coupled with a decline in b-wave amplitudes – resulted in an

increase in the drift:b-wave ratio between 0 and 1 cd/m$^2$ background luminance (Figures 5.3B-C & 5.4). There was also a striking difference between the drift:b-wave ratio between two brightest luminance conditions, which may indicate continued rod contributions to the 10 cd/m$^2$ background ERG. Furthermore, the drift:b ratio peaked between 1 and 10 cd/m$^2$ background luminance, depending on stimulus strength, and declined with the strongest background luminance (Figure 5.4).

To better characterize photoreceptor contributions to the On-response, we fit an equation described by Birch & Hood to the leading edge of the rod a-wave. For these calculations, the model first subtracted the response at 42 cd/m$^2$ (essentially the same photopic subtraction used when modeling the a-wave of the short flash ERG). Model parameters are also included from short-flash ERGs for comparison. The model demonstrated similar changes in the amplitude (Figure 5.5 – first row) and sensitivity (Figure 5.5 – second row) parameters with increasing background luminance, up to 1 cd/m$^2$. The amplitude and sensitivity parameters of the short and On-Off scotopic ERGs were similar. However, we did find a substantial difference in the time delay parameter, ($t_d$) which was higher for the On-Off compared to short flash ERG (Figure 5.5 – third row). This suggests that there is a part of the flash-offset response that initiates the a-wave that is lost with the longer flash duration.

To further interrogate postreceptoral rod pathways, particularly the large negative response seen most obviously in the responses with a 1 cd/m$^2$ background, we isolated the PII response by subtracting the modeled PIII process (as shown in Figure 5.6A). With increasing background the isolated PII response decreased. This demonstrated that the negative shape in the 1 cd/m$^2$ (which was also present to a lesser extent in the 0.1 cd/m$^2$ background) was mainly attributable to the rod-driven PIII component. Furthermore, the negative ‘drift’ (as defined

above) present at all backgrounds was essentially eliminated in the isolated PII response, which further supports that the negativity present with sustained flash (as compared to short flash stimuli) is driven by sustained rod activation.

Examination of the isolated PII component revealed further differences with increases in both stimulus strength and background luminance. Although the peak amplitude of both the 0 (dark-adapted) and 0.01 cd/m$^2$ background recordings were similar across all tested stimuli, there was an evident shift to a shorter peak time with the brighter background. This was also apparent in the 0.1 and 1 cd/m$^2$ background recordings in addition to substantial declines in amplitude. We also observed a narrowing (time between the beginning of the leading slope and return to baseline) of the isolated PII response with increasing background luminance, which may reflect a shift in rod signaling pathways.

**5.4. Discussion**

The light-adapted Off response in the dog (d-wave) has a small positive component but is predominantly negative. The amplitude of this response scales with stimulus strength and background luminance (see Figure 5.1). This shape of Off response is similar to that of the rat and in contrast to that of primates where a more prominent positive d-wave is present. This difference is probably due to differences between the species in the relative contributions of ON and OFF pathways. The cessation of ON bipolar cell driven responses as they hyperpolarize with cessation of the light stimulus to the photoreceptors probably drives the negative Off response in the On-Off ERG. The relatively small positive component to the dog Off response suggests that the OFF bipolar cell contributions towards shaping the waveform are relatively small in this species. When extrapolated to the On response it also seems likely that OFF bipolar cells make less of a contribution to the photopic a-wave of the dog than they do in primates [255].

The amplitude and shape of the On-Off ERG changes with increases in background luminance. When moving from dark-adapted to partial light adaptation the photoreceptor-driven a-wave has a significantly slower decline in amplitude compared to the postreceptoral b-wave of the On response. This disparity results in a 'negative type' ERG appearance. Similar findings have been reported in human studies of the short-flash ERG and have been posited to reflect a mechanism for maintenance of retinal sensitivity across a wide range of luminance [275–278]. The findings reported here suggest that there is a similar occurrence in dogs.

We applied the Birch & Hood model of the rod-driven a-wave to parameterize the PIII response. The most significant difference in model parameters was seen in the 'time delay' parameter $t_d$ between the short flash and On-Off durations, with smaller decreases in the amplitude parameter $R_{max}$ that mirrored the changes in a-wave amplitude with increasing background luminance. As the dog demonstrates relatively small photopic amplitudes (compared to humans), our results support the conclusion that the responses are primarily rod-driven and a reduction in rod responses leads to a commensurate decrease in a-wave amplitudes. Additionally, the time delay parameter is effectively the time from flash onset to beginning of the a-wave – so while there is likely some component of the Off response that drives the initial slope of the a-wave, it appears to have relatively small contributions to the amplitude of this response.

Using the calculated a-wave model parameters, we subtracted the PIII component from the waveform to isolate the PII component which predominantly results from activity in the ON pathway. This calculation eliminated the large negativity present in the mesopic background conditions. This suggests that the decline in amplitude of the isolated PII component (which was relatively much greater than the decline in PIII amplitude) is likely attributable at least in part to saturation kinetics to maintain retinal sensitivity across increasing background luminance (as

discussed above). However, both the waveform narrowing and move to earlier peak times suggest changes in rod signaling pathways with shifts from scotopic to mesopic luminance conditions. The changes in the isolated PII response may indicate rod contributions to the 'push-pull' mechanism describing the factors that affect the b-wave (mainly driven by ON bipolar cell responses but with influences to the amplitude and shape by OFF bipolar cells) [241,247]. The reduction in activity in the rod BC pathway may also represent the switching of rod signaling from rod bipolar cells to direct contact with cones or cone bipolar cells in mesopic light levels. This process is thought to be important to prevent saturation of inner retinal pathways by rod responses thus expanding the range of luminances the retina can respond to [244–246].

Although not performed here, drug dissection studies could be used to further assess the contributions from different pathways to the On-Off ERG in the dog. Evidence from drug dissection studies of the On-Off ERG in primates suggests that the positive b-wave is mainly driven by ON bipolar cells whereas the positive d-wave is driven by the cessation of OFF bipolar cell activity (using L-AP4 and PDA to block the activity of the ON and OFF bipolar cells, respectively) [247]. From a comparison of primate and rodent drug dissection studies, it is plausible that the difference in Off response is due to relative contributions of the ON and OFF pathways. In fact, the On response appears to be largely similar in both monkey and rat (albeit with some difference in the response shape) – whereas the PDA-sensitive component appears to drive the difference between the ERGs of these species, with a very strong corneal-negative component at flash onset and corneal positive component at flash offset in the primate that is not seen in the rodent [253].

In this study, we designed a protocol with increasing background luminance using long-duration flashes to characterize changes in rod contributions to the On response of the canine

ERG. We showed that the positive PII response saturates at dimmer background luminance than the rod-driven PIII, indicating a role of the On response in maintaining retinal sensitivity with shifts from scotopic to mesopic lighting. Furthermore, we demonstrated that the rod-driven PIII is responsible for the large negativity present in the On-Off ERG waveforms recorded with mesopic background conditions. This suggests that the shape of the isolated PII indicates potential changes in rod signaling pathways with increasing background luminance. Overall, this study suggests a significant role, and possible changes in signaling, of rod pathways in retinal responses in mesopic background conditions that merit future investigation in dogs and other species.

# APPENDIX

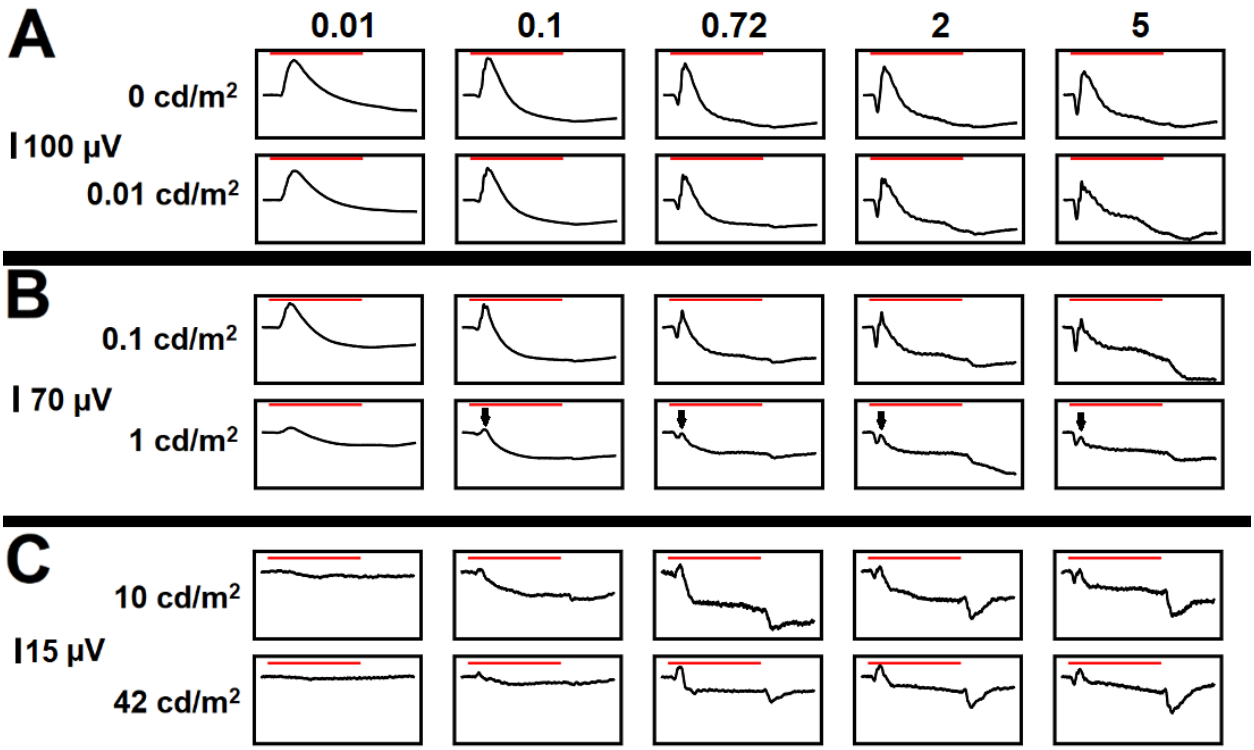


**Figure 5.1. Representative long flash ERG tracings**

Flash duration is noted in red in each panel. Responses were elicited from flash stimuli of 250 mSec duration. Stimulus flash strengths ranged from 0.01 to 5 cd.s/$m^2$ and are labeled above the columns in (A), and background luminances ranged from 0 to 42 cd/$m^2$ and are labeled to the left of each row. An amplitude scale is provided in each figure. The small b-wave superimposed on the large negative deflection is denoted by arrows in the 1 cd/$m^2$ background.

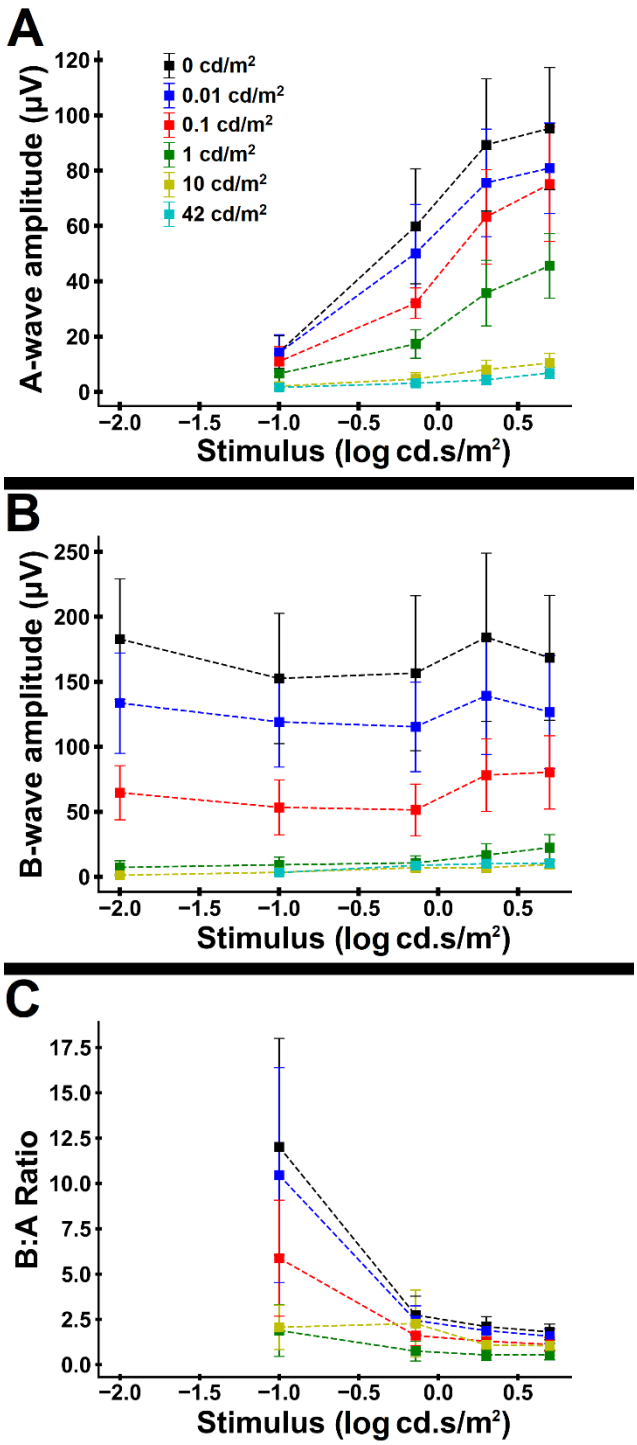


**Figure 5.2. Variation in amplitude parameters with stimulus strength and background luminance**

**Figure 5.2. (cont'd)**

Comparison of average a-wave amplitude (A), b-wave amplitude (B), and log B:A-wave amplitude ratio (C) versus stimulus strength. Different colors were used to denote background luminance.

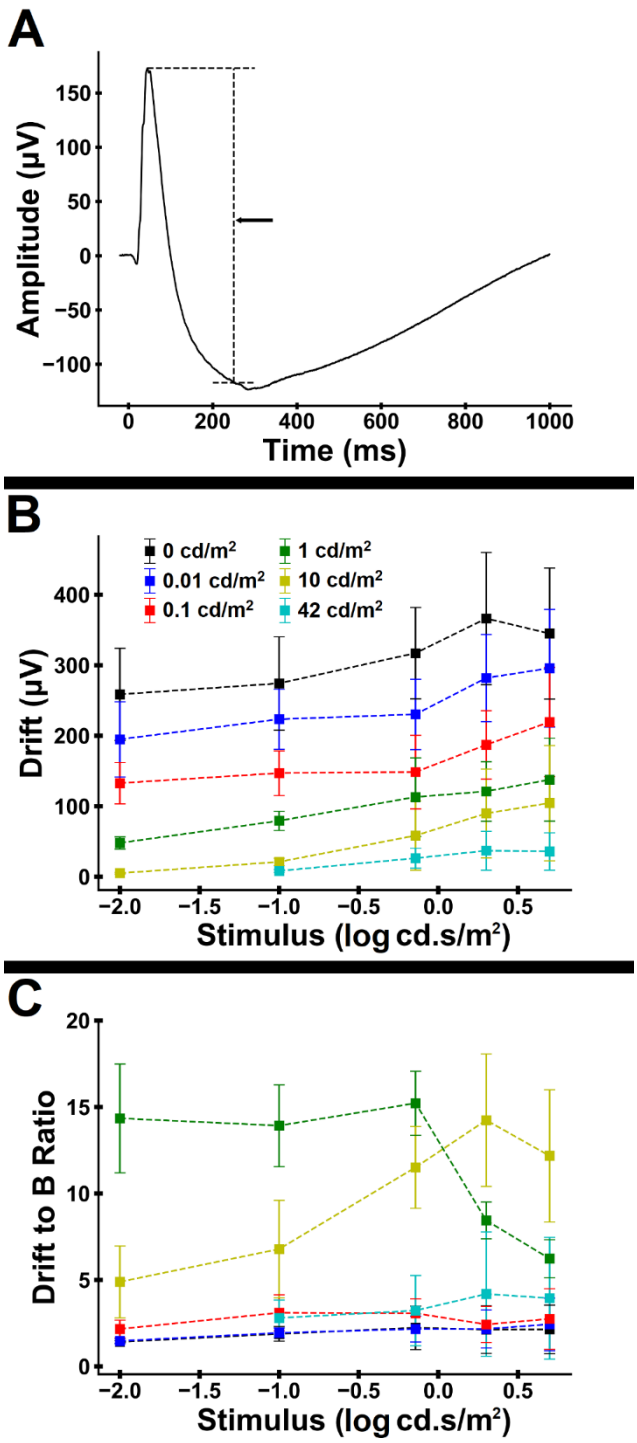


**Figure 5.3. Variation in drift with stimulus strength**

With 'drift' defined as the absolute change in amplitude between the peak of the b-wave and amplitude at flash cessation, not including the negative off response component (see arrow in A),

**Figure 5.3 (cont'd)**

comparison of average drift amplitude (B) and drift:b-wave ratio (C) versus stimulus strength. Different colors were used to denote background luminance.

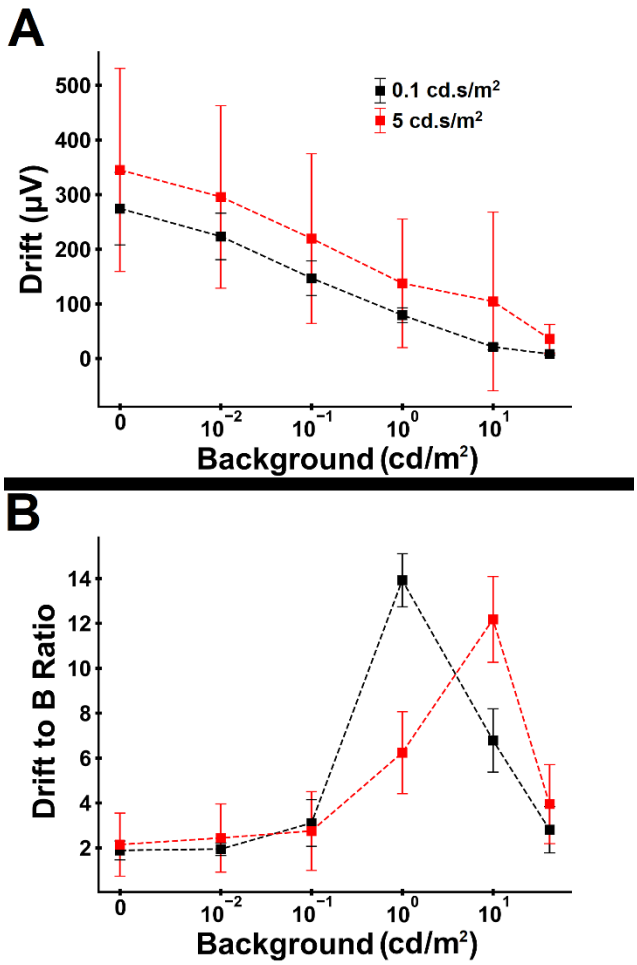


**Figure 5.4. Variation in drift with background luminance**

Comparison of average drift amplitude (A) and drift:b-wave ratio (B) versus background luminance for the 0.1 and 5 cd.s/m$^2$ flash stimuli. Different colors were used to denote stimulus strength.

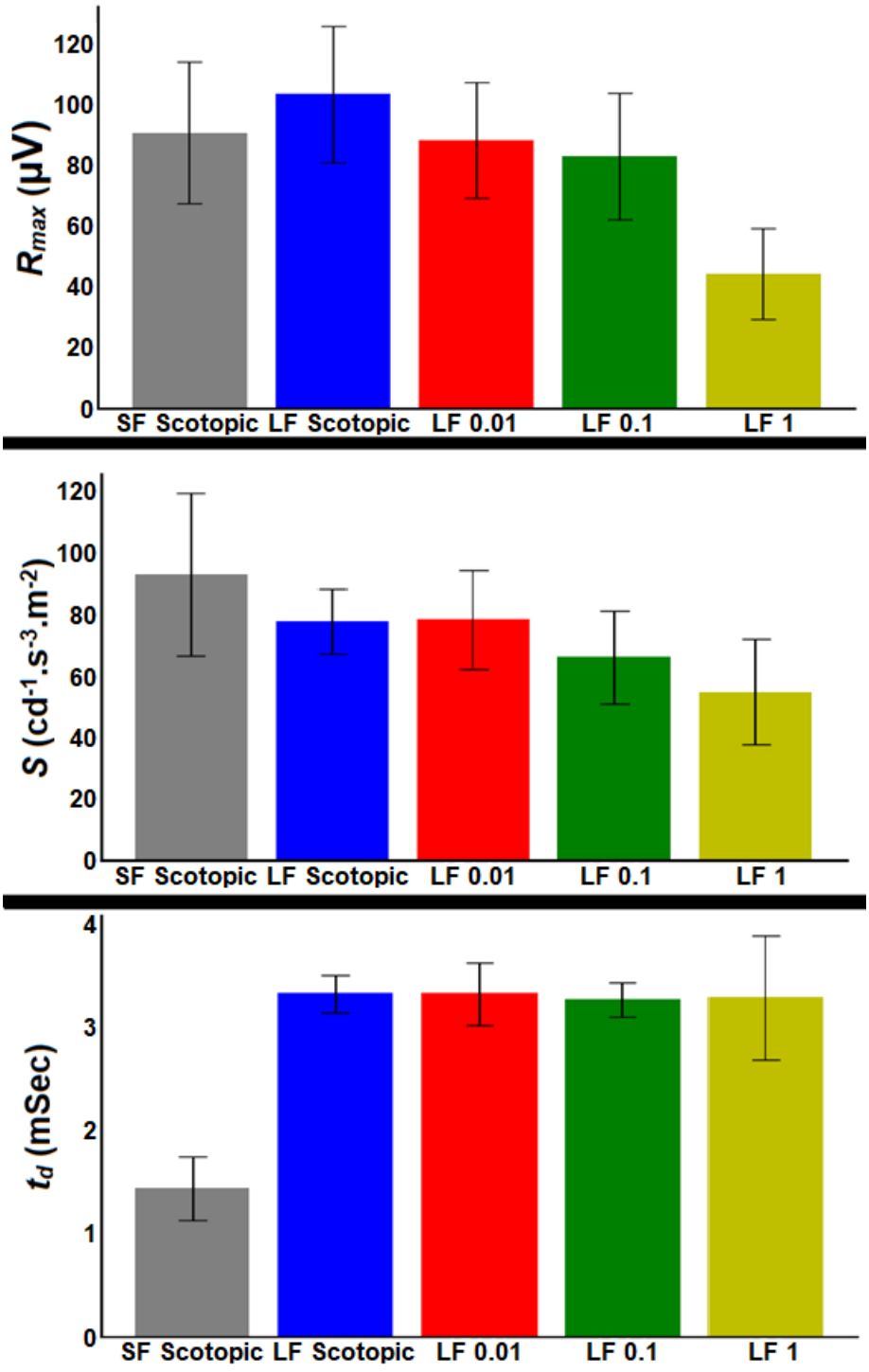


**Figure 5.5. Changes in a-wave model parameters by background luminance**

Amplitude parameters are shown in the first row, sensitivity in the second, and time delay in the third. 'SF' and 'LF' are used as abbreviations for short flash and long flash, respectively, and the corresponding background luminance is provided after these.

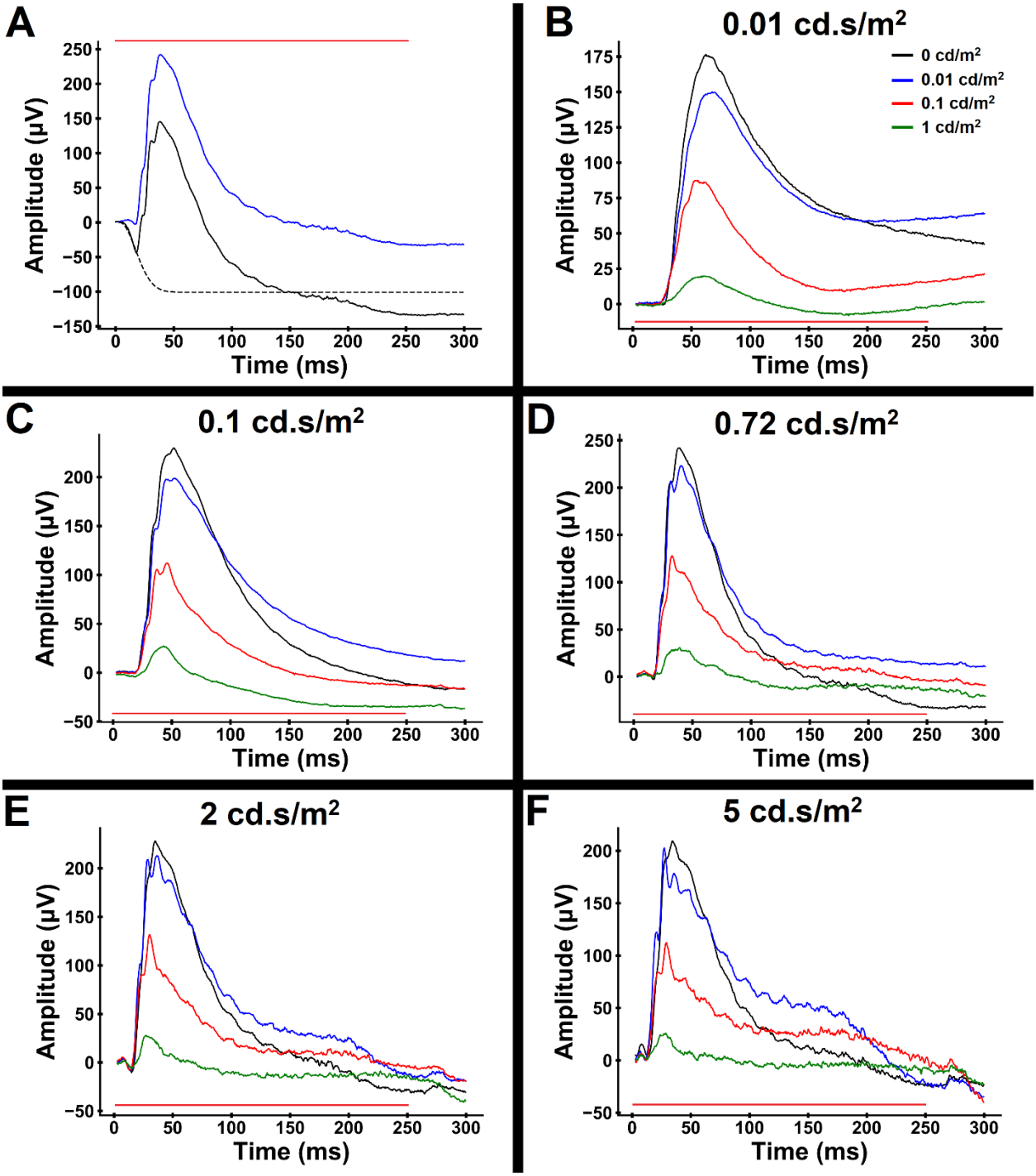


**Figure 5.6. Isolating the PII response**

Using the calculated model parameters for the rod a-wave, the PII contribution (in blue) was isolated by subtracting the modeled PIII (dashed black line) from the ERG waveform in background light of 0. 0.01, 0.1 and 1 cd/m$^2$ (A). This is shown in a representative dog (from

**Figure 5.6 (cont'd)**

Figure 1). The calculation was performed in the 0.01, 0.1, 0.72, 2, and 5 cd.s/$m^2$ (B-F, respectively) and background luminance is denoted by different colors.

# CHAPTER 6.

# CONCLUSION

**Summary of Findings**

Through application of select mathematical models and modalities to normal dogs and dogs lacking rod function, this research has established baseline features of normal canine retinal function. Specifically, this research demonstrates that existing rod and cone a-wave models intended to assess photoreceptor function, and the Naka-Rushton b-wave model for assessment of retinal function, can be applied to the dog ERG to further characterize normal retinal function in this species. This research further shows the utility of models in monitoring disease progression and the results of gene augmentation therapy treatment in dogs with inherited retinal disease. Finally, this research derives mathematical models in normal dogs for several expanded ERG protocols that provide additional tools for detecting and characterizing altered retinal function.

Dogs are frequently used as large animal models of inherited retinal disease in humans, due in part to the similarity of the canine *area centralis* to the human macula with central fovea [7,12,269]. Multiple dog models have been used to characterize inherited retinal disease and develop translational therapies for rescue of retinal function [5,8–10]. Compared to humans, the dog has several notable differences in retinal function as characterized by the full-field ERG. These include relatively higher amplitude scotopic and lower amplitude photopic responses, a predominantly negative d-wave, and a small x-wave [99,190,193]. Methods that are commonly applied to the human ERG, including mathematical models and extended protocols, are infrequently used in dog studies. Assessing the utility of these methods in dogs provides valuable information about normal function as well as additional techniques for characterizing, monitoring, and quantifying the effects of gene augmentation therapy in dogs with inherited retinal disease.

Through assessment of several mathematical models, this thesis has shown that good model fits can be acquired for the a- and b-waves of phenotypically normal dogs. Additionally, we established baseline model parameters in a colony of normal research dogs. We used these results to quantify reduced retinal function in dogs with inherited retinal dystrophy, and to assess the degree of rescue in dogs treated with gene augmentation therapy. Furthermore, we correlated the parameters derived from dogs with inherited retinal dystrophy with physiologic bases of abnormal retinal function. For example, the reduced cone a-wave amplitude parameter $R_{mp3}$ reflects the shortening of cone OS in young *pde6a* dogs [159], while the reduced rod a-wave sensitivity parameter *S* quantifies abnormal channel kinetics in young *cngb1* dogs [152]. We also demonstrated several potential frequency-based approaches for the assessment and analysis of canine ERGs, such as the Fourier transform for quantification of signal-to-noise ratio and the discrete wavelet transform for differentiating retinal cell types by frequency band.

To further characterize canine retinal function, we tested ERG protocols that varied in stimulus color, background luminance, flash frequency, as well as flash duration. Based on Naka-Rushton fitting of the dark-adapted b-waves and comparison to dogs lacking rod function, we developed a short dark-adapted protocol with red and blue flashes that demonstrates the x-wave in phenotypically normal dogs and enables assessment of dogs with decreased rod or cone function. We showed that luminance:response series of the blue-background ERG demonstrates a quantifiable gain-control mechanism between rod photoreceptors and bipolar cells, which has been described in human studies. Additionally, we used expanded flicker protocols to derive accurate mathematical models of response amplitude in normal dogs using constant luminance, increasing frequency and the 6Hz luminance:response series. We further developed in-depth protocols for assessing on and off pathways in the normal canine retina and demonstrated how

rod pathways change with increasing background luminance in the long flash ERG. We showed that the isolated PII response declines in amplitude at much dimmer background luminances compared to the rod-driven response resulting in a large underlying negativity in mesopic backgrounds and suggests that changes in rod signaling through alternative pathways may help maintain retinal sensitivity in mesopic lighting.

**Future Directions**

Based on these results, future studies should consider incorporating the methods presented when planning or analyzing ERG studies in dogs. This thesis demonstrated that accurate parameters for mathematical models of the rod- and cone-driven a-wave can be derived using the ISCEV/ECVO standard flashes [1,13]. These models provide an additional tool for post-recording ERG analysis and can be used to quantify altered retinal function and determine potential physiological and biochemical bases for these changes. They also enable longitudinal assessment of changes in retinal function and quantification of recovery with gene augmentation therapy treatment. The short dark-adapted chromatic flashes can be easily incorporated into existing protocols for a succinct assessment of dark-adapted rod and cone function. Although the other methods require more extensive protocol alterations, they could be considered when assessing amplitude gain from rod to bipolar cells (blue-background ERG) or abnormal 30Hz photopic flicker recordings.

To better understand and apply these results, future studies could expand these protocols and assess their applicability in additional dogs, both normal and models of inherited retinal disease. This includes applicability to dogs without cone function (as in achromatopsia) and dogs with specific defects in photoreceptor to bipolar cell signaling (as in models of CSNB). Additionally, the protocols could be expanded to assess responses to weaker and stronger flash

stimuli (in the chromatic and blue-background ERG) and higher frequency flashes in the flicker ERG (that approach the CFF). Further research is needed to assess the reliability of these methods with different testing conditions. ERG responses differ based on breed, age, anesthetic protocol, choice and positioning of lenses, length of dark or light adaptation, background noise, and pupil dilation [43,46,48–51,53]. These factors impede the establishment of global normative values and could be assessed for effects on measured responses and calculated parameters. Postreceptoral pathways can be further characterized with drug dissection to preferentially inhibit different populations of retinal cells, which would be particularly valuable in the long flash ERG to determine how photoreceptors respond at flash offset as well as characterize the relative contributions of ON and OFF bipolar cells. Additional studies could also quantify the types, morphology, and connections of different bipolar cells in the dog retina and compare these results to ERG findings in dogs and other species. Finally, future studies could be performed to correlate both normal and abnormal ERG recordings with structural findings such as those characterized by OCT.

**Contributions to Knowledge**

The full-field ERG is an invaluable tool in the diagnosis, characterization, and monitoring of global retinal function. The dog is used to develop and test translational therapies for the treatment of human retinal disease. Many methods used in the analysis of human retinal function are untested or infrequently used in dog ERG studies. This thesis demonstrates the utility of several expanded protocols and mathematical models of the ERG waveforms in characterizing retinal function in normal dogs and dogs with inherited retinal disease. Furthermore, this research establishes normal baseline parameters of canine retinal function, provides mathematical models for assessment of expanded protocols, and suggests simple techniques to

incorporate into future ERG protocols and analysis. These findings better characterize different contributions to the canine ERG and provide additional tools for future studies.

# REFERENCES

## REFERENCES


1. McCulloch DL, Marmor MF, Brigell MG, et al. ISCEV Standard for full-field clinical electroretinography (2015 update). *Doc Ophthalmol*. 2015;130(1):1-12. doi:10.1007/s10633-014-9473-7

2. Arden GB, Carter RM, Hogg CR, et al. A modified ERG technique and the results obtained in X-linked retinitis pigmentosa. *British Journal of Ophthalmology*. 1983;67(7):419-430. doi:10.1136/bjo.67.7.419

3. Berson EL, Rosner B, Weigel-DiFranco C, Dryja TP, Sandberg MA. Disease progression in patients with dominant retinitis pigmentosa and rhodopsin mutations. *Invest Ophthalmol Vis Sci*. 2002;43(9):3027-3036.

4. Bainbridge JWB, Mehat MS, Sundaram V, et al. Long-Term Effect of Gene Therapy on Leber's Congenital Amaurosis. *N Engl J Med*. 2015;372(20):1887-1897. doi:10.1056/NEJMoa1414221

5. Petersen-Jones SM, Occelli LM, Winkler PA, et al. Patients and animal models of CNGβ1-deficient retinitis pigmentosa support gene augmentation approach. *J Clin Invest*. 2018;128(1):190-206. doi:10.1172/JCI95161

6. Petersen-Jones SM, Komáromy AM. Dog models for blinding inherited retinal dystrophies. *Hum Gene Ther Clin Dev*. 2015;26(1):15-26. doi:10.1089/humc.2014.155

7. Bunel M, Chaudieu G, Hamel C, et al. Natural models for retinitis pigmentosa: progressive retinal atrophy in dog breeds. *Hum Genet*. 2019;138(5):441-453. doi:10.1007/s00439-019-01999-6

8. Somma AT, Moreno JCD, Sato MT, et al. Characterization of a novel form of progressive retinal atrophy in Whippet dogs: a clinical, electroretinographic, and breeding study. *Vet Ophthalmol*. 2017;20(5):450-459. doi:10.1111/vop.12448

9. Occelli LM, Schön C, Seeliger MW, et al. Gene Supplementation Rescues Rod Function and Preserves Photoreceptor and Retinal Morphology in Dogs, Leading the Way Towards Treating Human PDE6A-Retinitis Pigmentosa. *Hum Gene Ther*. Published online December 6, 2017. doi:10.1089/hum.2017.155

10. Acland GM, Aguirre GD, Ray J, et al. Gene therapy restores vision in a canine model of childhood blindness. *Nat Genet*. 2001;28(1):92-95. doi:10.1038/ng0501-92

11. Narfström K, Tullis GE, Seeliger M. Effective Treatment for the Canine RPE65 Null Mutation, a Hereditary Retinal Dystrophy Comparable to Human Leber's Congenital Amaurosis. In: Tombran-Tink J, Barnstable CJ, eds. *Retinal Degenerations*. Humana Press; 2007:415-431. doi:10.1007/978-1-59745-186-4_22

12. Mowat FM, Petersen-Jones SM, Williamson H, et al. Topographical characterization of cone photoreceptors and the area centralis of the canine retina. *Mol Vis*. 2008;14:2518-2527.

13. Ekesten B, Komáromy AM, Ofri R, Petersen-Jones SM, Narfström K. Guidelines for clinical electroretinography in the dog: 2012 update. *Doc Ophthalmol*. 2013;127(2):79-87. doi:10.1007/s10633-013-9388-8

14. Fain GL, Matthews HR, Cornwall MC, Koutalos Y. Adaptation in vertebrate photoreceptors. *Physiol Rev*. 2001;81(1):117-151. doi:10.1152/physrev.2001.81.1.117

15. Hood DC, Birch DG. Phototransduction in human cones measured using the a-wave of the ERG. *Vision Research*. 1995;35(20):2801-2810. doi:10.1016/0042-6989(95)00034-W

16. Kraft TW, Schneeweis DM, Schnapf JL. Visual transduction in human rod photoreceptors. *J Physiol (Lond)*. 1993;464:747-765. doi:10.1113/jphysiol.1993.sp019661

17. Thomas MM, Lamb TD. Light adaptation and dark adaptation of human rod photoreceptors measured from the a-wave of the electroretinogram. *J Physiol (Lond)*. 1999;518 ( Pt 2):479-496. doi:10.1111/j.1469-7793.1999.0479p.x

18. Hood DC, Birch DG. Light adaptation of human rod receptors: the leading edge of the human a-wave and models of rod receptor activity. *Vision Research*. 1993;33(12):1605-1618. doi:10.1016/0042-6989(93)90027-T

19. Massof RW, Wu L, Finkelstein D, Perry C, Starr SJ, Johnson MA. Properties of electroretinographic intensity-response functions in retinitis pigmentosa. *Doc Ophthalmol*. 1984;57(3):279-296.

20. Peachey NS, Alexander KR, Fishman GA. Visual adaptation and the cone flicker electroretinogram. *Invest Ophthalmol Vis Sci*. 1991;32(5):1517-1522.

21. Pugh EN, Lamb TD. Amplification and kinetics of the activation steps in phototransduction. *Biochimica et Biophysica Acta (BBA) - Bioenergetics*. 1993;1141(2-3):111-149. doi:10.1016/0005-2728(93)90038-H

22. Tanimoto N, Sothilingam V, Kondo M, Biel M, Humphries P, Seeliger MW. Electroretinographic assessment of rod- and cone-mediated bipolar cell pathways using flicker stimuli in mice. *Sci Rep*. 2015;5:10731. doi:10.1038/srep10731

23. Hood DC, Birch DG. Rod phototransduction in retinitis pigmentosa: estimation and interpretation of parameters derived from the rod a-wave. *Invest Ophthalmol Vis Sci*. 1994;35(7):2948-2961.

24. McCall MA, Gregg RG. Comparisons of structural and functional abnormalities in mouse b-wave mutants. *J Physiol (Lond)*. 2008;586(18):4385-4392. doi:10.1113/jphysiol.2008.159327

25. Marmor MF, Lurie M. Characterizing the C-Wave of the Electroretinogram. In: Zauberman H, ed. *Proceedings of the Conference on Subretinal Space, Jerusalem, October 14–19, 1979*. Springer Netherlands; 1981:259-266.

26. Evans LS, Peachey NS, Marchese AL. Comparison of three methods of estimating the parameters of the Naka-Rushton equation. *Doc Ophthalmol*. 1993;84(1):19-30. doi:10.1007/BF01203279

27. Gotch F. The time relations of the photo-electric changes in the eyeball of the frog. *J Physiol (Lond)*. 1903;29(4-5):388-410. doi:10.1113/jphysiol.1903.sp000965

28. Einthoven W, Jolly WA. The form and magnitude of the electrical response of the eye to stimulation by light at various intensities. *Quarterly Journal of Experimental Physiology*. 1908;1(4):373-416.

29. Granit R. The components of the retinal action potential in mammals and their relation to the discharge in the optic nerve. *The Journal of Physiology*. 1933;77(3):207-239. doi:10.1113/jphysiol.1933.sp002964

30. Brown KT, Wiesel TN. Analysis of the intraretinal electroretinogram in the intact cat eye. *J Physiol (Lond)*. 1961;158:229-256. doi:10.1113/jphysiol.1961.sp006767

31. Derwent JJK, Linsenmeier RA. Intraretinal analysis of the *a* -wave of the electroretinogram (ERG) in dark-adapted intact cat retina. *Vis Neurosci*. 2001;18(3):353-363. doi:10.1017/S0952523801183021

32. Tomita T, Funaishi A. STUDIES ON INTRARETINAL ACTION POTENTIAL WITH LOW-RESISTANCE MICROELECTRODE. *Journal of Neurophysiology*. 1952;15(1):75-84. doi:10.1152/jn.1952.15.1.75

33. Tomita T, Torihama Y. Further study on the intraretinal action potentials and on the site of ERG generation. *Jpn J Physiol*. 1956;6(2):118-136. doi:10.2170/jjphysiol.6.118

34. Frishman LJ, Steinberg RH. Intraretinal analysis of the threshold dark-adapted ERG of cat retina. *Journal of Neurophysiology*. 1989;61(6):1221-1232. doi:10.1152/jn.1989.61.6.1221

35. Criswell MH, Karwoski CJ, Proenza LM. Species differences in the intraretinal electroretinogram within the leopard frog complex. *Vision Research*. 1979;19(3):339-341. doi:10.1016/0042-6989(79)90180-9

36. Green DG, Kapousta-Bruneau NV. A dissection of the electroretinogram from the isolated rat retina with microelectrodes and drugs. *Vis Neurosci*. 1999;16(4):727-741. doi:10.1017/S0952523899164125

37. Jamison JA, Bush RA, Lei B, Sieving PA. Characterization of the rod photoresponse isolated from the dark-adapted primate ERG. *Vis Neurosci*. 2001;18(3):445-455. doi:10.1017/s0952523801183112

38. Hanawa I, Tateishi T. The effect of aspartate on the electroretinogram of the vertebrate retina. *Experientia*. 1970;26(12):1311-1312.

39. Slaughter MM, Miller RF. 2-amino-4-phosphonobutyric acid: a new pharmacological tool for retina research. *Science*. 1981;211(4478):182-185.

40. Bush RA, Sieving PA. A proximal retinal component in the primate photopic ERG a-wave. *Invest Ophthalmol Vis Sci*. 1994;35(2):635-645.

41. Robson JG, Frishman LJ. Dissecting the dark-adapted electroretinogram. *Doc Ophthalmol*. 1998;95(3-4):187-215.

42. Dang TM, Tsai TI, Vingrys AJ, Bui BV. Post-receptoral contributions to the rat scotopic electroretinogram a-wave. *Doc Ophthalmol*. 2011;122(3):149-156. doi:10.1007/s10633-011-9269-y

43. Andréeasson SOL, Sandberg MA, Berson EL. Narrow-Band Filtering for Monitoring Low-Amplitude Cone Electroretinograms in Retinitis Pigmentosa. *American Journal of Ophthalmology*. 1988;105(5):500-503. doi:10.1016/0002-9394(88)90241-3

44. Bayer AU, Mittag T, Cook P, Brodie SE, Podos SM, Maag K-P. Comparisons of the amplitude size and the reproducibility of three different electrodes to record the corneal flash electroretinogram in rodents. *Documenta Ophthalmologica*. 1999;98(3):233-246. doi:10.1023/A:1002416918247

45. Kurtenbach A, Kramer S, Strasser T, Zrenner E, Langrová H. The importance of electrode position in visual electrophysiology. *Doc Ophthalmol*. 2017;134(2):129-134. doi:10.1007/s10633-017-9579-9

46. Mentzer AE, Eifler DM, Montiani-Ferreira F, Tuntivanich N, Forcier JQ, Petersen-Jones SM. Influence of Recording Electrode Type and Reference Electrode Position on the Canine Electroretinogram. *Doc Ophthalmol*. 2005;111(2):95-106. doi:10.1007/s10633-005-4517-7

47. Yin H, Pardue MT. Performance of the DTL electrode compared to the Jet contact lens electrode in clinical testing. *Doc Ophthalmol*. 2004;108(1):77-86. doi:10.1023/B:DOOP.0000018395.78512.4e

48. Lin S-L, Shiu W-C, Liu P-C, Cheng F-P, Lin Y-C, Wang W-S. The Effects of Different Anesthetic Agents on Short Electroretinography Protocol in Dogs. *J Vet Med Sci*. 2009;71(6):763-768. doi:10.1292/jvms.71.763

49. Friedburg C, Thomas MM, Lamb TD. Time course of the flash response of dark- and light-adapted human rod photoreceptors derived from the electroretinogram. *The Journal of Physiology*. 2001;534(1):217-242. doi:10.1111/j.1469-7793.2001.t01-1-00217.x

50. Gagné A-M, Lavoie J, Lavoie M-P, Sasseville A, Charron M-C, Hébert M. Assessing the impact of non-dilating the eye on full-field electroretinogram and standard flash response. *Doc Ophthalmol*. 2010;121(3):167-175. doi:10.1007/s10633-010-9242-1

51. Sussadee M, Phavaphutanon J, Kornkaewrat K, Thayananuphat A. Normal clinical electroretinography parameters for poodle, Labrador retriever, Thai ridgeback, and Thai Bangkaew. *J Vet Sci*. 2015;16(1):67. doi:10.4142/jvs.2015.16.1.67

52. Westall CA, Dhaliwal HS, Panton CM, et al. Values of electroretinogram responses according to axial length. *Documenta Ophthalmologica*. 2001;102(2):115-130. doi:10.1023/A:1017535207481

53. Birch DG. Standardized Full-Field Electroretinography: Normal Values and Their Variation With Age. *Arch Ophthalmol*. 1992;110(11):1571. doi:10.1001/archopht.1992.01080230071024

54. Burns ME, Baylor DA. Activation, deactivation, and adaptation in vertebrate photoreceptor cells. *Annu Rev Neurosci*. 2001;24:779-805. doi:10.1146/annurev.neuro.24.1.779

55. Arshavsky VY, Lamb TD, Pugh EN. G Proteins and Phototransduction. *Annu Rev Physiol*. 2002;64(1):153-187. doi:10.1146/annurev.physiol.64.082701.102229

56. Hagins WA, Penn RD, Yoshikami S. Dark Current and Photocurrent in Retinal Rods. *Biophysical Journal*. 1970;10(5):380-412. doi:10.1016/S0006-3495(70)86308-1

57. Krizaj D, Copenhagen DR. Calcium regulation in photoreceptors. *Front Biosci*. 2002;7:d2023-2044.

58. Duvoisin RM, Morgans C, Taylor W. The mGluR6 receptors in the retina: Analysis of a unique G-protein signaling pathway. *Cellscience Reviews*. 2005;2(2):18.

59. Thoreson WB. Kinetics of synaptic transmission at ribbon synapses of rods and cones. *Mol Neurobiol*. 2007;36(3):205-223. doi:10.1007/s12035-007-0019-9

60. Hurley JB. Signal transduction enzymes of vertebrate photoreceptors. *J Bioenerg Biomembr*. 1992;24(2):219-226.

61. Lamb TD, Pugh EN. Dark adaptation and the retinoid cycle of vision. *Prog Retin Eye Res*. 2004;23(3):307-380. doi:10.1016/j.preteyeres.2004.03.001

62. Breton ME, Schueller AW, Lamb TD, Pugh EN. Analysis of ERG a-wave amplification and kinetics in terms of the G-protein cascade of phototransduction. *Invest Ophthalmol Vis Sci*. 1994;35(1):295-309.

63. Lamb TD, Pugh EN. A quantitative account of the activation steps involved in phototransduction in amphibian photoreceptors. *The Journal of Physiology*. 1992;449(1):719-758. doi:10.1113/jphysiol.1992.sp019111

64. Müller F, Kaupp UB. [Signal transduction in photoreceptor cells]. *Naturwissenschaften*. 1998;85(2):49-61.

65. Yau K-W, Hardie RC. Phototransduction motifs and variations. *Cell*. 2009;139(2):246-264. doi:10.1016/j.cell.2009.09.029

66. Robson JG, Saszik SM, Ahmed J, Frishman LJ. Rod and cone contributions to the a-wave of the electroretinogram of the macaque. *J Physiol (Lond)*. 2003;547(Pt 2):509-530. doi:10.1113/jphysiol.2002.030304

67. Wachtmeister L. Further studies of the chemical sensitivity of the oscillatory potentials of the electroretinogram (ERG). II. Glutamate-aspartate-and dopamine antagonists. *Acta Ophthalmol (Copenh)*. 1981;59(2):247-258.

68. Wakabayashi K, Gieser J, Sieving PA. Aspartate separation of the scotopic threshold response (STR) from the photoreceptor a-wave of the cat and monkey ERG. *Invest Ophthalmol Vis Sci*. 1988;29(11):1615-1622.

69. Bolnick DA, Walter AE, Sillman AJ. Barium suppresses slow PIII in perfused bullfrog retina. *Vision Res*. 1979;19(10):1117-1119.

70. Kofuji P, Ceelen P, Zahs KR, Surbeck LW, Lester HA, Newman EA. Genetic inactivation of an inwardly rectifying potassium channel (Kir4.1 subunit) in mice: phenotypic impact in retina. *J Neurosci*. 2000;20(15):5733-5740.

71. Witkovsky P, Dudek FE, Ripps H. Slow PIII component of the carp electroretinogram. *J Gen Physiol*. 1975;65(2):119-134. doi:10.1085/jgp.65.2.119

72. Nelson RF, Singla N. A spectral model for signal elements isolated from zebrafish photopic electroretinogram. *Vis Neurosci*. 2009;26(4):349-363. doi:10.1017/S0952523809990113

73. Sieving PA, Murayama K, Naarendorp F. Push-pull model of the primate photopic electroretinogram: a role for hyperpolarizing neurons in shaping the b-wave. *Vis Neurosci*. 1994;11(3):519-532.

74. Cameron AM, Mahroo O a. R, Lamb TD. Dark adaptation of human rod bipolar cells measured from the b-wave of the scotopic electroretinogram. *J Physiol (Lond)*. 2006;575(Pt 2):507-526. doi:10.1113/jphysiol.2006.108027

75. Robson JG, Maeda H, Saszik SM, Frishman LJ. In vivo studies of signaling in rod pathways of the mouse using the electroretinogram. *Vision Res*. 2004;44(28):3253-3268. doi:10.1016/j.visres.2004.09.002

76. Ueno S, Kondo M, Ueno M, Miyata K, Terasaki H, Miyake Y. Contribution of retinal neurons to d-wave of primate photopic electroretinograms. *Vision Res*. 2006;46(5):658-664. doi:10.1016/j.visres.2005.05.026

77. Lei B, Perlman I. The contributions of voltage- and time-dependent potassium conductances to the electroretinogram in rabbits. *Vis Neurosci*. 1999;16(4):743-754.

78. Miller RF, Dowling JE. Intracellular responses of the Müller (glial) cells of mudpuppy retina: their relation to b-wave of the electroretinogram. *J Neurophysiol*. 1970;33(3):323-341. doi:10.1152/jn.1970.33.3.323

79. Newman EA. Potassium conductance block by barium in amphibian Müller cells. *Brain Res*. 1989;498(2):308-314.

80. Dong CJ, Hare WA. Contribution to the kinetics and amplitude of the electroretinogram b-wave by third-order retinal neurons in the rabbit retina. *Vision Res*. 2000;40(6):579-589.

81. Dong C-J, Hare WA. GABAc feedback pathway modulates the amplitude and kinetics of ERG b-wave in a mammalian retina in vivo. *Vision Res*. 2002;42(9):1081-1087.

82. Dong C-J, Agey P, Hare WA. Origins of the electroretinogram oscillatory potentials in the rabbit retina. *Vis Neurosci*. 2004;21(4):533-543. doi:10.1017/S0952523804214043

83. Peachey NS, Alexander KR, Fishman GA. Rod and cone system contributions to oscillatory potentials: an explanation for the conditioning flash effect. *Vision Res*. 1987;27(6):859-866.

84. Speros P, Price J. Oscillatory potentials. History, techniques and potential use in the evaluation of disturbances of retinal circulation. *Surv Ophthalmol*. 1981;25(4):237-252.

85. Gauthier M, Gauvin M, Lina J-M, Lachapelle P. The effects of bandpass filtering on the oscillatory potentials of the electroretinogram. *Doc Ophthalmol*. 2019;138(3):247-254. doi:10.1007/s10633-019-09683-w

86. Gauvin M, Dorfman AL, Trang N, et al. Assessing the Contribution of the Oscillatory Potentials to the Genesis of the Photopic ERG with the Discrete Wavelet Transform. *Biomed Res Int*. 2016;2016:2790194. doi:10.1155/2016/2790194

87. Sieving PA, Frishman LJ, Steinberg RH. Scotopic threshold response of proximal retina in cat. *J Neurophysiol*. 1986;56(4):1049-1061. doi:10.1152/jn.1986.56.4.1049

88. Sieving PA, Nino C. Scotopic threshold response (STR) of the human electroretinogram. *Invest Ophthalmol Vis Sci*. 1988;29(11):1608-1614.

89. Yanase J, Ogawa H, Ohtsuka H. Scotopic threshold response of the electroretinogram of dogs. *Am J Vet Res*. 1996;57(3):361-366.

90. Frishman L, Wang MH. Electroretinogram of Human , Monkey and Mouse. In: ; 2010.

91. Saszik SM, Robson JG, Frishman LJ. The scotopic threshold response of the dark-adapted electroretinogram of the mouse. *J Physiol (Lond)*. 2002;543(Pt 3):899-916. doi:10.1113/jphysiol.2002.019703

92. Steinberg RH, Schmidt R, Brown KT. Intracellular responses to light from cat pigment epithelium: origin of the electroretinogram c-wave. *Nature*. 1970;227(5259):728-730.

93. Skoog KO, Nilsson SE. The c-wave of the human D.C. registered ERG. I. A quantitative study of the relationship between c-wave amplitude and stimulus intensity. *Acta Ophthalmol (Copenh)*. 1974;52(5):759-773.

94. Nilsson SE, Andersson BE. Corneal D.C. recordings of slow ocular potential changes such as the ERG c-wave and the light peak in clinical work. Equipment and examples of results. *Doc Ophthalmol*. 1988;68(3-4):313-325.

95. Nilsson SEG, Wrigstad A, Narfström K. Changes in the DC electroretinogram in briard dogs with hereditary congenital night blindness and partial day blindness. *Experimental Eye Research*. 1992;54(2):291-296. doi:10.1016/S0014-4835(05)80218-0

96. Naarendorp F, Williams GE. The *d* -wave of the rod electroretinogram of rat originates in the cone pathway. *Vis Neurosci*. 1999;16(1):91-105. doi:10.1017/S0952523899161054

97. Xu X, Karwoski C. Current source density analysis of the electroretinographic d wave of frog retina. *J Neurophysiol*. 1995;73(6):2459-2469. doi:10.1152/jn.1995.73.6.2459

98. Lei B. The ERG of guinea pig (Cavis porcellus): comparison with I-type monkey and E-type rat. *Doc Ophthalmol*. 2003;106(3):243-249.

99. Kondo M, Das G, Imai R, et al. A Naturally Occurring Canine Model of Autosomal Recessive Congenital Stationary Night Blindness. *PLoS ONE*. 2015;10(9):e0137072. doi:10.1371/journal.pone.0137072

100. Szikra T, Witkovsky P. Contributions of AMPA- and kainate-sensitive receptors to the photopic electroretinogram of the Xenopus retina. *Vis Neurosci*. 2001;18(2):187-196.

101. Khan NW, Kondo M, Hiriyanna KT, Jamison JA, Bush RA, Sieving PA. Primate Retinal Signaling Pathways: Suppressing ON-Pathway Activity in Monkey With Glutamate Analogues Mimics Human CSNB1-NYX Genetic Night Blindness. *J Neurophysiol*. 2005;93(1):481-492. doi:10.1152/jn.00365.2004

102. Cone RA, Pak WL. The Early Receptor Potential. In: Loewenstein WR, ed. *Principles of Receptor Physiology*. Vol 1. Springer Berlin Heidelberg; 1971:345-365. doi:10.1007/978-3-642-65063-5_12

103. Sieving PA, Fishman GA, Salzano T, Rabb MF. Acute macular neuroretinopathy: early receptor potential change suggests photoreceptor pathology. *Br J Ophthalmol*. 1984;68(4):229-234. doi:10.1136/bjo.68.4.229

104. Graham SL, Klistorner A. Electrophysiology: a review of signal origins and applications to investigating glaucoma. *Aust N Z J Ophthalmol*. 1998;26(1):71-85.

105. Peachey NS, Alexander KR, Fishman GA, Derlacki DJ. Properties of the human cone system electroretinogram during light adaptation. *Appl Opt*. 1989;28(6):1145-1150. doi:10.1364/AO.28.001145

106. Rosolen SG, Rigaudière F, LeGargasson J-F, et al. Comparing the photopic ERG i-wave in different species. *Vet Ophthalmol*. 2004;7(3):189-192. doi:10.1111/j.1463-5224.2004.04022.x

107. Colotto A, Falsini B, Salgarello T, Iarossi G, Galan ME, Scullica L. Photopic negative response of the human ERG: losses associated with glaucomatous damage. *Invest Ophthalmol Vis Sci*. 2000;41(8):2205-2211.

108. Machida S, Gotoh Y, Tanaka M, Tazawa Y. Predominant loss of the photopic negative response in central retinal artery occlusion. *Am J Ophthalmol*. 2004;137(5):938-940. doi:10.1016/j.ajo.2003.10.023

109. Viswanathan S, Frishman LJ, Robson JG, Harwerth RS, Smith EL. The photopic negative response of the macaque electroretinogram: reduction by experimental glaucoma. *Invest Ophthalmol Vis Sci*. 1999;40(6):1124-1136.

110. Hamilton R, Graham K. Dark-adapted red flash ERGs in healthy adults. *Doc Ophthalmol*. 2018;137(1):1-8. doi:10.1007/s10633-018-9642-1

111. Adrian ED. The electric response of the human eye. *J Physiol (Lond)*. 1945;104(1):84-104. doi:10.1113/jphysiol.1945.sp004109

112. Adrian ED. Rod and cone components in the electric response of the eye. *The Journal of Physiology*. 1946;105(1):24-37. doi:10.1113/jphysiol.1946.sp004148

113. Lim S-H, Ohn Y-H. Study of Blue and Red Flash in Dark-Adapted Electroretinogram. *Korean J Ophthalmol*. 2005;19(2):106. doi:10.3341/kjo.2005.19.2.106

114. Luo X, Frishman LJ. Retinal Pathway Origins of the Pattern Electroretinogram (PERG). *Invest Ophthalmol Vis Sci*. 2011;52(12):8571. doi:10.1167/iovs.11-8376

115. Bach M, Brigell MG, Hawlina M, et al. ISCEV standard for clinical pattern electroretinography (PERG): 2012 update. *Doc Ophthalmol*. 2013;126(1):1-7. doi:10.1007/s10633-012-9353-y

116. Grozdanic SD, Kecova H, Harper MM, Nilaweera W, Kuehn MH, Kardon RH. Functional and structural changes in a canine model of hereditary primary angle-closure glaucoma. *Invest Ophthalmol Vis Sci*. 2010;51(1):255-263. doi:10.1167/iovs.09-4081

117. Holder GE. Pattern electroretinography (PERG) and an integrated approach to visual pathway diagnosis. *Prog Retin Eye Res*. 2001;20(4):531-561.

118. Miura G, Wang MH, Ivers KM, Frishman LJ. Retinal pathway origins of the pattern ERG of the mouse. *Exp Eye Res*. 2009;89(1):49-62. doi:10.1016/j.exer.2009.02.009

119. Hood DC, Bach M, Brigell M, et al. ISCEV standard for clinical multifocal electroretinography (mfERG) (2011 edition). *Doc Ophthalmol*. 2012;124(1):1-13. doi:10.1007/s10633-011-9296-8

120. Lai TYY, Chan W-M, Lai RYK, Ngai JWS, Li H, Lam DSC. The Clinical Applications of Multifocal Electroretinography: A Systematic Review. *Survey of Ophthalmology*. 2007;52(1):61-96. doi:10.1016/j.survophthal.2006.10.005

121. Barnes CS, Alexander KR, Fishman GA. A distinctive form of congenital stationary night blindness with cone ON-pathway dysfunction. *Ophthalmology*. 2002;109(3):575-583.

122. Sustar M, Stirn-Kranjc B, Hawlina M, Brecelj J. Photopic ON- and OFF-responses in complete type of congenital stationary night blindness in relation to stimulus intensity. *Doc Ophthalmol*. 2008;117(1):37-46. doi:10.1007/s10633-007-9101-x

123. Quigley M, Roy MS, Barsoum-Homsy M, Chevrette L, Jacob JL, Milot J. On- and off-responses in the photopic electroretinogram in complete-type congenital stationary night blindness. *Doc Ophthalmol*. 1996;92(3):159-165.

124. Sustar M, Holder GE, Kremers J, et al. ISCEV extended protocol for the photopic On–Off ERG. *Doc Ophthalmol*. 2018;136(3):199-206. doi:10.1007/s10633-018-9645-y

125. Shirato S, Maeda H, Miura G, Frishman LJ. Postreceptoral contributions to the light-adapted ERG of mice lacking b-waves. *Exp Eye Res*. 2008;86(6):914-928. doi:10.1016/j.exer.2008.03.008

126. Sieving PA. Photopic ON- and OFF-pathway abnormalities in retinal dystrophies. *Trans Am Ophthalmol Soc*. 1993;91:701-773.

127. Kremers J, Pangeni G, Tsaousis KT, McKeefry D, Murray IJ, Parry NRA. Incremental and decremental L- and M-cone driven ERG responses: II Sawtooth stimulation. *J Opt Soc Am A*. 2014;31(4):A170. doi:10.1364/JOSAA.31.00A170

128. Viswanathan S, Frishman LJ, Robson JG. Inner-retinal contributions to the photopic sinusoidal flicker electroretinogram of macaques. *Documenta Ophthalmologica*. 2002;105(2):223-242. doi:10.1023/A:1020505104334

129. Kondo M, Sieving PA. Primate photopic sine-wave flicker ERG: vector modeling analysis of component origins using glutamate analogs. *Invest Ophthalmol Vis Sci*. 2001;42(1):305-312.

130. Jacobs GH, Neitz J. Spectral sensitivity of cat cones to rapid flicker. *Exp Brain Res*. 1986;62(2):446-448.

131. Verma R, Pianta MJ. The contribution of human cone photoreceptorsto the photopic flicker electroretinogram. *Journal of Vision*. 2009;9(3):9-9. doi:10.1167/9.3.9

132. Calderone JB, Jacobs GH. Spectral properties and retinal distribution of ferret cones. *Vis Neurosci*. 2003;20(1):11-17. doi:10.1017/S0952523803201024

133. Healy K, McNally L, Ruxton GD, Cooper N, Jackson AL. Metabolic rate and body size are linked with perception of temporal information. *Animal Behaviour*. 2013;86(4):685-696. doi:10.1016/j.anbehav.2013.06.018

134. Byosiere S-E, Chouinard PA, Howell TJ, Bennett PC. What do dogs (Canis familiaris) see? A review of vision in dogs and implications for cognition research. *Psychon Bull Rev*. 2018;25(5):1798-1813. doi:10.3758/s13423-017-1404-7

135. Coile DC, Pollitz CH, Smith JC. Behavioral determination of critical flicker fusion in dogs. *Physiology & Behavior*. 1989;45(6):1087-1092. doi:10.1016/0031-9384(89)90092-9

136. Jacobs GH, Deegan JF, Crognale MA, Fenwick JA. Photopigments of dogs and foxes and their implications for canid vision. *Vis Neurosci*. 1993;10(1):173-180. doi:10.1017/S0952523800003291

137. Cideciyan AV, Jacobson SG. Negative electroretinograms in retinitis pigmentosa. *Invest Ophthalmol Vis Sci*. 1993;34(12):3253-3263.

138. Mowat FM, Wise E, Oh A, Foster ML, Kremers J. In vivo electroretinographic differentiation of rod, short-wavelength and long/medium-wavelength cone responses in dogs using silent substitution stimuli. *Exp Eye Res*. 2019;185:107673. doi:10.1016/j.exer.2019.05.013

139. Naka KI, Rushton WAH. S-potentials from luminosity units in the retina of fish (Cyprinidae). *The Journal of Physiology*. 1966;185(3):587-599. doi:10.1113/jphysiol.1966.sp008003

140. Tzekov RT, Sohocki MM, Daiger SP, Birch DG. Visual phenotype in patients with Arg41Gln and Ala196+1bp mutations in the CRX gene. *Ophthalmic Genetics*. 2000;21(2):89-99. doi:10.1076/1381-6810(200006)2121-8FT089

141. Velten IM, Horn FK, Korth M, Velten K. The b-wave of the dark adapted flash electroretinogram in patients with advanced asymmetrical glaucoma and normal subjects. *Br J Ophthalmol*. 2001;85(4):403-409. doi:10.1136/bjo.85.4.403

142. Tzekov RT, Locke KG, Hood DC, Birch DG. Cone and Rod ERG Phototransduction Parameters in Retinitis Pigmentosa. *Invest Ophthalmol Vis Sci*. 2003;44(9):3993. doi:10.1167/iovs.02-1104

143. Krauss GL, Johnson MA, Miller NR. Vigabatrin-associated retinal cone system dysfunction: Electroretinogram and ophthalmologic findings. *Neurology*. 1998;50(3):614-618. doi:10.1212/WNL.50.3.614

144. Charng J, He Z, Vingrys AJ, et al. Retinal Electrophysiology Is a Viable Preclinical Biomarker for Drug Penetrance into the Central Nervous System. *Journal of Ophthalmology*. 2016;2016:1-12. doi:10.1155/2016/5801826

145. Cideciyan AV. Leber congenital amaurosis due to RPE65 mutations and its treatment with gene therapy. *Progress in Retinal and Eye Research*. 2010;29(5):398-427. doi:10.1016/j.preteyeres.2010.04.002

146. McAnany JJ, Park JC. Temporal Frequency Abnormalities in Early-Stage Diabetic Retinopathy Assessed by Electroretinography. *Invest Ophthalmol Vis Sci*. 2018;59(12):4871. doi:10.1167/iovs.18-25199

147. Barraco R, Persano Adorno D, Brai M. ERG signal analysis using wavelet transform. *Theory Biosci*. 2011;130(3):155-163. doi:10.1007/s12064-011-0124-1

148. Gauvin M, Little JM, Lina J-M, Lachapelle P. Functional decomposition of the human ERG based on the discrete wavelet transform. *Journal of Vision*. 2015;15(16):14. doi:10.1167/15.16.14

149. Gauvin M, Lina J-M, Lachapelle P. Advance in ERG Analysis: From Peak Time and Amplitude to Frequency, Power, and Energy. *BioMed Research International*. 2014;2014:1-11. doi:10.1155/2014/246096

150. Komáromy AM, Abrams KL, Heckenlively JR, et al. Sudden acquired retinal degeneration syndrome (SARDS) - a review and proposed strategies toward a better understanding of pathogenesis, early diagnosis, and therapy. *Vet Ophthalmol*. 2016;19(4):319-331. doi:10.1111/vop.12291

151. Johnson MA, Jeffrey BG, Messias AMV, Robson AG. ISCEV extended protocol for the stimulus–response series for the dark-adapted full-field ERG b-wave. *Doc Ophthalmol*. 2019;138(3):217-227. doi:10.1007/s10633-019-09687-6

152. Winkler PA, Ekenstedt KJ, Occelli LM, et al. A Large Animal Model for CNGB1 Autosomal Recessive Retinitis Pigmentosa. Hollander AI den., ed. *PLoS ONE*. 2013;8(8):e72229. doi:10.1371/journal.pone.0072229

153. Kanamaru C, Yamada Y, Hayashi S, et al. Retinal toxicity induced by small-molecule Hsp90 inhibitors in beagle dogs. *J Toxicol Sci*. 2014;39(1):59-69.

154. Sidjanin DJ. Canine CNGB3 mutations establish cone degeneration as orthologous to the human achromatopsia locus ACHM3. *Human Molecular Genetics*. 2002;11(16):1823-1833. doi:10.1093/hmg/11.16.1823

155. Marinho LLP, Occelli LM, Pasmanter N, Somma AT, Montiani-Ferreira F, Petersen-Jones SM. Autosomal recessive night blindness with progressive photoreceptor degeneration in a dog model. *Investigative Ophthalmology & Visual Science*. 2019;60(9):465-465.

156. Das RG, Becker D, Jagannathan V, et al. Genome-wide association study and whole-genome sequencing identify a deletion in LRIT3 associated with canine congenital stationary night blindness. *Sci Rep*. 2019;9(1):14166. doi:10.1038/s41598-019-50573-7

157. Wiik AC, Wade C, Biagi T, et al. A deletion in nephronophthisis 4 (NPHP4) is associated with recessive cone-rod dystrophy in standard wire-haired dachshund. *Genome Research*. 2008;18(9):1415-1421. doi:10.1101/gr.074302.107

158. Turney C, Chong NHV, Alexander RA, et al. Pathological and Electrophysiological Features of a Canine Cone–Rod Dystrophy in the Miniature Longhaired Dachshund. *Invest Ophthalmol Vis Sci*. 2007;48(9):4240. doi:10.1167/iovs.04-0737

159. Tuntivanich N, Pittler SJ, Fischer AJ, et al. Characterization of a Canine Model of Autosomal Recessive Retinitis Pigmentosa due to a *PDE6A* Mutation. *Invest Ophthalmol Vis Sci*. 2009;50(2):801. doi:10.1167/iovs.08-2562

160. Suber ML, Pittler SJ, Qin N, et al. Irish setter dogs affected with rod/cone dysplasia contain a nonsense mutation in the rod cGMP phosphodiesterase beta-subunit gene. *Proceedings of the National Academy of Sciences*. 1993;90(9):3968-3972. doi:10.1073/pnas.90.9.3968

161. Petersen–Jones SM, Entz DD, Sargan DR. cGMP phosphodiesterase-α mutation causes progressive retinal atrophy in the Cardigan Welsh corgi dog. *Investigative ophthalmology & visual science*. 1999;40(8):1637-1644.

162. Torres NV, Santos G. The (Mathematical) Modeling Process in Biosciences. *Front Genet*. 2015;6. doi:10.3389/fgene.2015.00354

163. Michaelis L, Menten ML, Johnson KA, Goody RS. The original Michaelis constant: translation of the 1913 Michaelis-Menten paper. *Biochemistry*. 2011;50(39):8264-8269. doi:10.1021/bi201284u

164. Hood DC, Birch DG. The A-wave of the human electroretinogram and rod receptor function. *Invest Ophthalmol Vis Sci*. 1990;31(10):2070-2081.

165. Perlman I. Relationship between the amplitudes of the b wave and the a wave as a useful index for evaluating the electroretinogram. *Br J Ophthalmol*. 1983;67(7):443-448. doi:10.1136/bjo.67.7.443

166. Naka KI, Rushton WAH. The generation and spread of S-potentials in fish (Cyprinidae). *The Journal of Physiology*. 1967;192(2):437-461. doi:10.1113/jphysiol.1967.sp008308

167. Evans LS, Peachey NS, Marchese AL. Comparison of three methods of estimating the parameters of the Naka-Rushton equation. *Doc Ophthalmol*. 1993;84(1):19-30.

168. Annear MJ, Bartoe JT, Barker SE, et al. Gene therapy in the second eye of RPE65-deficient dogs improves retinal function. *Gene Ther*. 2011;18(1):53-61. doi:10.1038/gt.2010.111

169. Newville M, Stensitzki T, Allen DB, Ingargiola A. *LMFIT: Non-Linear Least-Square Minimization and Curve-Fitting for Python*. Zenodo; 2014. doi:10.5281/ZENODO.11813

170. Luenberger DG. *Optimization by Vector Space Methods*. Nachdr. Wiley; 1998.

171. Levenberg K. A method for the solution of certain non-linear problems in least squares. *Quart Appl Math*. 1944;2(2):164-168. doi:10.1090/qam/10666

172. Marquardt DW. An Algorithm for Least-Squares Estimation of Nonlinear Parameters. *Journal of the Society for Industrial and Applied Mathematics*. 1963;11(2):431-441. doi:10.1137/0111030

173. Seabold, Skipper, Perktold, Josef. Statsmodels: Econometric and statistical modeling with python. *Proceedings of the 9th Python in Science Conference*. Published online 2010.

174. Brigham EO. *The Fast Fourier Transform and Its Applications*. Prentice Hall; 1988.

175. Atkinson KE. *An Introduction to Numerical Analysis*. Wiley; 1989. Accessed January 20, 2020. http://catalog.hathitrust.org/api/volumes/oclc/17551990.html

176. Wachtmeister L. Oscillatory potentials in the retina: what do they reveal. *Progress in Retinal and Eye Research*. 1998;17(4):485-521. doi:10.1016/S1350-9462(98)00006-8

177. Parry HB, Tansley K, Thomson LC. The electroretinogram of the dog. *J Physiol (Lond)*. 1953;120(1-2):28-40. doi:10.1113/jphysiol.1953.sp004870

178. Thompson DA, Fujinami K, Perlman I, Hamilton R, Robson AG. ISCEV extended protocol for the dark-adapted red flash ERG. *Documenta Ophthalmologica*. 2018;136(3):191–197. doi:10.1007/s10633-018-9644-z

179. Brigell M, Jeffrey BG, Mahroo OA, Tzekov R. ISCEV extended protocol for derivation and analysis of the strong flash rod-isolated ERG a-wave. *Doc Ophthalmol*. 2020;140(1):5-12. doi:10.1007/s10633-019-09740-4

180. McCulloch DL, Kondo M, Hamilton R, et al. ISCEV extended protocol for the stimulus–response series for light-adapted full-field ERG. *Doc Ophthalmol*. 2019;138(3):205-215. doi:10.1007/s10633-019-09685-8

181. Frishman L, Sustar M, Kremers J, et al. ISCEV extended protocol for the photopic negative response (PhNR) of the full-field electroretinogram. *Doc Ophthalmol*. 2018;136(3):207-211. doi:10.1007/s10633-018-9638-x

182. Perlman I, Kondo M, Chelva E, Robson AG, Holder GE. ISCEV extended protocol for the S-cone ERG. *Doc Ophthalmol*. 2020;140(2):95-101. doi:10.1007/s10633-019-09730-6

183. Thompson DA, Fujinami K, Perlman I, Hamilton R, Robson AG. ISCEV extended protocol for the dark-adapted red flash ERG. *Doc Ophthalmol*. 2018;136(3):191-197. doi:10.1007/s10633-018-9644-z

184. Kremers J. The assessment of L- and M-cone specific electroretinographical signals in the normal and abnormal human retina. *Progress in Retinal and Eye Research*. 2003;22(5):579-605. doi:10.1016/S1350-9462(03)00049-1

185. Arden G, Wolf J, Berninger T, Hogg CR, Tzekov R, Holder GE. S-cone ERGs elicited by a simple technique in normals and in tritanopes. *Vision Res*. 1999;39(3):641-650. doi:10.1016/s0042-6989(98)00182-5

186. Armington JC. A Component of the Human Electroretinogram Associated with Red Color Vision*. *J Opt Soc Am*. 1952;42(6):393. doi:10.1364/JOSA.42.000393

187. De Rouck A, Francois J, Verriest G. Pathology of the x-wave of the human electroretinogram. I. Red-blindness and other congenital functional abnormalities. *Br J Ophthalmol*. 1956;40(7):439-443. doi:10.1136/bjo.40.7.439

188. Kellner U, Foerster MH. Color electroretinography: A method for separation of dysfunctions of cones. *Doc Ophthalmol*. 1992;80(1):13-23. doi:10.1007/BF00161227

189. Kremers J, Jertila M, Link B, Pangeni G, Horn FK. Spectral characteristics of the PhNR in the full-field flash electroretinogram of normals and glaucoma patients. *Doc Ophthalmol*. 2012;124(2):79-90. doi:10.1007/s10633-011-9304-z

190. Narfström K, Andersson B-E, Andreasson S, Gouras P. Clinical electroretinography in the dog with ganzfeld stimulation: A practical method of examining rod and cone function. *Doc Ophthalmol*. 1995;90(3):279-290. doi:10.1007/BF01203863

191. Aguirre GD, Rubin LF. The electroretinogram in dogs with inherited cone degeneration. *Invest Ophthalmol*. 1975;14(11):840-847.

192. Aguirre G. Retinal degenerations in the dog. I. Rod dysplasia. *Experimental Eye Research*. 1978;26(3):233-253. doi:10.1016/0014-4835(78)90072-6

193. Narfström K, Ekesten B. Electroretinographic evaluation of Papillons with and without hereditary retinal degeneration. *Am J Vet Res*. 1998;59(2):221-226.

194. Aguirre GD, Rubin LF. Progressive retinal atrophy (rod dysplasia in the Norwegian Elkhound. *J Am Vet Med Assoc*. 1971;158(2):208-218.

195. Maehara S, Osawa A, Itoh N, et al. Detection of cone dysfunction induced by digoxin in dogs by multicolor electroretinography. *Vet Ophthalmol*. 2005;8(6):407-413. doi:10.1111/j.1463-5224.2005.00415.x

196. Baylor DA, Lamb TD, Yau KW. Responses of retinal rods to single photons. *J Physiol (Lond)*. 1979;288:613-634.

197. Baylor DA, Nunn BJ, Schnapf JL. The photocurrent, noise and spectral sensitivity of rods of the monkey Macaca fascicularis. *J Physiol (Lond)*. 1984;357:575-607. doi:10.1113/jphysiol.1984.sp015518

198. Burkhardt DA. Light adaptation and photopigment bleaching in cone photoreceptors in situ in the retina of the turtle. *J Neurosci*. 1994;14(3 Pt 1):1091-1105.

199. Koenig D, Hofer H. The absolute threshold of cone vision. *J Vis*. 2011;11(1). doi:10.1167/11.1.21

200. Korenbrot JI. Speed, adaptation, and stability of the response to light in cone photoreceptors: the functional role of Ca-dependent modulation of ligand sensitivity in cGMP-gated ion channels. *J Gen Physiol*. 2012;139(1):31-56. doi:10.1085/jgp.201110654

201. Normann RA, Werblin FS. Control of Retinal Sensitivity. *The Journal of General Physiology*. 1974;63(1):37-61. doi:10.1085/jgp.63.1.37

202. Rufiange M, Rousseau S, Dembinska O, Lachapelle P. Cone-dominated ERG luminance–response function: the Photopic Hill revisited. *Documenta Ophthalmologica*. 2002;104(3):231-248. doi:10.1023/A:1015265812018

203. Wali N, Leguire LE. The photopic hill: A new phenomenon of the light adapted electroretinogram. *Doc Ophthalmol*. 1992;80(4):335-342. doi:10.1007/BF00154382

204. Bloomfield SA, Dacheux RF. Rod vision: pathways and processing in the mammalian retina. *Prog Retin Eye Res*. 2001;20(3):351-384. doi:10.1016/s1350-9462(00)00031-8

205. Deans MR, Volgyi B, Goodenough DA, Bloomfield SA, Paul DL. Connexin36 is essential for transmission of rod-mediated visual signals in the mammalian retina. *Neuron*. 2002;36(4):703-712. doi:10.1016/s0896-6273(02)01046-2

206. Field GD, Chichilnisky EJ. Information processing in the primate retina: circuitry and coding. *Annu Rev Neurosci*. 2007;30:1-30. doi:10.1146/annurev.neuro.30.051606.094252

207. Sharpe LT, Stockman A. Rod pathways: the importance of seeing nothing. *Trends Neurosci*. 1999;22(11):497-504. doi:10.1016/s0166-2236(99)01458-7

208. Tsukamoto Y, Morigiwa K, Ueda M, Sterling P. Microcircuits for night vision in mouse retina. *J Neurosci*. 2001;21(21):8616-8623.

209. Tsukamoto Y, Morigiwa K, Ishii M, et al. A novel connection between rods and ON cone bipolar cells revealed by ectopic metabotropic glutamate receptor 7 (mGluR7) in mGluR6-deficient mouse retinas. *J Neurosci*. 2007;27(23):6261-6267. doi:10.1523/JNEUROSCI.5646-06.2007

210. Tsukamoto Y, Omi N. Some OFF bipolar cell types make contact with both rods and cones in macaque and mouse retinas. *Front Neuroanat*. 2014;8:105. doi:10.3389/fnana.2014.00105

211. Sustar M, Hawlina M, Brecelj J. ON- and OFF-response of the photopic electroretinogram in relation to stimulus characteristics. *Doc Ophthalmol*. 2006;113(1):43-52. doi:10.1007/s10633-006-9013-1

212. Pretterer G, Bubna-Littitz H, Windischbauer G, Gabler C, Griebel U. Brightness discrimination in the dog. *Journal of Vision*. 2004;4(3):10. doi:10.1167/4.3.10

213. Heck J. The Flicker Electroretinogram of the Human Eye. *Acta Physiologica Scandinavica*. 1957;39(2-3):158-166. doi:10.1111/j.1748-1716.1957.tb01417.x

214. Lei B. Rod-driven OFF pathway responses in the distal retina: dark-adapted flicker electroretinogram in mouse. *PLoS ONE*. 2012;7(8):e43856. doi:10.1371/journal.pone.0043856

215. Tuntivanich N, Pittler SJ, Fischer AJ, et al. Characterization of a Canine Model of Autosomal Recessive Retinitis Pigmentosa due to a *PDE6A* Mutation. *Investigative Opthalmology & Visual Science*. 2009;50(2):801. doi:10.1167/iovs.08-2562

216. Gum GG, Gelatt KN, Samuelson DA. Maturation of the retina of the canine neonate as determined by electroretinography and histology. *Am J Vet Res*. 1984;45(6):1166-1171.

217. Seeliger MW, Brombas A, Weiler R, et al. Modulation of rod photoreceptor output by HCN1 channels is essential for regular mesopic cone vision. *Nat Commun*. 2011;2(1):532. doi:10.1038/ncomms1540

218. Montgomery DC. *Design and Analysis of Experiments*. Tenth edition. Wiley; 2020.

219. Massof RW, Jones AE. Electroretinographic evidence for a photopic system in the rat. *Vision Res*. 1972;12(7):1231-1239. doi:10.1016/0042-6989(72)90194-0

220. Jacobs GH, Jones AE, De Valois RL. Electroretinogram of the squirrel monkey. *J Comp Physiol Psychol*. 1963;56:405-409. doi:10.1037/h0046899

221. Donner K. Noise and the absolute thresholds of cone and rod vision. *Vision Res*. 1992;32(5):853-866. doi:10.1016/0042-6989(92)90028-h

222. Dunn FA, Doan T, Sampath AP, Rieke F. Controlling the gain of rod-mediated signals in the Mammalian retina. *J Neurosci*. 2006;26(15):3959-3970. doi:10.1523/JNEUROSCI.5148-05.2006

223. Frishman LJ, Robson JG, Reddy MG. Effects of background light on the human dark-adapted electroretinogram and psychophysical threshold. *J Opt Soc Am A*. 1996;13(3):601. doi:10.1364/JOSAA.13.000601

224. Shapley R, Enroth-Cugell C. Chapter 9 Visual adaptation and retinal gain controls. *Progress in Retinal Research*. 1984;3:263-346. doi:10.1016/0278-4327(84)90011-7

225. Li B, Barnes GE, Holt WF. The decline of the photopic negative response (PhNR) in the rat after optic nerve transection. *Doc Ophthalmol*. 2005;111(1):23-31. doi:10.1007/s10633-005-2629-8

226. Perlman I, Normann RA. Light adaptation and sensitivity controlling mechanisms in vertebrate photoreceptors. *Prog Retin Eye Res*. 1998;17(4):523-563. doi:10.1016/s1350-9462(98)00005-6

227. Smith EL, Harwerth RS, Crawford ML, Duncan GC. Contribution of the retinal ON channels to scotopic and photopic spectral sensitivity. *Vis Neurosci*. 1989;3(3):225-239. doi:10.1017/s0952523800009986

228. Burns ME, Baylor DA. Activation, deactivation, and adaptation in vertebrate photoreceptor cells. *Annu Rev Neurosci*. 2001;24:779-805. doi:10.1146/annurev.neuro.24.1.779

229. Arshavsky VY, Lamb TD, Pugh EN. G Proteins and Phototransduction. *Annu Rev Physiol*. 2002;64(1):153-187. doi:10.1146/annurev.physiol.64.082701.102229

230. Hagins WA, Penn RD, Yoshikami S. Dark Current and Photocurrent in Retinal Rods. *Biophysical Journal*. 1970;10(5):380-412. doi:10.1016/S0006-3495(70)86308-1

231. Fain GL, Matthews HR, Cornwall MC, Koutalos Y. Adaptation in vertebrate photoreceptors. *Physiol Rev*. 2001;81(1):117-151. doi:10.1152/physrev.2001.81.1.117

232. Kraft TW, Schneeweis DM, Schnapf JL. Visual transduction in human rod photoreceptors. *J Physiol (Lond)*. 1993;464:747-765. doi:10.1113/jphysiol.1993.sp019661

233. Thomas MM, Lamb TD. Light adaptation and dark adaptation of human rod photoreceptors measured from the a-wave of the electroretinogram. *The Journal of Physiology*. 1999;518 ( Pt 2):479–496. doi:10.1111/j.1469-7793.1999.0479p.x

234. Euler T, Haverkamp S, Schubert T, Baden T. Retinal bipolar cells: elementary building blocks of vision. *Nat Rev Neurosci*. 2014;15(8):507-519. doi:10.1038/nrn3783

235. Nelson R, Kolb H. ON and OFF Pathways in the Vertebrate Retina and Visual System. :76.

236. Wässle H. Parallel processing in the mammalian retina. *Nat Rev Neurosci*. 2004;5(10):747-757. doi:10.1038/nrn1497

237. Duvoisin RM, Morgans C, Taylor W. The mGluR6 receptors in the retina: Analysis of a unique G-protein signaling pathway. *Cellscience Reviews*. 2005;2(2):18.

238. Thoreson WB. Kinetics of synaptic transmission at ribbon synapses of rods and cones. *Mol Neurobiol*. 2007;36(3):205-223. doi:10.1007/s12035-007-0019-9

239. Rufiange M, Rousseau S, Dembinska O, Lachapelle P. Cone-dominated ERG luminance–response function: the Photopic Hill revisited. *Documenta Ophthalmologica*. 2002;104(3):231–248. doi:10.1023/A:1015265812018

240. Wali N, Leguire LE. The photopic hill: A new phenomenon of the light adapted electroretinogram. *Doc Ophthalmol*. 1992;80(4):335-342. doi:10.1007/BF00154382

241. Sieving PA, Murayama K, Naarendorp F. Push-pull model of the primate photopic electroretinogram: a role for hyperpolarizing neurons in shaping the b-wave. *Vis Neurosci*. 1994;11(3):519-532.

242. Bloomfield SA, Dacheux RF. Rod vision: pathways and processing in the mammalian retina. *Prog Retin Eye Res*. 2001;20(3):351-384. doi:10.1016/s1350-9462(00)00031-8

243. Deans MR, Volgyi B, Goodenough DA, Bloomfield SA, Paul DL. Connexin36 is essential for transmission of rod-mediated visual signals in the mammalian retina. *Neuron*. 2002;36(4):703-712. doi:10.1016/s0896-6273(02)01046-2

244. Hornstein EP, Verweij J, Li PH, Schnapf JL. Gap-junctional coupling and absolute sensitivity of photoreceptors in macaque retina. *J Neurosci*. 2005;25(48):11201-11209. doi:10.1523/JNEUROSCI.3416-05.2005

245. Schneeweis DM, Schnapf JL. Photovoltage of rods and cones in the macaque retina. *Science*. 1995;268(5213):1053-1056. doi:10.1126/science.7754386

246. Verweij J, Dacey DM, Peterson BB, Buck SL. Sensitivity and dynamics of rod signals in H1 horizontal cells of the macaque monkey retina. *Vision Res*. 1999;39(22):3662-3672. doi:10.1016/s0042-6989(99)00093-0

247. Bush RA, Sieving PA. A proximal retinal component in the primate photopic ERG a-wave. *Invest Ophthalmol Vis Sci*. 1994;35(2):635-645.

248. Robson JG, Saszik SM, Ahmed J, Frishman LJ. Rod and cone contributions to the a-wave of the electroretinogram of the macaque. *J Physiol (Lond)*. 2003;547(Pt 2):509-530. doi:10.1113/jphysiol.2002.030304

249. Cameron AM, Mahroo O a. R, Lamb TD. Dark adaptation of human rod bipolar cells measured from the b-wave of the scotopic electroretinogram. *The Journal of Physiology*. 2006;575(Pt 2):507–526. doi:10.1113/jphysiol.2006.108027

250. Robson JG, Maeda H, Saszik SM, Frishman LJ. In vivo studies of signaling in rod pathways of the mouse using the electroretinogram. *Vision Res*. 2004;44(28):3253-3268. doi:10.1016/j.visres.2004.09.002

251. Naarendorp F, Williams GE. The *d* -wave of the rod electroretinogram of rat originates in the cone pathway. *Vis Neurosci*. 1999;16(1):91-105. doi:10.1017/S0952523899161054

252. Xu X, Karwoski C. Current source density analysis of the electroretinographic d wave of frog retina. *Journal of Neurophysiology*. 1995;73(6):2459-2469. doi:10.1152/jn.1995.73.6.2459

253. Lei B. The ERG of guinea pig (Cavis porcellus): comparison with I-type monkey and E-type rat. *Documenta Ophthalmologica*. 2003;106(3):243-249. doi:10.1023/A:1022940517793

254. Kondo M, Miyake Y, Horiguchi M, Suzuki S, Tanikawa A. Recording Multifocal Electroretinogram On and Off Responses in Humans. 1998;39(3):7.

255. Ueno S, Kondo M, Ueno M, Miyata K, Terasaki H, Miyake Y. Contribution of retinal neurons to d-wave of primate photopic electroretinograms. *Vision Research*. 2006;46(5):658-664. doi:10.1016/j.visres.2005.05.026

256. Granit R. The components of the retinal action potential in mammals and their relation to the discharge in the optic nerve. *The Journal of Physiology*. 1933;77(3):207-239. doi:10.1113/jphysiol.1933.sp002964

257. Müller F, Kaupp UB. [Signal transduction in photoreceptor cells]. *Naturwissenschaften*. 1998;85(2):49-61.

258. Green DG. Scotopic and photopic components of the rat electroetinogram. *J Physiol*. 1973;228(3):781-797. doi:10.1113/jphysiol.1973.sp010112

259. Granit R, Therman PO. Excitation and inhibition in the retina and in the optic nerve. *The Journal of Physiology*. 1935;83(3):359-381. doi:10.1113/jphysiol.1935.sp003235

260. Wündsch L, Lützow A v. The effect of aspartate on the ERG of the isolated rabbit retina. *Vision Research*. 1971;11(10):1207-1208. doi:10.1016/0042-6989(71)90154-4

261. Vinberg FJ, Strandman S, Koskelainen A. Origin of the fast negative ERG component from isolated aspartate-treated mouse retina. *Journal of Vision*. 2009;9(12):9-9. doi:10.1167/9.12.9

262. Arden GB. Voltage gradients across the receptor layer of the isolated rat retina. *J Physiol*. 1976;256(2):333-360.1. doi:10.1113/jphysiol.1976.sp011328

263. Hanawa I, Tateishi T. The effect of aspartate on the electroretinogram of the vertebrate retina. *Experientia*. 1970;26(12):1311-1312.

264. Veske A, Nilsson SE, Narfström K, Gal A. Retinal dystrophy of Swedish briard/briard-beagle dogs is due to a 4-bp deletion in RPE65. *Genomics*. 1999;57(1):57-61. doi:10.1006/geno.1999.5754

265. Kondo M, Das G, Imai R, et al. A Naturally Occurring Canine Model of Autosomal Recessive Congenital Stationary Night Blindness. *PLoS ONE*. 2015;10(9):e0137072. doi:10.1371/journal.pone.0137072

266. Somma AT, Moreno JCD, Sato MT, et al. Characterization of a novel form of progressive retinal atrophy in Whippet dogs: a clinical, electroretinographic, and breeding study. *Vet Ophthalmol*. 2017;20(5):450-459. doi:10.1111/vop.12448

267. Marinho LLP, Occelli LM, Pasmanter N, Somma AT, Montiani-Ferreira F, Petersen-Jones SM. Autosomal recessive night blindness with progressive photoreceptor degeneration in a dog model. *Investigative Ophthalmology & Visual Science*. 2019;60(9):465-465.

268. Pasmanter N, Petersen-Jones SM. A review of electroretinography waveforms and models and their application in the dog. *Vet Ophthalmol*. 2020;23(3):418-435. doi:10.1111/vop.12759

269. Petersen-Jones SM, Komáromy AM. Dog models for blinding inherited retinal dystrophies. *Hum Gene Ther Clin Dev*. 2015;26(1):15-26. doi:10.1089/humc.2014.155

270. Occelli LM, Schön C, Seeliger MW, et al. Gene Supplementation Rescues Rod Function and Preserves Photoreceptor and Retinal Morphology in Dogs, Leading the Way Towards Treating Human PDE6A-Retinitis Pigmentosa. *Hum Gene Ther*. Published online December 6, 2017. doi:10.1089/hum.2017.155

271. Petersen-Jones SM, Occelli LM, Winkler PA, et al. Patients and animal models of CNGβ1-deficient retinitis pigmentosa support gene augmentation approach. *The Journal of Clinical Investigation*. 2018;128(1):190–206. doi:10.1172/JCI95161

272. Brigell M, Jeffrey BG, Mahroo OA, Tzekov R. ISCEV extended protocol for derivation and analysis of the strong flash rod-isolated ERG a-wave. *Doc Ophthalmol*. 2020;140(1):5-12. doi:10.1007/s10633-019-09740-4

273. Hood DC, Birch DG. Assessing abnormal rod photoreceptor activity with the a-wave of the electroretinogram: Applications and methods. *Doc Ophthalmol*. 1996;92(4):253-267. doi:10.1007/BF02584080

274. Team PC. Python: A dynamic, open source programming language. *Python Software Foundation*. 2015;78.

275. Donner K. Noise and the absolute thresholds of cone and rod vision. *Vision Res*. 1992;32(5):853-866. doi:10.1016/0042-6989(92)90028-h

276. Dunn FA, Doan T, Sampath AP, Rieke F. Controlling the gain of rod-mediated signals in the Mammalian retina. *J Neurosci*. 2006;26(15):3959-3970. doi:10.1523/JNEUROSCI.5148-05.2006

277. Frishman LJ, Robson JG, Reddy MG. Effects of background light on the human dark-adapted electroretinogram and psychophysical threshold. *J Opt Soc Am A*. 1996;13(3):601. doi:10.1364/JOSAA.13.000601

278. Shapley R, Enroth-Cugell C. Chapter 9 Visual adaptation and retinal gain controls. *Progress in Retinal Research*. 1984;3:263-346. doi:10.1016/0278-4327(84)90011-7